



FACULTAD DE CIENCIAS  
UNIVERSIDAD DE CANTABRIA

---

**Search for dark matter production in  
association with top quarks in the  
dilepton final state at  $\sqrt{s} = 13$  TeV**

---

A thesis submitted in fulfillment of the requirements for the  
**Degree of Doctor of Philosophy**

---

Written by  
**Cédric Prieëls**

Under the supervision of  
**Jónatan Piedra Gómez**  
**Pablo Martínez Ruiz del Árbol**

Santander, June 2020





FACULTAD DE CIENCIAS  
UNIVERSIDAD DE CANTABRIA

---

**Búsqueda de materia oscura en  
asociación con quarks top en el estado  
final dileptónico a  $\sqrt{s} = 13$  TeV**

---

Memoria para optar al  
**Grado de doctor**

---

Escrita por  
**Cédric Prieëls**  
  
Bajo la supervisión de  
**Jónatan Piedra Gómez**  
**Pablo Martínez Ruiz del Árbol**

Santander, Junio 2020



# **Abstract**



# **Resumen**



# Acknowledgments



# Acronyms used

<b>ADMX</b>	Axion Dark Matter Experiment	<b>DY</b>	Drell-Yan
<b>ALICE</b>	A Large Ion Collider Experiment	<b>ECAL</b>	Electromagnetic Calorimeter
<b>AMS</b>	Alpha Magnetic Spectrometer	<b>EDM</b>	Event Data Model
<b>AOD</b>	Analysis Object Data	<b>EFT</b>	Effective Field Theory
<b>ATLAS</b>	A Toroidal LHC ApparatuS	<b>EWK</b>	Electroweak
<b>BDT</b>	Boosted Decision Trees	<b>FR</b>	Fake Rate
<b>BR</b>	Branching Ratio	<b>FSR</b>	Final State Radiation
<b>BSM</b>	Beyond the Standard Model	<b>GEM</b>	Gas Electron Multiplier
<b>BW</b>	Breit-Wigner	<b>GSF</b>	Gaussian Sum Filter
<b>CAST</b>	CERN Axion Solar Telescope	<b>HCAL</b>	Hadronic Calorimeter
<b>CERN</b>	European Council for Nuclear Research	<b>HLT</b>	High-Level Trigger
<b>CL</b>	Confidence Level	<b>HO</b>	Hadron Outer
<b>CMB</b>	Cosmic Microwave Background	<b>IACT</b>	Imaging Atmospheric Cherenkov Telescopes
<b>CMS</b>	Compact Muon Solenoid	<b>IAXO</b>	International AXion Observatory
<b>CSC</b>	Cathode Strip Chamber	<b>ISR</b>	Initial State Radiation
<b>CR</b>	Control Region	<b>KF</b>	Kalman Filter
<b>CSV</b>	Combined Secondary Vertex	<b>L1</b>	Level-1 Trigger
<b>CTA</b>	Cherenkov Telescope Array	<b>LAT</b>	Fermi Large Telescope
<b>DAQ</b>	Data Acquisition System	<b>LEP</b>	Large Electron Positron collider
<b>DAS</b>	Data Aggregation System	<b>LHC</b>	Large Hadron Collider
<b>DCS</b>	Detector Control System	<b>LNGS</b>	Laboratori Nazionali del Gran Sasso
<b>DQM</b>	Data Quality Monitoring	<b>LO</b>	Leading Order
<b>DM</b>	Dark Matter	<b>LS</b>	Long Shutdown
<b>DMWG</b>	Dark Matter Working Group	<b>LSP</b>	Lightest Supersymmetric Particle
<b>DNN</b>	Deep Neural Network	<b>MACHO</b>	Massive Compact Halo Object
<b>DT</b>	Drift tube	<b>MC</b>	Monte Carlo

<b>MET</b>	Missing Transverse Energy	<b>QFT</b>	Quantum Field Theory
<b>MFV</b>	Minimal Flavour Violation	<b>RMS</b>	Root Mean Square
<b>ML</b>	Machine Learning	<b>RPC</b>	Resistive Plate Chamber
<b>MPI</b>	Multiple Parton Interaction	<b>SC</b>	Super Cluster
<b>MSSM</b>	Minimal Supersymmetric Standard Model	<b>SD</b>	Spin Dependent
<b>MVA</b>	Multi-Variate Analysis	<b>SF</b>	Scale Factors
<b>NFW</b>	Navarro-Frenk-White	<b>SI</b>	Spin Independent
<b>NLO</b>	Next to Leading Order	<b>SM</b>	Standard Model
<b>PDF</b>	Parton Density Function	<b>SPS</b>	Super Proton Synchrotron
<b>PF</b>	Particle Flow	<b>SR</b>	Signal Region
<b>POG</b>	Physics Object Group	<b>TEC</b>	Tracker EndCap
<b>PR</b>	Prompt Rate	<b>TIB/TBD</b>	Tracker Inner Barrel and Disks
<b>PS</b>	Proton Synchrotron	<b>TOB</b>	Tracker Outer Barrel
<b>PU</b>	Pile Up	<b>UE</b>	Underlying Event
<b>PUPPI</b>	Pileup Per Particle Identification	<b>UED</b>	Universal Extra Dimensions
<b>PV</b>	Primary Vertex	<b>VBF</b>	Vector Boson Fusion
<b>QCD</b>	Quantum ChromoDynamics	<b>WIMP</b>	Weakly Interactive Massive Particle
		<b>WP</b>	Working Point

# Contents

<b>1</b>	<b>Introduction</b>	<b>1</b>
<b>2</b>	<b>The dark matter case</b>	<b>5</b>
2.1	The Standard Model . . . . .	5
2.2	At the origins of dark matter . . . . .	6
2.2.1	Zwicky and the virial theorem . . . . .	7
2.2.2	Spiral galaxies rotation curves . . . . .	7
2.2.3	Cosmic Microwave Background (CMB) anisotropies . . . . .	8
2.2.4	Gravitational lensing . . . . .	10
2.3	Dark matter properties . . . . .	11
2.4	Dark matter candidates . . . . .	13
2.5	Dark matter searches . . . . .	18
2.5.1	Direct searches . . . . .	19
2.5.2	Indirect searches . . . . .	22
2.5.3	Collider production . . . . .	26
2.6	Dark Matter (DM) production at the Large Hadron Collider (LHC) . . . . .	29
2.6.1	The single top production channel . . . . .	31
2.6.2	The $t\bar{t}$ production channel . . . . .	32
2.6.3	The dilepton final state . . . . .	32
2.7	Previous relevant results . . . . .	33
<b>3</b>	<b>Event selection</b>	<b>37</b>
3.1	Objects selection . . . . .	37
3.1.1	Triggers selection . . . . .	37
3.1.2	Electrons selection . . . . .	39
3.1.3	Muons selection . . . . .	40
3.1.4	Jet selection . . . . .	42
3.2	Signals regions . . . . .	43
3.2.1	$t/\bar{t}$ +DM region . . . . .	44
3.2.2	$t\bar{t}$ +DM region . . . . .	44

3.3	Control regions . . . . .	47
3.3.1	Drell-Yan (DY) control region . . . . .	47
3.3.2	Top control region . . . . .	47
3.3.3	ttV control region . . . . .	47
3.3.4	Same sign control region . . . . .	47
3.4	Background-signal discrimination . . . . .	52
3.4.1	Discriminating variables . . . . .	52
3.4.2	Neural network . . . . .	53
<b>4</b>	<b>Results and interpretations</b>	<b>55</b>
4.1	Systematics and uncertainties . . . . .	55
4.2	Results . . . . .	55
<b>5</b>	<b>Conclusions</b>	<b>57</b>
5.1	Future prospects . . . . .	57
<b>Appendices</b>		<b>59</b>
<b>A</b>	<b>Samples used</b>	<b>61</b>
A.1	Data samples . . . . .	61
A.2	Signal samples . . . . .	61
A.3	Backgrounds samples . . . . .	61
<b>B</b>	<b>Neural network optimization</b>	<b>69</b>
<b>Bibliography</b>		<b>75</b>



# Chapter 1

## Introduction

The Standard Model (SM) of particle physics [1] is nowadays the most accepted mathematical model used to describe the elementary particles and three of the 4 fundamental forces of nature (electromagnetic, weak and strong interactions, while the gravitational interaction is out of reach of this model). This model is quite simple in concept, but has been able to describe most of the phenomena observed in nature so far with an incredible level of precision, and has made a lot of predictions that have now been proven to be true, such as the postulate of the Higgs mechanism [4, 5] followed by the discovery of the Higgs boson itself [6, 7] by the Compact Muon Solenoid (CMS) [2] and A Toroidal LHC ApparatuS (ATLAS) [3] experiments analyzing the proton-proton collisions produced by the Large Hadron Collider (LHC) at a center of mass energy  $\sqrt{s} = 13$  TeV, announced at the European Council for Nuclear Research (CERN) on the 4th of July 2012.

However, as accurate as it seems to be, this theory, introduced in Section 2.1, is known to have several shortcomings which require further investigation. Eventual exotic particles which do not fit in the current model could be the sign of new physics and have therefore been extensively searched for over the course of the last decades in order to enhance our understanding of the Universe and all its constituents.

In this context, the first serious Dark Matter (DM) hypothesis was introduced in the 1970s because of gravitational anomalies observed by several astrophysicists, as a way to explain the apparent non-luminous missing mass in the Universe [8]. Indeed, the visible mass in most galaxies appears to be way too low to explain several astrophysical processes, such as the rotation curves of the galaxies [9], which seems to be incompatible with the well established laws of gravitation. Some additional measurements of the gravitational lensing (in the Bullet Cluster, for example [10]) and the anisotropies observed in the Cosmic Microwave Background (CMB) [11] are other evidences for the existence of DM, as explained in Section 2.2.

As far as we currently know from cosmological measurements, ordinary baryonic matter only constitutes around 5% of the Universe, while DM represents around 26% of the total energy density of the Universe (the rest is being considered as dark energy) [12]. Understanding the nature and properties of this new kind of exotic matter is therefore crucial to try and understand the laws of physics in the Universe, with many theorists and large experiments around the world currently involved in such searches.

Nowadays, the existence of DM is well motivated in the physics community, even though it has never been observed directly, since our only evidences so far for its existence come from its large-scale gravitational effects. While its mass, spin, nature and basic properties are still unknown and extensively studied, one of the best DM candidates are the so-called Weakly Interactive Massive Particles (WIMPs), predicted to interact both gravitationally and weakly with SM particles. This

would allow direct and indirect direction of such candidates, used as the driving process of many experiments over the last decades, trying to find the hint of a possible interaction between standard baryonic particles and DM particles, or even between several DM particles themselves. Dark matter production through the use of a particle accelerator colliding SM particles together, such as the LHC, is also a possibility, and will be considered as the main channel towards the eventual detection of this exotic matter throughout this work. The production through colliders is actually able to provide constraints on low dark matter masses as well, in a region where both the direct and indirect searches are less efficient, which makes the LHC a perfect tool to study this kind of Beyond the Standard Model (BSM) physics. These searches will be summarized in Section 2.5.

However, observing DM is still extremely difficult, mainly because it barely interacts with ordinary baryonic matter, except through gravity (we have to assume that it does interact with SM at least weakly for the sake of this work though, as we would not be able to discover it as an individual particle if it were not the case). This means that nowadays, all the experiments searching for DM have only been able to put constraints on the DM particle mass and on the interaction cross sections between the dark and standard sectors. Actually, even if the collisions between protons produced by the LHC do have a sufficient amount of energy to produce this kind of particles, we would not expect them to interact with our detector, making their detection even harder. The presence of such matter has to be inferred from the study of the interaction between SM particles and CMS itself, since a typical DM-like event consists of at least one energetic SM particle produced in association with a large imbalance in the momentum due to the presence of an eventual DM candidate that was able to escape our detection.

In the context of this work, DM is searched for in association with one or two top quarks which play the role of the SM particle allowing us to trigger the event. The top quark, the most massive of all the fundamental particles observed by far, is indeed an excellent object to study in this context, mainly because of its high mass and because of the expected Yukawa-like coupling structure of the new physics model [13]. However, this also means that the phenomenology of this quark is mostly driven by its large mass and that it decays before hadronization can occur, almost always into a W boson and a bottom quark. The final state of the process we are interested in is then made of some b jets, leptons and/or quarks and is mostly categorized depending on the decay of the W itself. This work will actually be focused on the two leptons final state, also known as the dileptonic channel, mostly because leptons are by reconstruction much cleaner than jets and because this channel does not have lots of background processes raising to a similar final state, even though its branching ratio is the smallest, as will be explained in Section 2.6.

The LHC has now been running for 10 years, and several similar searches have already been carried out and published in the past by the CMS and ATLAS collaborations, at different center of mass energies. First of all, at 8 TeV, several searches for a pair of top quarks were published by the CMS (in association with DM in the semileptonic [14] and dileptonic [15] final states) and ATLAS collaborations [16]. Then, at 13 TeV, the ATLAS collaboration published on one hand several studies, considering different final states and different luminosities ( $13.3 \text{ fb}^{-1}$  and  $36.1 \text{ fb}^{-1}$ ) [17, 18, 19]. On the other hand, the CMS collaboration published a few extremely important papers for this study [21, 22]. For the first time in 2019, the results obtained by the  $t/\bar{t}+\text{DM}$  and  $t\bar{t}+\text{DM}$  analyses have also been combined and published using the data collected during the year 2016 [23]. Our main objective is now to repeat and improve this analysis while considering the full Run II dataset, globally improving the analysis strategy and including the dileptonic final state for the first time in this combination.

After a general introduction about DM in Chapter 2, the experimental setup will be detailed in Chapter ???. This will include a discussion about the LHC, along with a complete description of CMS, the detector used to collect the data that will be analyzed throughout this work. The data has been collected during the years 2016, 2017 and 2018 and corresponds to an integrated luminosity of  $\sim 137 \text{ fb}^{-1}$ , collected during the Run II of operation of the LHC and at a center of mass energy  $\sqrt{s} = 13 \text{ TeV}$ . A particular care will be given to the explanation of the Particle Flow (PF) algorithm, used to reconstruct the different objects of the analysis and that will be defined in Chapter ???, while the estimation of the different backgrounds and the selection of interesting events will be detailed throughout Chapters ?? and 3.

Distinguishing between the signal we are searching for and backgrounds having a much higher cross-section and kinematically really close, such as the SM  $t\bar{t}$  without production of DM is not a straightforward task (sometimes a production of missing transverse energy due to the presence of physical neutrinos is even obtained). To enhance the signal and to obtain some discrimination between these kind of processes, an algebraic reconstruction of the event and top-notch Machine Learning (ML) techniques are used in this work, in order to train a network of neurons to perform this task. The main objective is to make them learn how to combine the discriminating power of a set of input variables in order to create a single output variable describing the probability of a single event to be classified as signal or background. All this process will be detailed in Section 3.4.

Finally, a statistical interpretation of our data will be performed and different sources of systematic uncertainties will be considered in Chapter 4. This will allow us to set upper limits on the cross section production value of DM particles in our particular channel and for the simplified models considered in this analysis. The conclusions of this work and some additional future prospects will then finally be presented in Chapter 5.



# Chapter 2

## The dark matter case

In this chapter, some general explanations about the SM will first of all be given in Section 2.1 as a general introduction about today's most accepted mathematical model describing all the known particles and their interactions. The case for DM will then be presented in Section 2.2, along with a summary of the main evidences, mostly astrophysical, which lead to the introduction of this kind of Beyond the Standard Model (BSM) physics. Then, the main properties expected by such exotic matter will be introduced in Section 2.3 and nowadays's most accepted DM candidates, such as the Weakly Interactive Massive Particle (WIMP) will be presented in Section 2.4. The main ways we have to search (direct, indirect and collider searches) for this new exotic physics along with the main experiments dedicated to such searches will then be shown in Section 2.5. Finally, the searches performed in colliders such as the Large Hadron Collider (LHC) and our particular channels of interest (DM produced in association with either one or two top quarks) will be detailed in Section 2.6 and the latest similar results and exclusion limits published over the course of the previous years by the ATLAS and CMS collaborations will be shown in Section 2.7.

### 2.1 The Standard Model

The SM of particle physics is a relativistic Quantum Field Theory (QFT) able to mathematically summarize our current understanding of all the known particles and to describe three out of the four main interactions between these particles (the weak, strong and electromagnetic forces, while an explanation of the origin of the gravitational interaction is out of the reach of this theory).

If the neutrinos are considered to be normal Dirac fermions in the sense the antineutrinos are expected to be different than neutrinos (the question whether or not they could actually be Majorana particles is still well under discussion [25]), then the SM contains 26 free parameters, mainly the masses of the 12 predicted fermions, as shown in Figure 2.1, along with the couplings describing the strengths of the three interactions, two parameters describing the Higgs potential, eight mixing angles and, maybe, the phase of the eventual strong CP violation that will be mentioned in Section 2.4 (but in any case this parameter is expected to be close to 0). This is a quite high number of free parameters, but the value of most of them has now been derived experimentally.

The SM Lagrangian density in a differential volume element  $\mathcal{L} = \int L d^3x$ , accounting for the kinetic and potential energy of a system, takes the (very) simplified form given in Equation 2.1, where  $F_{\mu\nu}$  is the field strength tensor accounting for the different interactions,  $\psi$  is the interacting field describing quarks and leptons and  $\phi$  is the Brout-Englert-Higgs field while  $y_{ij}$  are the Yukawa couplings to this field, which depend on the mass of the particle considered and which will be

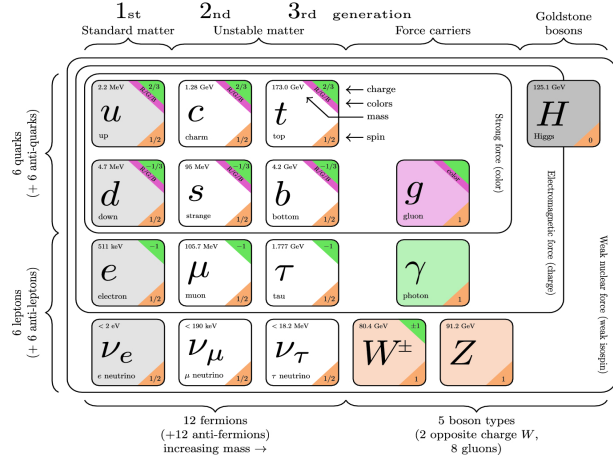


Figure 2.1: Representation of the 12 fermions of the SM [24] along with the main force carriers and the Higgs boson, discovered in 2012 and completing the SM.

e

described later on in Section 2.5.3.

$$\mathcal{L} = -\frac{1}{4}F_{\mu\nu}F^{\mu\nu} + i\bar{\psi}\not{D}\psi + \bar{\psi}_i y_{ij} \psi_j \phi + |D_\mu \phi|^2 - V(\phi) \quad (2.1)$$

A complete description of this model is out of the scope of this work but it is important to note that the SM, although mostly experimental, is still working extremely well today. Indeed, it managed to make a lot of predictions over the years, which is the best one can obtain from a mathematical model, and all of its major predictions revealed themselves to be true (we can quote for example that it successfully predicted the existence of the gluons, the top quarks, along with the W, Z and Higgs bosons [26]).

However, we know that the SM is not the final theory of particle physics since it is not able to explain all the observations which have been made. There are some open questions and many BSM theories trying to explain such observations, such as an eventual inclusion of the gravitational interaction within this model. We can quote for example as BSM theories the possible existence of the supersymmetry, telling us that each particle should have a superpartner whose spin differs by 1/2 or the possible existence of DM particles, the main subject of the following sections.

## 2.2 At the origins of dark matter

The origin of the concept of dark matter can be traced back to the 17 and 18th centuries, shortly after Newton's works on gravitation, even though this concept has changed quite a lot over the years. Back then, DM was more considered to be ordinary matter which simply did not emit any kind of electromagnetic radiation, being therefore invisible and dark, but which does have a strong gravitation impact because of its mass. It was for example considered in the 20th century to be found in massive astronomical objects able to absorb the light or other objects located behind them, such as black holes [27].

### 2.2.1 Zwicky and the virial theorem

In the 20th century, the first experimental evidences for the existence of dark matter were found. In 1933, Fritz Zwicky managed to determine the mass of the Coma Cluster using the virial theorem [28], which states that in a cluster in equilibrium under its own gravitation the kinetic energy must be comparable to its gravitational binding energy.

Mathematically, the virial theorem can be written in Equation 2.2, where the brackets represent the mean value of the quantity obtained over time or position, the universal constant of gravitation is  $G = 6.67 \cdot 10^{-11} \text{ m}^3 \text{ kg}^{-1} \text{ s}^{-2}$  and where the gravitation potential energy expression can be simplified assuming a spherical distribution of the masses and the same average density everywhere in the cluster considered.

$$2\langle T \rangle + \langle V \rangle = 0, \text{ where } \begin{cases} T = \frac{1}{2} \sum_i M_i v_i^2 = \frac{1}{2} M \langle v^2 \rangle \\ V = -4\pi G \int_0^R M \rho r dr \propto \frac{GM^2}{R} \end{cases} \quad (2.2)$$

Solving these simple equations gives us an approximate value of the mass of the cluster in Equation 2.3, where  $R$  is the radius of the cluster and  $\langle\langle v^2 \rangle\rangle$  is the squared velocity of all the galaxies averaged over position and time.

$$M \propto \frac{\langle\langle v^2 \rangle\rangle R}{G} \quad (2.3)$$

From this simple expression and astronomical observations, Zwicky then managed to compute the average mass to light ratio of its galaxies and concluded that the value obtained was around 400-500 times larger than the mass previously estimated by Edwin Hubble, who simply considered the number of visible galaxies within this cluster for his calculations. One plausible explanation for this discrepancy is to introduce the concept of DM, which contributes to the mass of the cluster without increasing the galactic luminosity.

Zwicky's results were actually quite controversial since they were based on statistical calculations relying on different hypotheses not always justified, such as the fact that the galaxies in the cluster must be gravitationally bound with each other and they were actually proven to be overestimated later on [29], but additional observations came to enforce the validity of his conclusions anyway.

### 2.2.2 Spiral galaxies rotation curves

Despite being controversial and slightly off, Zwicky's results were soon followed by a series of additional astronomical observations leading to the same conclusion, the possible existence of non-luminous matter in all the galaxies, called dark matter. The most famous of these results is the study of the observed and expected rotation curves of the stars within spiral galaxies such as the Milky Way in the 1970s [9].

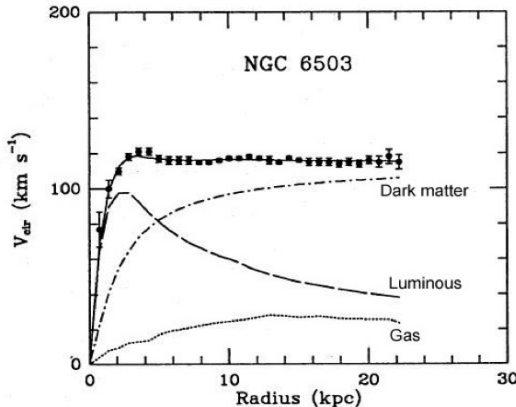
According to this study, if we assume that we can apply Newton's universal laws of gravitation at the galactic scale, then the stars within this kind of galaxies should rotate with a velocity depending on the radius to the galactic center obtained by the usual equation for centripetal acceleration in a gravitational field and represented in Equation 2.4, where  $M(r)$  accounts for the total mass

encountered in a radius  $r$ .

$$v_{\text{rotation}}(r) = \sqrt{\frac{GM(r)}{r}} \quad (2.4)$$

At first approximation, one can assume that most of the mass within this kind of galaxies comes from the inner core, which means that, at large radius, the velocity of individual stars is expected to decrease proportionally to  $r^{-1/2}$ . Any deviation to this rule suggests that either our understanding of gravity at large scales or our basic understanding of galaxies as a celestial body made of stars, dust and gas, has to be revised.

Actually, observations made by Vera Rubin and her team in the early 1970s with a new spectrograph designed to study the velocity curves of spiral galaxies with a degree of accuracy never reached before, did not confirm these expectations [30]. Indeed, according to these results, from a given value of the radius, the velocity curve appears to be flat instead of decreasing, as illustrated in Figure 2.2. This is another hint that can motivate the introduction of the concept of DM.



K.G. Begeman, A.H. Broeils, R.H. Sanders. 1991. Mon.Not.RAS 249, 523.

Figure 2.2: Expected and observed rotation curves of the galaxy NGC 6503 [9]. The black dots correspond to the data and the *luminous* line corresponds to the rotation curve decreasing as  $r^{-1/2}$  expected from Newtonian dynamics.

### 2.2.3 Cosmic Microwave Background (CMB) anisotropies

The CMB is a mostly uniform background of primary radio waves emitted when the Universe became transparent around 380 000 years after the Big Bang and was discovered accidentally in the 1940s [31]. Studying it is extremely important, as it is actually made of the oldest and cleanest electromagnetic radiation we can find in the Universe. Precise measurements of this radiation are actually critical in many different fields of physics, since any proposed model of the Universe must be able to explain this radiation, its temperature and anisotropies.

Recent measurements determined that the CMB can be considered as emitting a thermal black body spectrum at a temperature of  $(2.72548 \pm 0.00057)\text{K}$  [32]. However, we now know that this temperature is actually not constant as some small anisotropies can be observed (at the  $10^{-5}$  level), depending on the value of the solid angle of observation, as represented in Figure 2.3.

We see these fluctuations projected over a 2D sphere, and it is therefore natural to introduce at this point Laplace's spherical harmonics,  $Y_{lm}(\theta, \phi)$ , a complete set of orthogonal functions obtained

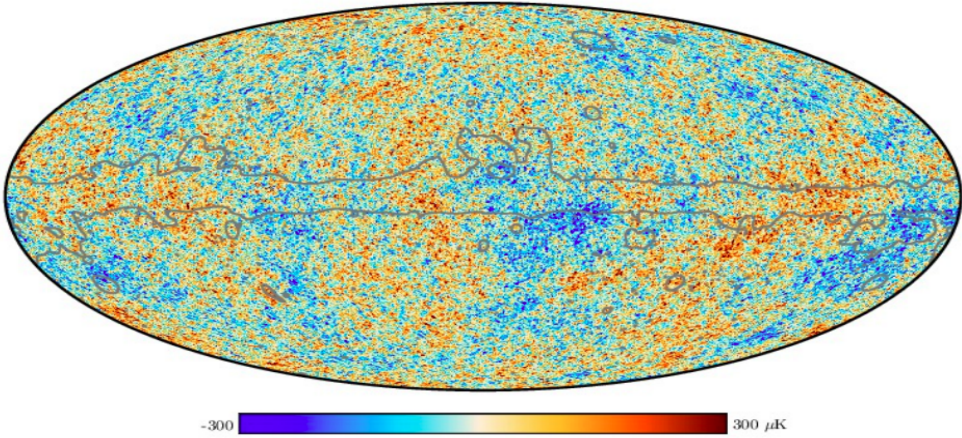


Figure 2.3: Anisotropies at the  $10^{-5}$  level in the temperature of the CMB, as observed by the Planck satellite in 2018 [33].

by solving Laplace's equation  $\nabla\psi = 0$  on a sphere and defined by a few parameters such as  $l$ , the multipole, representing a given solid angle in the sky ( $l = 100$  corresponds to  $\sim 1^\circ$ ) and  $m$ , the number of poles, such as  $-l \leq m \leq l$  [34].

It is possible to show that these spherical harmonics form a complete orthonormal basis on this space and therefore that any function that can be defined on the sphere may be expanded into these harmonics using coefficients called  $a_{lm}$ . The temperature fluctuations, whose value depend on the two usual spherical angles  $\theta$  and  $\phi$  can therefore be expanded using these generic functions, according to Equation 2.5.

$$\frac{\Delta T}{T}(\theta, \phi) = \sum_{l=0}^{\infty} \sum_{m=-l}^{m=l} a_{lm} Y_{lm}(\theta, \phi) \quad (2.5)$$

The information about the anisotropies can actually be extracted from the variance of these harmonic coefficients  $a_{lm}$  of the expansion since the CMB is assumed to be a gaussian random field. The power spectrum of the CMB can be extracted according to Equation 2.6, and from which most of the cosmological information of the CMB is derived.

$$D_l = \frac{l(l-1)C_l}{2\pi} = \sum_m |a_{lm}^2| \quad (2.6)$$

Interestingly enough, this spectrum is directly affected by the value of the density of the dark matter in the Universe, and this is something that will be often discussed in the remaining of this chapter. Doing a multi-parameters fit on the observed data represented in the power spectrum (cf. Figure 2.4) is then able to give us directly the energy density of baryonic  $\Omega_b$  and dark  $\Omega_\chi$  matter, along with other important parameters of the  $\Lambda_{CDM}$  cosmological model. Today's most precise measurements have been obtained in 2018 using the Planck satellite, and lead to the determination of these two quantities:  $\Omega_b h^2 = 0.02220 \pm 0.00020$  and  $\Omega_\chi h^2 = 0.1185 \pm 0.0015$  [35]. This is one of the strongest constraint we have on DM so far, since any DM candidate will need to comply with this measurement.

By dividing these results with the value of the scaling factor for the Hubble expansion rate  $h = 0.674$  [36], we can obtain from these numbers a proportion of 4.9% of ordinary baryonic matter and 26.1%

of dark matter in the Universe.

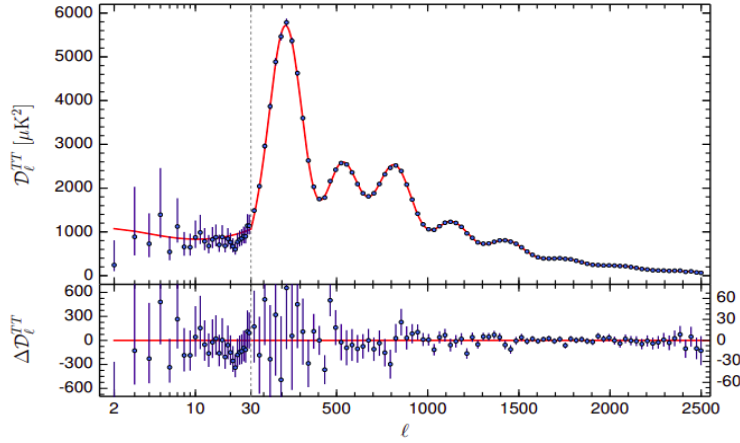


Figure 2.4: Power spectrum of the CMB obtained by Planck, representing the fluctuations of the temperature of the radiation with respect to the angular angle of observation [35].

## 2.2.4 Gravitational lensing

The last evidence supporting the existence of dark matter has been obtained by observing several clusters of galaxies in the Universe, such as the Bullet Cluster, and by studying their mass distribution through gravitational lensing.

The gravitational lensing effect is a consequence of the general relativity, a theory developed by Einstein as a way to represent gravity using the geometry of spacetime, stating that massive objects lying between distant sources and an observer should act as a lens and bend the light emitted by the source. This deviation of the light is actually proportional to the mass of the object in between the source and the observer, meaning that the gravitational lensing can give us a way to measure the mass distribution of massive objects, such as galaxy clusters. This mass distribution can then be compared to the luminous distribution of the cluster, to see if we can observe a discrepancy between the two measurements, which could be another hint of the existence of DM.

The bullet Cluster is particularly interesting in this context since it actually provides an evidence for the eventual existence of DM which does not rely on any mathematical assumption (other than the general relativity principle) and cannot at principle be explained by alternate laws of gravitation. In this case, some observations clearly showed that the spatial deviations between the center of the total mass and the center of the baryonic luminous mass cannot be explained with an alteration of the gravitational force law alone, with a statistical significance of  $8\sigma$  [37].

As seen in Figure 2.5, the image taken by Chandra clearly shows an offset between the visible plasma of the cluster and the actual mass distribution measured through gravitational lensing (green contours). The center of the luminous mass of the cluster does not seem to match the one obtained considering its non-luminous counterpart as well, which is another evidence of the possible existence of DM within galaxy clusters.

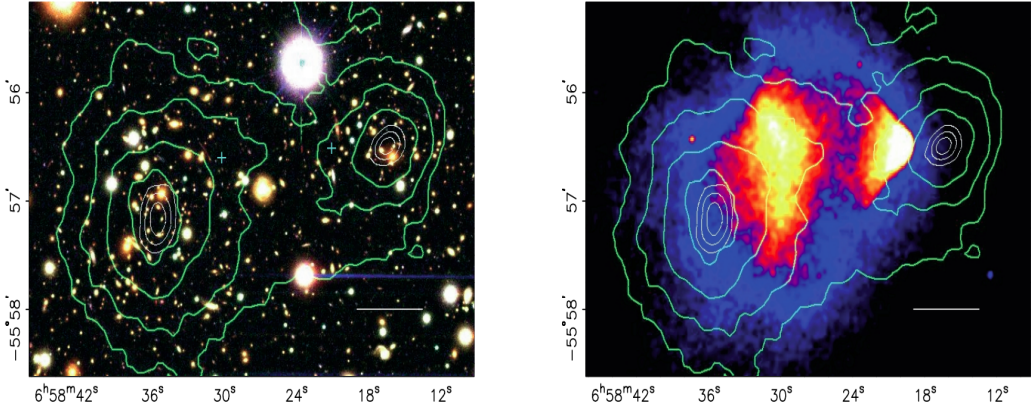


Figure 2.5: Mass distributions obtained by the Magellan telescope in the visible (on the left) and the Chandra telescope on the X-rays spectrum (on the right) telescopes of the Bullet Cluser. Being shifted compared to each other, this is yet another clear evidence for the existence of DM [37].

## 2.3 Dark matter properties

All the previous observations allow us to list some of the most important properties that any dark matter candidate should have. Even though several theories exist, each giving slightly different properties to the DM, we will consider in this work the following mostly accepted properties for such particles:

- First of all, we will assume that DM is a **particle**. As far as we know, the Universe is simply composed of particles so there is no objective reason to think that DM, being matter with a certain mass, might not be made of some kind of indivisible particles at some level.
- Then, the DM candidate should of course be **dark**. This means that it should not interact at all with electromagnetic radiation such as light, and that it should therefore be **electrically neutral**. However, it has to interact at least gravitationally because of the observations for the evidence of such a particle explained before, mostly relying on gravitational effects, and we assume in this work that it interacts weakly as well to have a chance to discover it with particle accelerators.
- It has to be **non-baryonic**, mainly because the energy density for the baryonic matter obtained by observing the power spectrum of the CMB is too low to account for DM as well, as explained in Section 2.2.3. Indeed, according to these results, baryonic matter accounts for around 5% while dark matter accounts for more than 25% of the energy density of the Universe.
- We will also only consider **cold** dark matter, since the widely accepted  $\Lambda_{CDM}$  cosmological model is actually based on this assumption. By cold, we do not refer to the temperature of these particles but actually to their size, and therefore to the velocity by which they can travel in the Universe. Large scale structures of the Universe such as we can observe them today cannot actually be explained if DM is made of hot/relativistic particles, as represented in Figure 2.6. However, although not really as popular, it is important to note that alternative models with warm DM have also been developed and still exist today.
- It is interesting to report as well that DM particles are expected to be found near the electroweak symmetry breaking scale, between **10 GeV and 1 TeV**. This is a consequence

of the expected production mechanism of such particles, the so-called thermal freeze-out [38]. This principle tells us that at some point in history, DM was supposed to be in thermal equilibrium with other primordial SM particles, meaning that its production and annihilation rates were equal. However, because of the expansion of the Universe, at some point DM particles were simply too far apart from each other and these reactions maintaining this equilibrium were not efficient enough any more. At this stage, the abundance of DM became fixed: this is the freeze-out, as represented in Figure 2.7.

This principle is interesting because, as a rule of thumb, we can say that if a particle interacts heavily, it will stay longer in equilibrium and its freeze-out abundance will therefore be smaller, so there is a mathematical relation between the strength of the SM/DM interaction  $g$ , the mass of the DM particle  $m_\chi$  and its relic abundance  $\Omega_\chi$  that has been precisely measured, as expressed in Equation 2.7 [39].

$$\Omega_\chi \propto \frac{m_\chi^2}{g^4} \quad (2.7)$$

By using a typical value for  $g$  of the order of the Fermi coupling constant  $G_0^F \simeq 4.54 \cdot 10^{14} \text{ J}^{-2}$  we can see that, in order to observe a freeze-out abundance comparable to the one observed recently by the Planck satellite, the DM candidate should have a mass between 10 GeV and 1 TeV as previously stated. The measurement of the CMB power spectrum is therefore able to put constraints on the DM cross-section with the baryonic sector, and all the DM candidates quoted in Section 2.4 will have to respect this criteria.

In any case, DM is not expected to have a mass lower than 300 eV since at this scale, the phase space density that would be needed to explain the relic abundance of DM would simply violate the Pauli-exclusion principle [42].

- Finally, the DM particles should be **long-lived**. Indeed, we expect that they were produced 13.8 billion years ago during the Big Bang, but it seems they are still present in the Universe since we still see their effect today. They should then be stable particles, or their lifetime should at least be larger than the age of the Universe itself.



Figure 2.6: Computer simulations for cold (on the left) and warm (on the right) DM scenarios and their impact on a galactic halo at 0 redshift [40].

All these properties narrow quite a lot the number of possible DM candidates, as we will now see in the following section.

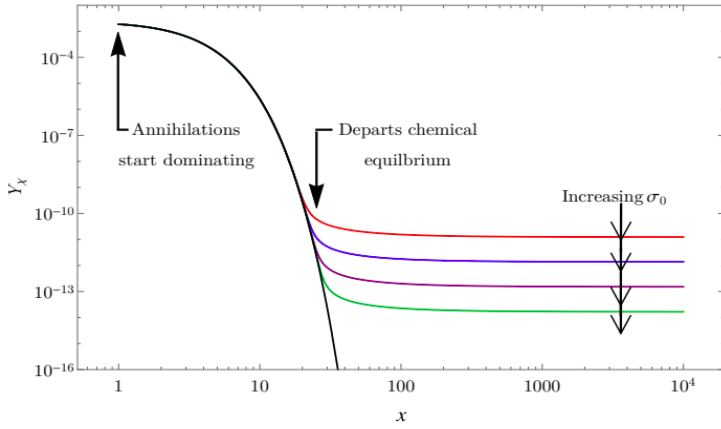


Figure 2.7: Schematic representation of the freeze-out process, representing the abundance of a 500 GeV DM as  $Y_\chi$  with respect to the time and the impact of increasing cross-section annihilation values on this freeze-out abundance [41].

## 2.4 Dark matter candidates

Several different categories of particles could pretend to be good candidates for dark matter but only the most interesting ones will be quoted here, since an extensive list of all the different possible candidates is out of the scope of this work. Two SM particles will first of all be investigated, before introducing some BSM theories providing additional DM candidates with the expected properties.

### Massive Compact Halo Objects (MACHOs)

The first obvious DM candidates are the so-called MACHOs. These objects are massive astronomical non-luminous bodies (such as black holes) made of baryonic matter and very hard to detect, that could be responsible of the gravitational lensing observed and that could explain the apparent missing mass in the Universe. However, as we saw in Section 2.3, DM is not expected to be made of such ordinary matter, mainly because observational data of the CMB and the deduced baryonic density of energy in the Universe is able to rule out this possibility.

Several different experiments did try to search for such DM anyway, and managed to constrain the properties of this kind of objects. The main way to search for such massive objects is through their gravitational microlensing effect since, according to the general relativity principle, they should bend the light of luminous objects located behind them, such as stars, and this bending actually depends on the mass of the eventual MACHO. Experiments like the MACHO project and EROS observed in this context  $\Theta(10^7)$  stars for several years, looking for microlensing events in order to constrain this particular DM model. Results published in 2000 from the MACHO project, after studying almost 12 million stars, actually observed between 13 and 17 such events, lower than expected if DM was only made of MACHOs.

The collaboration actually managed to exclude at the 95% Confidence Level (CL) the possibility of the dark halo to be entirely made of such baryonic particles [43]. On the other hand, the EROS collaboration only observed 1 microlensing after studying more than 30 millions of bright stars during 6.7 years, while  $\sim 39$  events were expected [44]. Both results have also been combined in order to obtain the exclusion plot represented in Figure 2.8. From this study, MACHOs with low

masses of the order of a fraction of the mass of the Sun  $M_\odot$  ( $10^{-7}M_\odot < m < 10^{-3}M_\odot$ ) should make up less than 25% of the dark matter halo for most models considered at the 95% CL [45].

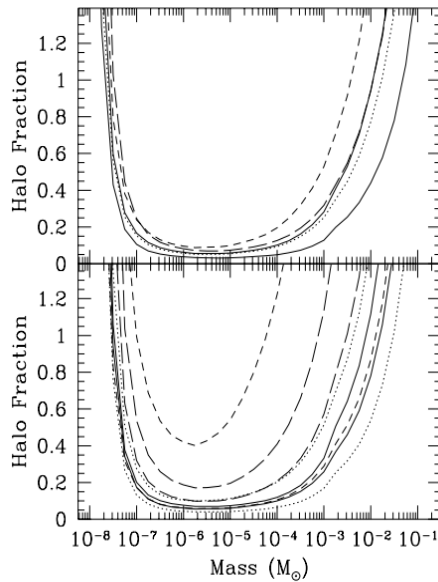


Figure 2.8: Halo fraction upper limits at the 95% CL compared to the mass of the lensing object for different MACHO models considered by the EROS (on the top) and the MACHO (on the bottom) collaborations [45].

### Active neutrinos

SM *active* neutrinos  $\nu$  (as opposed to *sterile* neutrinos, that will be the subject of the discussion in the next section) have been considered as good DM candidates for a long time as well, since they are electrically neutral and long-lived SM particles, two important properties of any DM candidate. They have a few particular properties that might be interesting in this context.

- First of all, even though it has still not been measured precisely, the sum of their masses has recently been measured to be lower than 0.17 eV at the 95% CL from cosmological studies [49]. Even though this is not fully understood, such value is incredibly low compared to other SM particles, this particularity usually being referred to as the *mass puzzle* of the neutrinos.
- Their low mass has a consequence in the sense that it means that the gravitational interaction between two neutrinos is usually considered to be negligible and that we can consider that they only interact weakly, making it hard to study their properties. Their actual cross-section of interaction, as represented in Figure 2.9 and which of course depends on their energies and on the channel of interaction (neutral or charged current considered), is therefore usually extremely low, making it hard to detect neutrinos.

This figure clearly shows that an approximate value of the cross section for such neutrinos is of the order of magnitude of  $10^{-38} \text{ cm}^2 \text{ GeV}^{-1}$ , which is typically tens of orders of magnitude lower than the interaction cross section of a photon ( $\sigma_\gamma \sim 10^{-25} \text{ cm}^2$  [47]). This means that the typical neutrinos of a few MeV produced by nuclear reactors have a mean free path of approximately 10 light years in steel.

- Neutrinos are also the only SM particle only observed in their left-handed chirality state, while anti-neutrinos can only be observed in their right-hand state. This could mean two

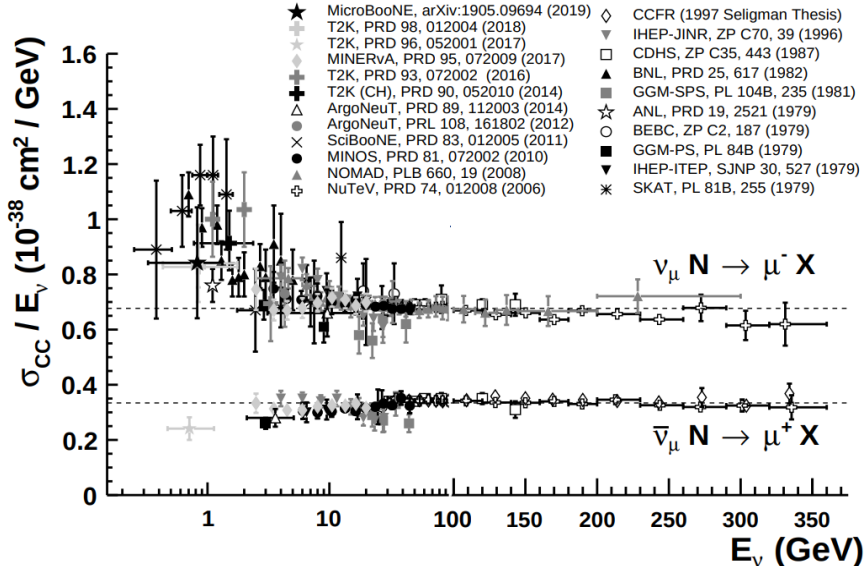


Figure 2.9: Neutrino cross section of interaction from the charged current as measured by different experiments over a large range of energies, for both neutrinos  $\nu$  and antineutrinos  $\bar{\nu}$  [46].

things: either right-handed neutrinos do not exist in nature for some reason, or we have just not been able to detect them because their interaction with baryonic matter is too weak. Right-handed neutrinos, also referred to as *sterile* neutrinos, do not fit in the current SM but could actually also be a strong BSM DM candidate, as we will discuss in the next subsection.

However, two physical reasons can explain why we do not really believe that DM could be made of neutrinos any more. First of all, their relative abundance does not match the expected one for DM from the freeze-out mechanism explained in Section 2.3. Indeed, their freeze-out abundance can be computed quite easily from Equation 2.8 [48], where the sum of the masses of the three neutrino flavors has been calculated to be lower than 0.17 eV [49] instead of the 11.5 eV expected to obtain the correct DM relic abundance as observed today from the power spectrum of the CMB.

$$\Omega_\nu h^2 = \sum_{i=1}^3 \frac{m_{\nu_i}}{93 \text{ eV}} \quad (2.8)$$

Additionally, for several reasons explained in Section 2.3, a good DM candidate is expected to be cold, i.e. non-relativistic. However, being extremely light, neutrinos are expected to be ultra-relativistic and could therefore not be responsible of the emergence of large scale structures as observed today. We can therefore most probably rule out the possibility of DM being made of SM neutrinos.

### Sterile neutrinos

The most obvious SM particles being ruled out as DM candidates, it is now time to introduce other BSM theories introducing additional particles that could have the properties searched for. The first one of these theories introduces the so-called sterile neutrinos, usually referring to right-handed SM neutrinos, as discussed in the previous subsection.

If they exist, sterile neutrinos are expected to interact in an even weaker way than SM active neutrinos, they could be very long-lived as well and in principle, nothing prevents us from considering that they could have a mass superior to 0.4 keV, giving therefore the correct DM relic abundance [42]. A superior bound of 50 keV on such particles can also be obtained considering limits on the observation of the monochromatic decay  $\gamma$  line originating from the one loop radiative decay  $N \rightarrow \nu + \gamma$  of such particles.

Several experiments are already searching for this kind of particles at this level of energy. Most of these experiments focus on the analysis of  $\gamma$ -rays and are actually searching for this particular monochromatic line resulting of the decay of sterile neutrinos. Two independent groups actually announced in 2014 the observation of an unidentified emission line at 3.57 keV (Figure 2.10) which did not match any known atomic emission line and which is actually consistent with an eventual DM signal [50, 51], since most of the possible instrumental contamination effects have been ruled out over the course of the last few years.

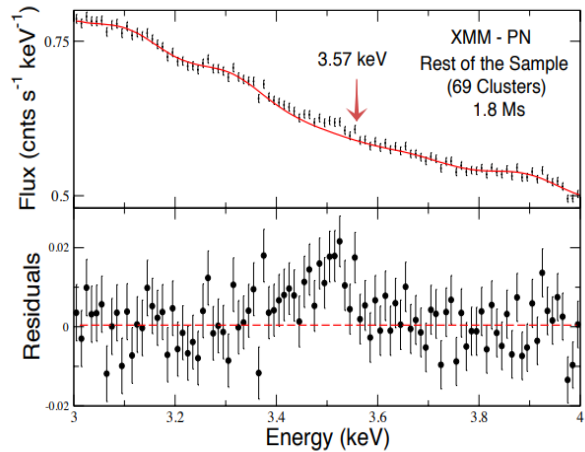


Figure 2.10: 3.57 keV emission line detected with a  $4.5\sigma$  CL by the XMM-Newton telescope in 2014, which could be a hint of the presence of DM [50].

However, some additional studies of the galactic center pointed out the fact that this observation might actually come from the observation of a potassium K XVIII transition line [52]. Recent observations actually ruled out at the 99% CL an eventual DM origin for this particular line [53], but further studies are still ongoing.

## Axions

Axions could also explain the particle nature of DM, since their existence is enough to explain 100% of the DM in the Universe, unlike most of the other candidates presented so far. Axions are hypothetical stable neutral particles, with masses of the order of the meV, introduced as a consequence of the strong-CP violation issue of Quantum ChromoDynamics (QCD). This issue is the following: the usual  $\Theta$  term of the QCD Lagrangian, the QCD vacuum angle shown in Equation 2.9 [54] should be responsible of breaking the CP symmetry, but this effect has actually never been observed so far: this is the so-called the strong CP problem.

Two ways to explain that we have never observed this phenomena exist: the first is to assume that one of the quarks of the SM is massless but this does not match the current observations and measurements. The second consists in assuming that the parameter  $\Theta$ , the QCD vacuum angle, is small enough so that this term becomes negligible. However, by definition, the  $\Theta$  angle should

be between 0 and  $2\pi$ , so there is no physical reason for this parameter to be small, unless some new physics can be introduced, such as the theory developed in 1977 by Peccei and Quinn [55] by relaxing  $\Theta$  from a parameter to a dynamic variable and absorbing it through the introduction of a new pseudoscalar particle that was called the axion.

$$\mathcal{L}_\Theta = \frac{\Theta}{32\pi^2} \epsilon_{\mu\nu\rho\sigma} G_a^{\mu\mu} G_a^{\rho\sigma} \quad (2.9)$$

By definition, it is possible to show that axions satisfy two of the previous criteria for a good DM candidate, since they are non-relativistic and their abundance might be enough to account for the dark matter energy density observed, because their actual abundance can easily be computed from Equation 2.10 [56], from which we could conclude that an axion having a mass of  $\sim 20 \text{ }\mu\text{eV}$  could account for the DM relic density of the Universe, as observed today.

$$\Omega_a \simeq \left( \frac{6\text{ }\mu\text{eV}}{m_a} \right)^{7/6} \quad (2.10)$$

Several axion search experiments have therefore been set up, such as the Axion Dark Matter Experiment (ADMX), a resonant microwave cavity installed at the University of Washington, the CERN Axion Solar Telescope (CAST), a CERN experiment observing the Sun which came online in 2002 and which managed in 2014 to turn up definitely the existence of solar axions [57], or the International AXion Observatory (IAXO), whose aim will be to search for axions with a much better signal to ratio noise than CAST. All the results obtained by these experiments along with their future projections are represented in Figure 2.11.

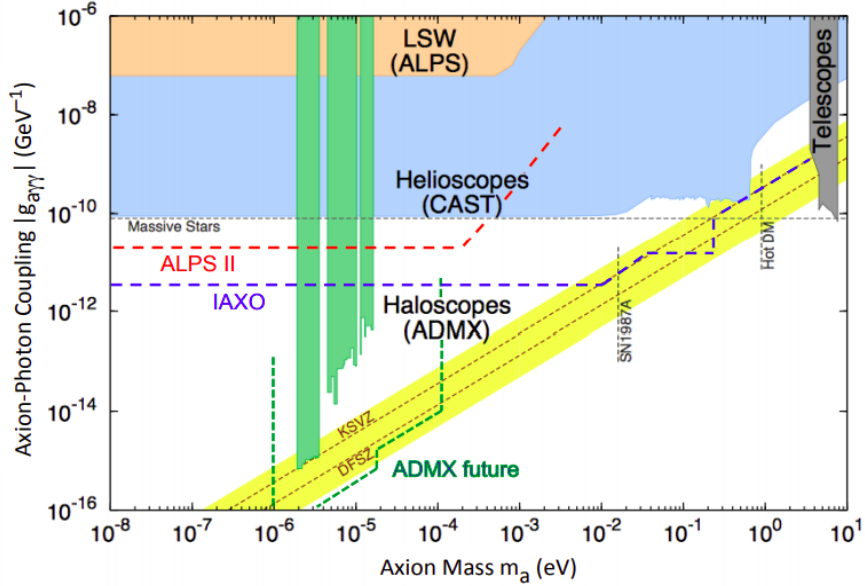


Figure 2.11: Axions exclusion summary plot and projected coverage of axion searches experiments, such as ADMX, CAST and IAXO [56].

## Weakly Interactive Massive Particles (WIMPs)

The actual DM candidates that will be mostly considered throughout this work are the so-called Weakly Interactive Massive Particles (WIMPs), which are expected to interact, even though very weakly, with ordinary baryonic matter and which have an expected mass in the range of 100 GeV to 1 TeV for reasonable electroweak production cross-section values, right where we expect DM to be found from its relic density: this is the so-called "WIMP miracle", an important concept that can be translated mathematically as well. Indeed, because of the freeze-out scenario explained in Section 2.3, we can find an expression relating the relic abundance of DM  $\Omega_\chi$  with its annihilation cross section  $\langle \sigma_A v \rangle$  through Equation 2.11 [65].

$$\Omega_\chi h^2 \sim \frac{3 \cdot 10^{-27} \text{ cm}^3 \text{ s}^{-1}}{\langle \sigma_A v \rangle} \quad (2.11)$$

This equation implies that, since we do know the current abundance of DM in the Universe, the total annihilation cross section of DM should be equal to  $\sim 3 \cdot 10^{-27} \text{ cm}^3 \text{ s}^{-1}$ , which corresponds to the typical value given by WIMPs for a range of dark matter masses matching the expected one.

Several strategies can be used to detect such particles, as we will see in Section 2.5. This kind of particle basically arises in various BSM theories, such as the Lightest Supersymmetric Particle (LSP) in SUSY. According to this theory, each SM particle should have a superpartner whose quantum numbers would be identical except for their spins, which would differ by one half. All of these superpartners would then be potentially new and undiscovered particles, giving us a perfect DM candidate in most of the Minimal Supersymmetric Standard Model (MSSM) theories, the neutralino  $\chi$  [58].

The WIMPs are also interesting in the sense that introducing them in the terms of this supersymmetric theory would not only give us a strong DM candidate, but would also solve the hierarchy problem, the apparent large discrepancy between multiple aspects of the weak and gravitational forces, such as their respective strength, differing by a factor  $10^{24}$ .

## 2.5 Dark matter searches

As previously stated, several cosmological evidences allow us to introduce the concept of dark matter, but its properties such as its mass, coupling and interaction cross-section are difficult to study in this context. Several different ways can then be used to try and detect DM particles in order to study them, as represented in Figure 2.12, strategies which can usually be divided into three categories: the direct and indirect searches, mostly relying on the production of baryonic matter from the interaction between two DM particles or on the observation of the interaction between the dark and baryonic sectors, and the production in colliders, usually able to probe lower DM candidates masses and which will actually be the main focus of this work.

A discussion about these different detection strategies along with the main results obtained by different experiments in each case will now be presented.

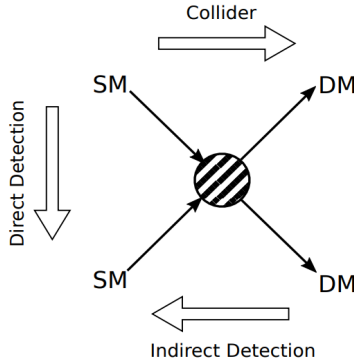


Figure 2.12: Schematic view of the three main DM detection strategies: direct, indirect and collider production searches [59].

### 2.5.1 Direct searches

From cosmological observations, we know that we live in a halo of dark matter. In this case, WIMPs should cross the Earth every day and, even if they interact only weakly, we should be able to directly detect them through their interaction with ordinary baryonic matter, for example because of their scattering with the nuclei of the atoms. Indeed, the transfer of momentum between these two particles in this case might be detectable with the correct experimental device, typically placed deep underground to have the lowest possible background, which is the main source of perturbations of such experiments.

To study this particular category of searches, let's first of all introduce the rate of expected WIMP scattering off a target nucleus of mass  $m_N$  with Equation 2.12, rate which ends up being described by a simple steeply falling exponential function as shown in Figure 2.13 [60], where  $E_{nr}$  is the nuclear recoil energy measured,  $m_\chi$  is the WIMP mass,  $\sigma$  its cross section,  $\rho_0 = 0.3 \text{ GeV cm}^{-3}$  is the local dark matter density and  $f(v)$  the normalized WIMP velocity distribution.

$$\frac{dR}{dE_{nr}} = \frac{\rho_0 M}{m_N m_\chi} \int_{v_{\min}}^{v_{\text{esc}}} v f(v) \frac{d\sigma}{dE_{nr}} dv \propto \exp\left(-\frac{E_{nr}}{E_0} \frac{4m_\chi m_N}{(m_\chi + m_N)^2}\right) \quad (2.12)$$

From this relation, the Equation 2.13 can be easily derived, representing this time the number of expected DM events in an experiment running during a time  $T$ , where  $\epsilon(E_{nr})$  is the efficiency of the detector for a given recoil energy.

$$N = T \int_{E_{\min}}^{E_{\max}} \epsilon(E_{nr}) \frac{dR}{dE_{nr}} dE_{nr} \quad (2.13)$$

The maximal velocity  $v_{\text{esc}}$  used as superior bound of the integral in Equation 2.12 has actually been measured to be in the range [498 – 608] km/s at the 90% CL [61], since any particle having a velocity higher than this would not be bound any more to the gravitational potential of a galaxy. This has an important consequence: all the direct and indirect detection experiments actually need to take into account the annual modulation of the observed count rate, due to the movement of the Earth around the Sun, as shown in Figure 2.14 [62], since this velocity is not negligible compared to the escape velocity  $v_{\text{esc}}$ .

From our perspective, it seems indeed that the velocity of the speed of WIMP particles arriving is

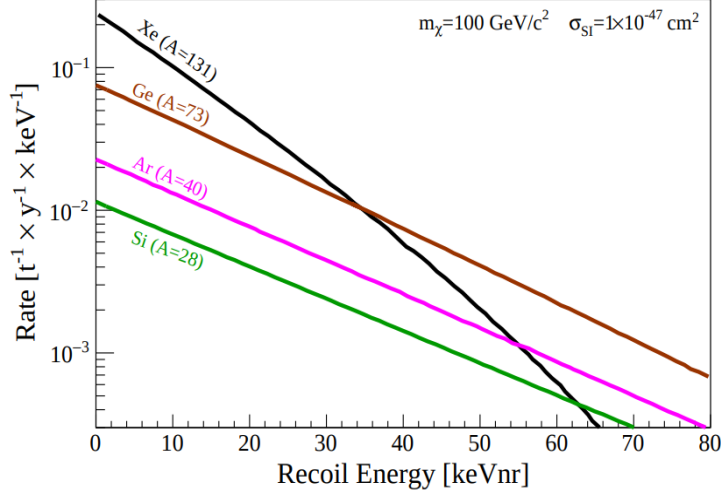


Figure 2.13: Nuclear recoil spectra induced in different materials for a given DM WIMP of 100 GeV, assuming a WIMP-nucleon Spin Independent (SI) cross section [60].

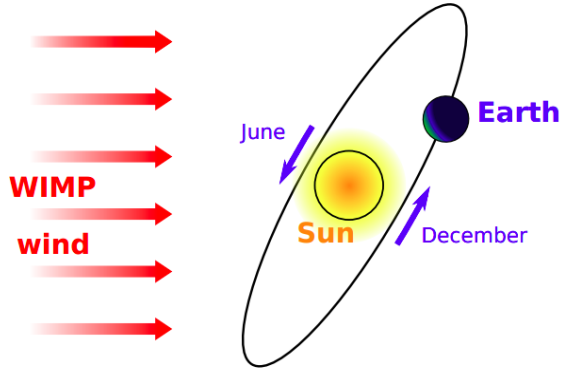


Figure 2.14: Schematic representation of the annual modulation of the WIMP wind introduced by the motion of rotation of the Earth around the Sun [62].

changing depending on the month of the year, since the Earth is sometimes moving in the direction of the WIMP source, and is sometimes moving away: the maximal velocity is reached around June. It is extremely important to take into account this effect since, as we saw on the previous equations such as Equation 2.11, the count rate of incoming particles  $N(t)$  actually depends on this velocity, and this modulation then introduces a periodical modulation that we need to take into account, as shown in Equation 2.14, where the periodical part usually introduces a  $\sim 5\%$  deviation [60].

$$N(t) = B + N_0 + N_m \cos(\omega(t - t_0)) \quad (2.14)$$

This effect is also important because an experiment performed during a long period of time can actually help us finding an eventual hint of DM particles, since our signal is expected to follow this periodical deviation while the background is expected to be constant. Moreover, this WIMP wind is expected to come from a particular region of the sky while the backgrounds are expected to be distributed uniformly, so this gives a clear way to isolate the signal.

Finally, it is also important to note that two different kinds of direct searches can be defined, depending on the category of the scattering between the DM and the nucleus: the Spin Independent (SI) (proceeding through the scalar term) and Spin Dependent (SD) (proceeding through the axial term of the Lagrangian) searches, since the interaction cross section  $\sigma$  of Equation 2.12 is expected to be different for DM particles having a spin 0 or not, as shown in Equation 2.15, where  $F$  is a factor accounting for the dependence of the scattering on the energy. This means that results obtained by either hypothesis cannot be compared with each other.

$$\frac{d\sigma}{dE_{nr}} \propto \sigma_{SI} F_{SI}^2(E_{nr}) + \sigma_{SD} F_{SD}^2(E_{nr}) \quad (2.15)$$

As previously stated, many experiments are dedicated to the direct search of DM particles, but in order to isolate an eventual DM signal, an environment with an ultra-low background is usually required, which is usually reduced either by placing the detector underground (to reduce the contamination due to cosmic rays), by increasing the statistics (by repeating the experiment and/or observing for a larger amount of time) or by choosing carefully the active material of the detector (to reduce the internal background coming from the detector itself). The impact these kind of parameters have on the final limits can be seen in Figure 2.15.

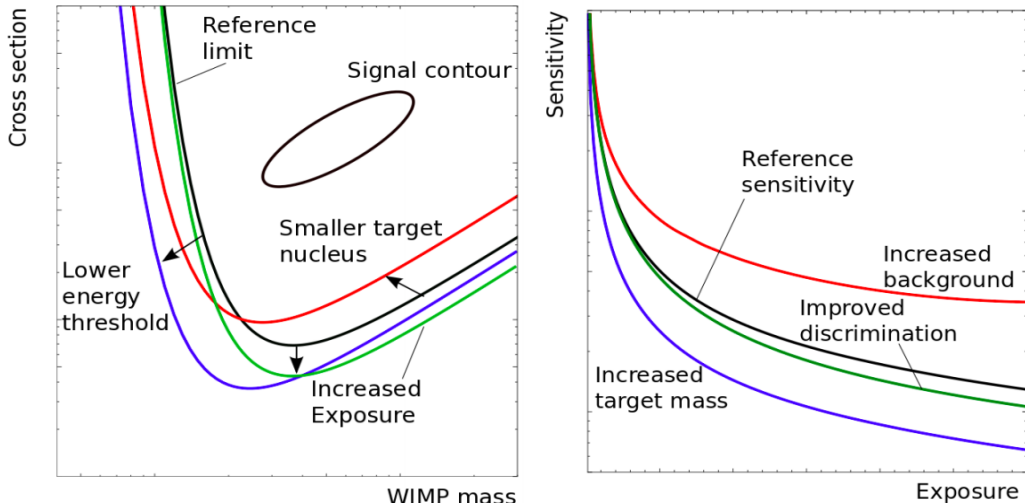


Figure 2.15: Impact of different experimental parameters on the final limits depending on the cross section and WIMP mass (on the left) or sensitivity and exposure (on the right), with respect to the expected limits (black curve) [63].

These detectors try to detect the scattering of an unknown exotic particle with an ordinary nucleus, which typically can give rise to different categories of signals. Some detectors try for example to detect the direct ionization of the target atom, while others focus on the emission of light coming from the desexcitation of the scattered nucleus, and some even search for the heat produced by these collisions under the form of phonons (collective excitation phenomena in condensed matter) in a crystal. These different search strategies have been summarized schematically in Figure 2.16.

As of today, no direct experiment has been able to detect serious hints for the existence of DM, and they have only been able to set limits on the scattering cross section depending on the models parameters, as seen in Figure 2.17 for multiple experiments at once.

However, the DAMA experiment at the Laboratori Nazionali del Gran Sasso (LNGS) did find an interesting result by showing the hints of an annual modulation signal compatible to the expected

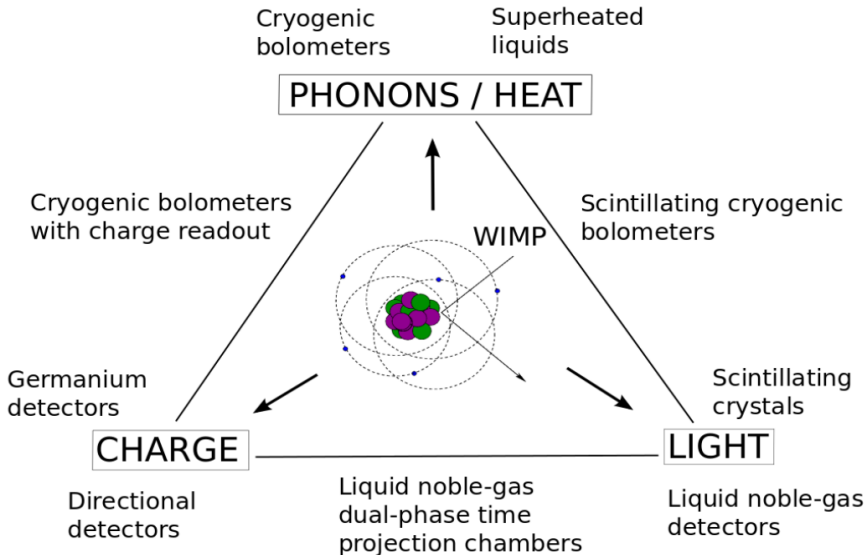


Figure 2.16: Schematic representation of the three main strategies to detect directly the interaction between DM particles and an ordinary nucleus [63].

one due to the WIMP wind in the 2-6 keV energy range, as seen on Figure 2.18 [64]. Further investigations about this modulation are still ongoing today, since no systematic effect able to account for the observed modulation amplitude and to simultaneously satisfy all the requirements of the signature has been found so far.

### 2.5.2 Indirect searches

The indirect detection of DM particles consists basically in searching for SM products coming from the annihilation of two DM particles or from its eventual direct decay, usually under the form of a flux of  $\gamma$ -rays, neutrinos, cosmic-rays or anti-matter appearing as an excess over the expected background. Indeed, many extensions to the SM, such as the supersymmetry SUSY or Universal Extra Dimensions (UED) do provide solid DM candidates (the lightest supersymmetric particle and the lightest Kaluza-Klein state, respectively) expected to interact with each other, resulting in the immediate production of SM (un)stable particles that can be detected by telescopes either placed on the ground or directly in space. Another point to make is that indirect searches are also usually affected by the annual fluctuation induced by the movement of the Earth around the Sun, as explained in Section 2.5.1.

Indirect searches are actually extremely useful since they are sensitive to the DM annihilation cross section, mass and the density profile of DM halos  $\rho(\vec{r}(s, \Omega))$ , usually represented by a Navarro-Frenk-White (NFW) profile, as shown in Equation 2.16, where  $r_s = 20$  kpc is the scale radius of the DM halo for the Milky Way and  $r$  is the distance to the center of the cluster considered, assumed to be spherical in this case [66].

$$\rho(r) \propto \frac{r_s}{r \cdot \left(1 + \left(\frac{r}{r_s}\right)^2\right)} \quad (2.16)$$

The flux coming from the annihilation of two DM particles is then expected to be proportional

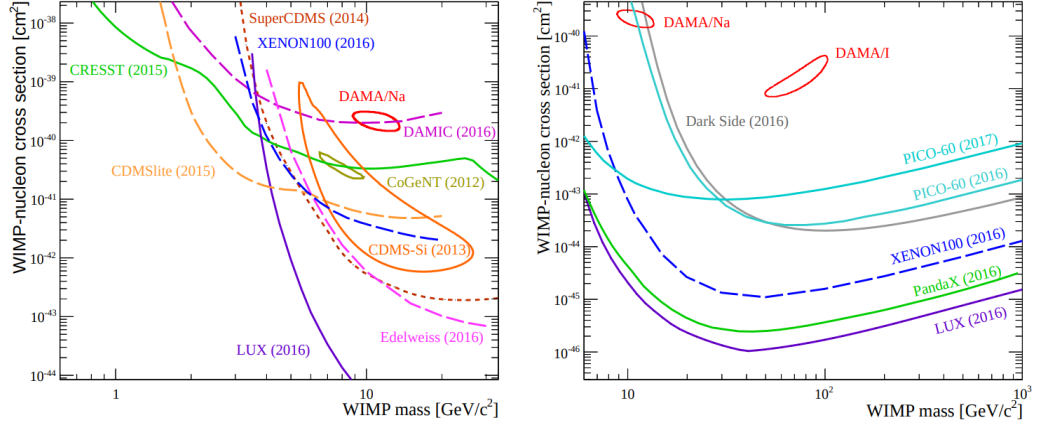


Figure 2.17: Exclusion limits obtained by various direct detection experiments considering a SI interaction cross section for low WIMP (on the left) or high WIMP masses (on the right) [63].

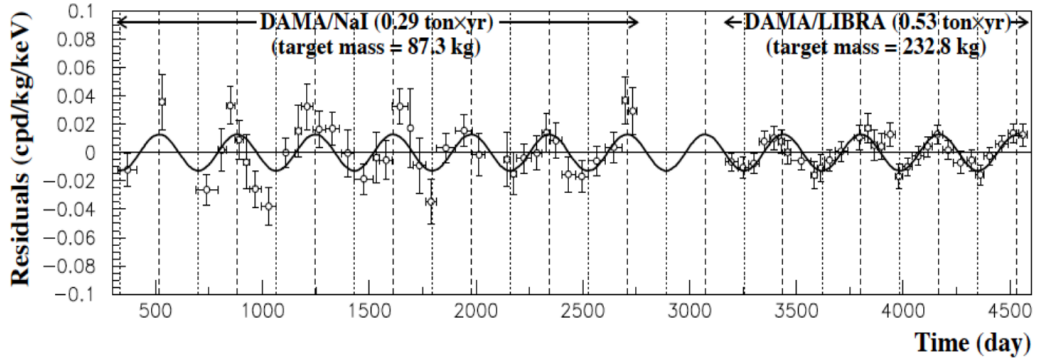


Figure 2.18: Observed and expected annual modulation in single hits events in the 2-6 keV energy range by the DAMA experiment [64].

to its annihilation cross section  $\sigma v$ , the solid angle of observation  $\Omega$  and the number of particles emitted by this annihilation  $\frac{dN}{dE}$ , according to Equation 2.17, where the integration is done over the line of sight  $l$  and the solid angle of observation  $\Omega$ .

$$\frac{d\Phi}{d\Omega dE} = \frac{\sigma v}{8\pi m_\chi^2} \cdot \frac{dN}{dE} \iint_{l,\Omega} \rho^2(\vec{r}(s, \Omega)) dl d\Omega \equiv P \cdot J(\Delta\Omega) \quad (2.17)$$

This equation is extremely important for two reasons. First of all, it shows that, if a signal is found in direct detection, we could use this detection to determine the new object mass and scattering cross section and then use this information in order to obtain the DM density profile this way: the data obtained by the different strategies of detection are actually complementary. The second reason is that as we can see, the flux of incoming particles can actually be divided into two factors:  $P$ , entirely dependent on the physics of the DM particle, and the  $J$ -factor  $J(\Delta\Omega)$ , depending only on the distribution of DM within the system considered. This  $J$ -factor is in this sense actually a measurement of the quality of an astronomical object for an indirect measurement, since the higher the flux received, the better the measurement will be in general (even though this is not the only factor which matters, since for example the galactic center has a higher  $J$ -factor than the best dwarf galaxy observable, but also has a lot of backgrounds affecting the measurement).

As different channels of observation are available for us to analyze the eventual annihilation of DM, several strategies can be used in order to detect DM indirectly, as we will now see, by searching different kinds of SM particles. Anyway, all these strategies have one goal in common: try to reduce the background, since the signal searched for is usually quite low while the uncertainties associated to the background in astrophysics are usually quite high.

### Through $\gamma$ -rays detection

The golden channel for such searches is through the production of  $\gamma$ -rays by DM annihilation  $\chi\chi \rightarrow \gamma + X$  or decay  $\chi \rightarrow \gamma + X$ , mainly because the energy scale of the WIMPs implies that most of the annihilation and decay radiation will be emitted in this range of energies and because  $\gamma$ -rays are usually not deflected when traveling to the observer (this means that the exact source of this kind of radiation can be quite easily and precisely pin-pointed). However, they do have one drawback as well: the Earth's atmosphere is usually opaque to this kind of radiation at this level of energy. This means that most of experiments searching for them simply cannot be performed from the ground and have to be sent to space.

One of the most famous detectors in this category is the Fermi Large Telescope (LAT), a pair production detector launched in June 2008 and mostly sensitive to  $\gamma$ -rays between 20 MeV and 300 GeV [67]. This experiment has managed to exclude a large portion of the phase space, as seen in Figure 2.19. The GAMMA-400 experiment, whose launch is scheduled in 2020, will pick up the work of LAT, by studying a similar range but with much improved angular and energy resolutions [68].

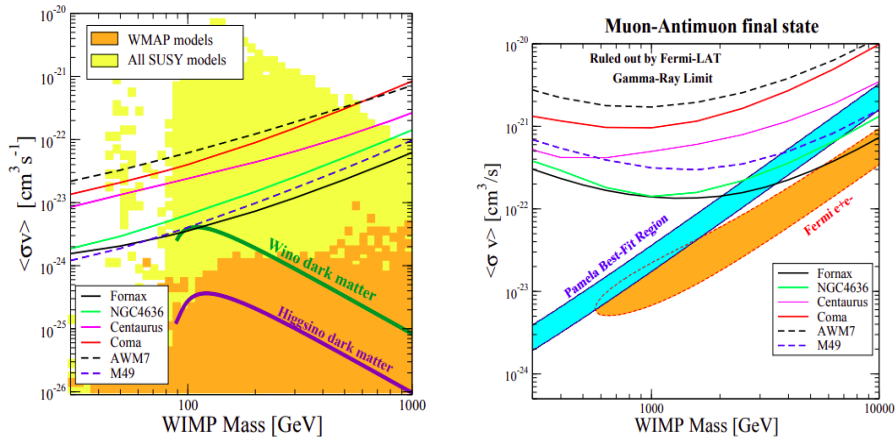


Figure 2.19: Upper limits on the DM annihilation cross section considering  $b\bar{b}$  (on the left) and  $\mu^+\mu^-$  (on the right) final states as a function of the WIMP mass, for different clusters studied [67].

It is much harder for DM to produce high energy  $\gamma$ -rays and therefore, the flux of such particles decreases quite quickly with energy, making it harder to study since telescopes then need a much larger effective area to pick up the same quantity of signal, and have therefore to be put on the ground. Such telescopes do exist, are called Imaging Atmospheric Cherenkov Telescopes (IACT) and have to take into account the atmospheric perturbations to work in an optimal way. They are usually sensitive to a range of energies going from  $\sim 10$  GeV up to  $\sim 100$  TeV, but can usually only study a small portion of the sky (up to a few degrees), forcing these experiments to choose carefully the objects to be studied. The Cherenkov Telescope Array (CTA) is a brand new telescope of this kind whose construction is supposed to start in 2020, that should improve greatly the sensitivity of high masses indirect DM searches.

## Through neutrinos detection

Interacting only weakly, neutrinos are another reliable source of data in the Universe since they are not supposed to be altered when traveling large distances as well, even though detecting neutrinos is much harder than detecting  $\gamma$ -rays and usually involves huge tanks of water in which neutrinos can be detected with the Cherenkov effect, which consists of the emission of an electromagnetic radiation when a charged particle moves through a dielectric medium with a speed greater than the speed of light in this medium.

The most famous detector of this kind, the IceCube neutrino observatory, actually uses the ice of the South Pole instead of water to detect these particles with photo-detectors, mainly because of the low interaction cross section of the neutrinos which then requires the installation of a huge volume of material to increase the probability of interaction. Super-Kamiokande (Super-K), in Japan, is another large Cherenkov experiment dedicated to the detection of cosmic neutrinos. Both detectors are also largely involved as direct searches experiments, since they are also sensitive to the eventual recoil between DM and ordinary matter nuclei.

The problem with this kind of experiment is the difficulty of actually detecting some neutrinos, along with the background levels from atmospheric neutrinos, as represented in Figure 2.20, typically several orders of magnitude larger than the signal. Multiple strategies therefore need to be put in place in order to reduce the background level in such experiments, such as the study of the directionality of the source and an appropriate choice of angle of observation, since most of the contamination is coming from tau neutrinos, themselves originating from muon neutrinos oscillation, strongly suppressed around the zenith.

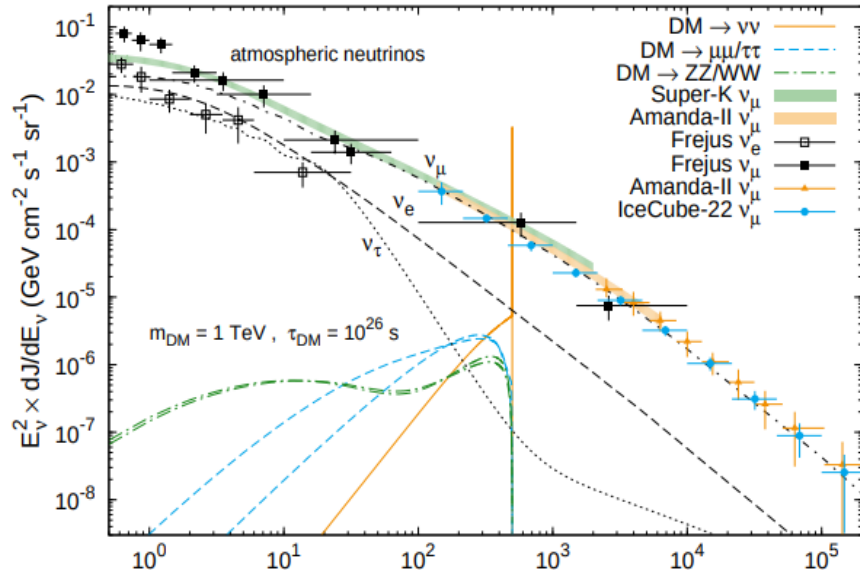


Figure 2.20: Neutrino spectra for a scalar DM candidate of 1 TeV for different indirect detection experiments and the corresponding background level expected [69].

## Through cosmic rays detection

Searching for anti-matter in the cosmic rays presents the advantage of being highly sensitive, because of the low levels of backgrounds this kind of searches implies. However, cosmic rays are

affected when traveling through the Universe, and determining the exact location of their emission can be quite challenging.

Among the most famous detectors of this kind, we can quote PAMELA, a spatial telescope dedicated to the study of such cosmic rays since 2006. CERN's Alpha Magnetic Spectrometer (AMS), installed in the International Space Station has also studied such radiation from a range of a few hundred MeV up to 1 TeV. The data collected by this detector is compared to the exclusion limits obtained by the IceCube detector in Figure 2.21.

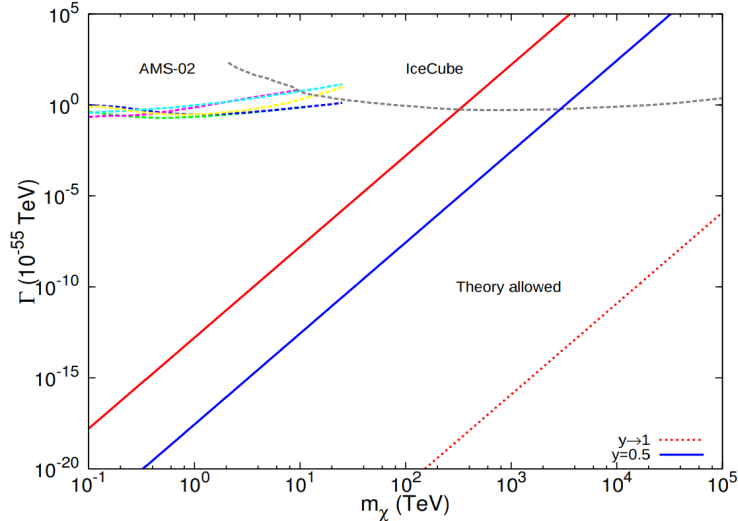


Figure 2.21: Limits of the decay width of the interaction with respect to the DM mass obtained by both IceCube and AMS [70].

### 2.5.3 Collider production

In this particular kind of searches, we are interested in the eventual direct production of DM candidates following the collision between two highly energetic SM particles, a perfectly viable scenario if we keep assuming that DM should at least interact weakly with ordinary matter if we want to be able to produce or detect it in a laboratory.

In this case, two main models for the interaction between SM and DM particles can be considered, each with a different level of complexity and different possible applications:

- The Effective Field Theory (EFT) approach is usually considered to be the easiest, even though it can still give us plenty of information about this kind of interaction. It relies on the assumption that the energy scale of the new exotic physics is much larger than the actual energy accessible with our experiment, since the momentum transfer of this interaction needs to be much smaller than the mediator mass in this case. According to this approach, represented in Figure 2.22, the interaction can be described using simplified operators (the most simple ones being either scalar  $\bar{\chi}\chi\bar{q}q$ , pseudoscalar  $\bar{\chi}\gamma^5\chi\bar{q}\gamma^5q$ , vector  $\bar{\chi}\gamma^\mu\chi\bar{q}\gamma_\mu q$  or axial-vector  $\bar{\chi}\gamma^\mu\gamma^5\chi\bar{q}\gamma_\mu\gamma^5q$ ) since, according to the assumption made, its mediator can usually be integrated out [59].

Despite of this strong assumption, this approach is actually quite useful anyway in the sense that it is able to provide us bounds on the new physics scale  $\Lambda$ , which can be related to the

different couplings of the interaction as in Equation 2.18, where  $g_q$  and  $g_\chi$  are the coupling between the mediator and the SM or DM particle, and  $m_{\text{med}}$  is the mass of the mediator.

$$\frac{1}{\Lambda^2} = \frac{g_q g_\chi}{m_{\text{med}}} \quad (2.18)$$

Additionally, direct searches experiments typically also introduce this kind of assumptions to extract constraints from their measurements, making it straightforward to compare the results obtained in both approaches. However, the transfer of momentum in the direct searches experiments is usually of the order of a few keV as seen in Equation 2.19, while in collider experiments such as the LHC, this is of the order of  $\Theta(\text{GeV-TeV})$ .

$$E = \frac{m_\chi v_\chi^2}{2} \simeq 100 \text{ GeV} \cdot 10^{-6} \simeq 50 \text{ keV} \quad (2.19)$$

This means that, especially due to the increasing center of mass energy given by the LHC over the last few years, the basic EFT assumption is usually not respected and gives information about an out of reach phase space region anyway, making its usefulness quite relative in most cases. This is why alternative models need to be developed as well.

- The simplified models attempt to solve the issue related to the approximation made by the EFT approach, by increasing the level of details regarding the interaction between the dark and baryonic sectors. This is usually done by explicitly taking into account the mediator of the interaction, which can be considered of two different types in the context of this work: either scalar  $\phi$  or pseudoscalar  $a$  (both having a spin 0), described by the Lagrangians in Equation 2.20, considering the DM candidate to be a Dirac fermion coupling to the SM through the mediator considered and under the assumption of Minimal Flavour Violation (MFV) (a proposal made to characterize the effects of flavor transitions in new theories of particle physics). In this equation, the sum runs over the three SM families and the parameters  $y_i^f = \sqrt{2} \frac{m_i^f}{v}$  are the Yukawa couplings, much larger for the top quarks because of their mass, which will allow us to simplify the following equations [71].

$$\begin{cases} \mathcal{L}_{\text{fermion},\phi} \propto -g_\chi \phi \bar{\chi} \chi - \frac{\phi}{\sqrt{2}} \sum_i (g_u y_i^u \bar{u}_i u_i + g_d y_i^d \bar{d}_i d_i + g_l y_i^l \bar{l}_i l_i) \\ \mathcal{L}_{\text{fermion},a} \propto -ig_\chi a \bar{\chi} \gamma^5 \chi - \frac{ia}{\sqrt{2}} \sum_i (g_u y_i^u \bar{u}_i \gamma^5 u_i + g_d y_i^d \bar{d}_i \gamma^5 d_i + g_l y_i^l \bar{l}_i \gamma^5 l_i) \end{cases} \quad (2.20)$$

An important parameter in this case is the decay width of this mediator  $\Gamma_{\text{med}}$ , given by Equation 2.21 for either a scalar mediator  $\phi$  or Equation 2.22 for a pseudoscalar mediator  $a$ , where the first term corresponds to the mediator decay to SM particles, the second to its decay to DM particles and the last term its possible decay to gluons.

$$\begin{cases} \Gamma_\phi = \sum_f N_C \frac{y_f^2 g_\nu^2 m_\phi}{16\pi} \left(1 - \frac{4m_f^2}{m_\phi^2}\right)^{3/2} + \frac{g_\chi^2 m_\phi}{8\pi} \left(1 - \frac{4m_f^2}{m_\phi^2}\right)^{3/2} + \frac{\alpha_S^2 g_\nu^2 m_\phi^3}{32\pi^3 \nu^2} \left| f_\phi \left( \frac{4m_t^2}{m_\phi^2} \right) \right|^2 \\ f_\phi(\tau) = \tau \left( 1 + (1 - \tau) \arctan^2 \left( \frac{1}{\sqrt{\tau - 1}} \right) \right) \end{cases} \quad (2.21)$$

$$\begin{cases} \Gamma_a = \sum_f N_C \frac{y_f^2 g_\nu^2 m_a}{16\pi} \left(1 - \frac{4m_f^2}{m_a^2}\right)^{1/2} + \frac{g_\chi^2 m_a}{8\pi} \left(1 - \frac{4m_f^2}{m_a^2}\right)^{1/2} + \frac{\alpha_S^2 g_\nu^2 m_a^3}{32\pi^3 \nu^2} \left|f_a\left(\frac{4m_t^2}{m_a^2}\right)\right|^2 \\ f_a(\tau) = \tau \arctan^2\left(\frac{1}{\sqrt{\tau-1}}\right) \end{cases} \quad (2.22)$$

In the case of the simplified models, the minimal set of parameters describing the interaction is therefore  $\{m_\chi, m_{\text{med}}, g_\chi, g_q\}$ .

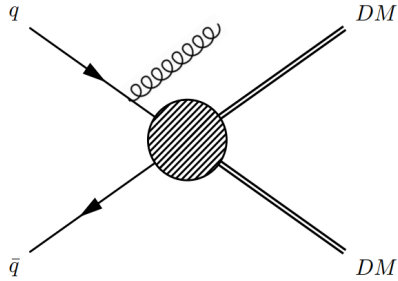


Figure 2.22: Schematic representation of a typical EFT modelization of an LHC event with an Initial State Radiation (ISR) object used to trigger the event [59].

An additional categorization of the DM production models can be done, by separating the so-called s-channel and t-channel models, as shown in Figure 2.23. In the first case, the most common one in collider searches, the mediator between the SM and DM is assumed to be a boson, and usually decays directly into a pair of DM particles. On the other hand, in the t-channel models, the mediator couples to one quark and one DM particle, with a colored exchange particle required.

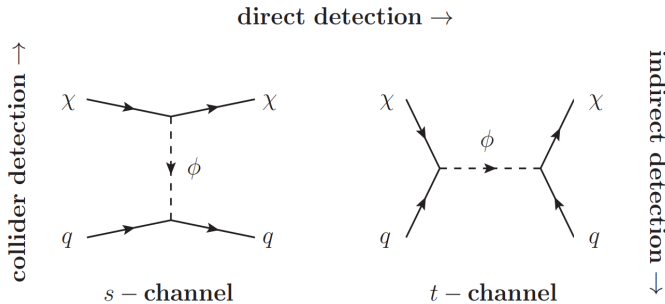


Figure 2.23: Schematic representation of a typical collider DM production through s-channel and t-channel processes [72].

In this work, simplified models with either scalar or pseudoscalar mediators will always be considered because of their relative simplicity and the lack of strong assumptions behind them. We will now study in particular the production and the search for DM within the LHC.

## 2.6 DM production at the LHC

The Large Hadron Collider (LHC), colliding protons at a center of mass energy of 13 TeV, is actually a perfect machine to study such processes, because of the expected range of masses (100 GeV to 1 TeV) for the best DM candidates, as discussed in Section 2.3. However, because of the weak interactions of such particles, they are not expected to interact at all with the detector, which will then basically search for missing transverse energy along with a SM particle triggering the event.

Several major categories of DM searches exist at the LHC, performed mainly by the CMS and ATLAS collaborations, depending on the strategy applied for such searches:

- First of all are the so-called **mono-X searches**, where X stands for a detectable SM particle used to trigger the event while the DM mediator usually decays into a pair of particles escaping the detector, leaving behind some Missing Transverse Energy (MET), a key variable to all these searches, as shown in Figure 2.24. Depending on the nature of the X particle, several searches can be performed: we can for example mention the mono- $\gamma$  [73, 74] or mono-jet [75, 76] 13 TeV searches performed by the ATLAS and CMS collaborations.

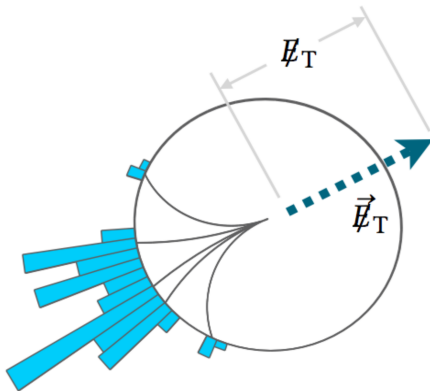


Figure 2.24: Schematic representation of a typical mono-X event, with an ISR jet in this case going back-to-back with some MET [59].

Additionally, if the DM mass is high enough, a coupling to the Higgs boson is also possible, or an eventual decay of the Higgs itself to a couple of DM particles  $H \rightarrow \chi\bar{\chi}$  is kinematically not impossible. This channel, known as the mono-Higgs, is sensitive to all the decays of the Higgs, even though the searches excluding most of the phase spaces are performed using the  $H \rightarrow b\bar{b}$  and  $H \rightarrow \gamma\gamma$  decays [77, 78].

- The searches for DM production in **association with heavy quark(s)** belong to the second category, such as the one performed in this work. Other analyses such as the one probing the  $b\bar{b} + \text{DM}$  to its different final states depending on the decay of the bottom quark (at 8 or 13 TeV) also belong to this group [16, 20].

These searches have to combine the discriminant power of several variables to separate the signal from the backgrounds, since the MET distribution on its own is usually not enough, but they present the advantage of being favored by the higher Yukawa coupling to more massive particles implied by the MFV assumption.

- **Dijet searches** provide the best exclusion limits for most of the spin-1 mediated models

considered (up to a few TeV for typical coupling choices) [79, 80]. In this case, the sensitivity is obtained by searching for either narrow or large resonances on the exponentially falling QCD background, while the other searches were mostly dedicated in searching for bumps in the MET spectrum.

- **Supersymmetric searches** can also be performed to search for DM which would solve the hierarchy problem while giving us perfect DM candidates such as the neutralino  $\chi$ , the lightest stable supersymmetric particle, obtained in many of the MSSM theories, having an hypothetical mass below the TeV scale [81].
- The **Higgs portal** to the dark sector is another interesting strategy. In some specific cases, when considering spin-0 mediated interactions between the dark and baryonic sectors, the Higgs could be considered as the mediator of the interaction as well, which only requires a minimal modification of the SM Lagrangian. It is then necessary to study the different Higgs production modes, such as the gluon fusion and Vector Boson Fusion (VBF) mechanisms, to search for an eventual invisible decay of the Higgs into a couple of DM particles, assuming that its mass is lower than  $\sim 62.5$  GeV,  $m_H/2$  [82].
- Finally, and this is quite new, **long-lived searches** can also be performed. These are interesting because they can extend the current searches performed to also consider the eventual creation of long-lived particles which would decay a few centimeters further than the primary vertex of the  $pp$  collision [83]. Typical SM signatures do not usually include such events, making this channel relatively background-free, even though the reconstruction of the different objects is much harder in this case.

All the results from the different searches performed by the CMS collaboration using the full 35.9  $\text{fb}^{-1}$  dataset collected at 13 TeV can be summarized in Figure 2.25 for spin-0 mediators and in Figure 2.26 when considering spin-1 mediators.

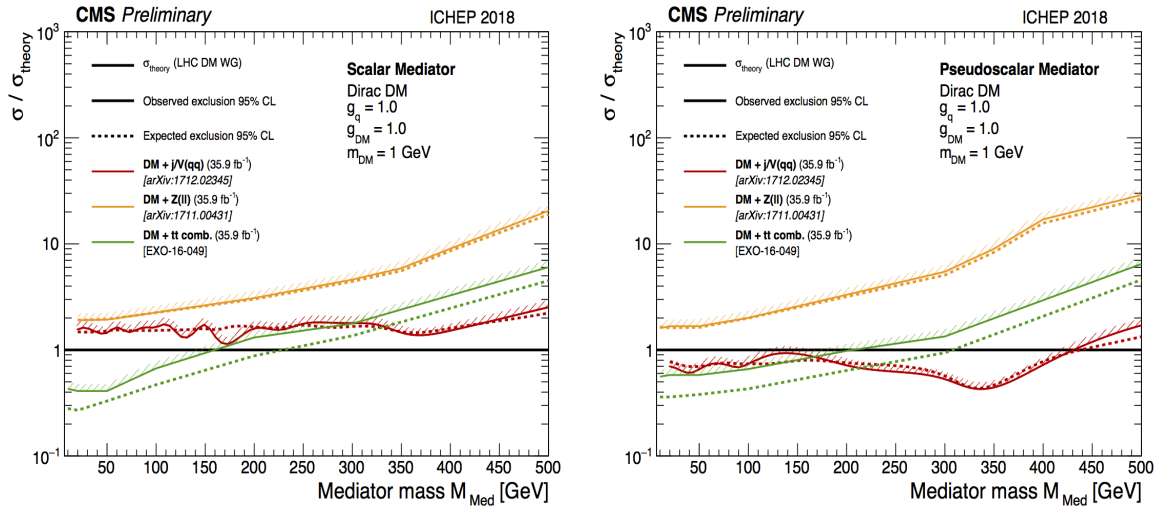


Figure 2.25: Observed and expected 95% exclusion limits obtained by different searches of the CMS collaboration as a function the spin-0 scalar (on the left) or pseudoscalar (on the right) mediator.

These results have also been compared to the results obtained by several direct detection experiments in Figure 2.27, considering both the Spin Dependent (SD) and Spin Independent (SI) cases, as explained in Section 2.5.1.

This particular analysis and our signal of interest, the search for DM production together with a single or a pair of top quarks falls into the second category and will now be detailed. It is already

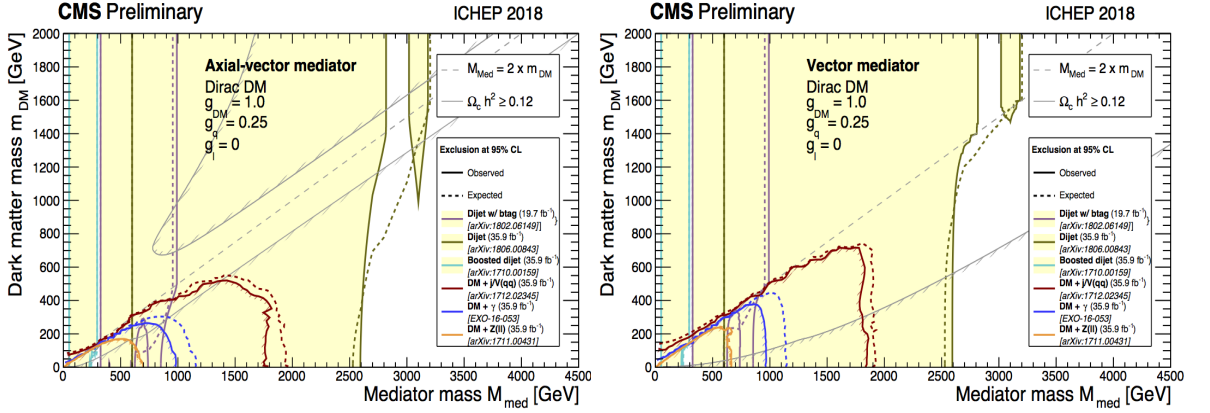


Figure 2.26: Observed and expected 95% exclusion limits obtained by different searches of the CMS collaboration as a function of the spin-1 mediator, considering axial-vector (on the left) and axial (on the right) interactions.

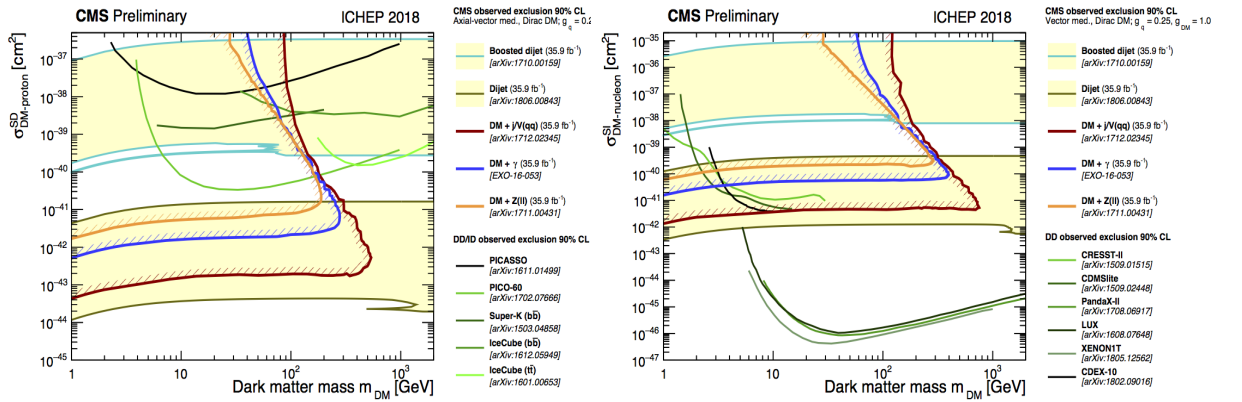


Figure 2.27: CMS 90% exclusion limits compared to the most famous direct detection experiments for the SD (on the left) and SI (on the right) scenarios, obtained using similar couplings.

important to note that this analysis has been performed considering the DM candidate to be a Dirac fermion with all the couplings equal and set to 1, as recommended by the Dark Matter Working Group (DMWG) [84].

### 2.6.1 The single top production channel

The first kind of signal considered in this analysis is the production of DM in association with a single top quark, known as  $t/\bar{t}$ +DM analysis. This process is expected to be mediated by a spin-0 mediator, either scalar or pseudoscalar, and is associated with a light quark and a W boson (the mono-top analysis is dealing with the case where a single top is created without any additional particle).

Three different Feynman diagrams can be associated to this particular analysis depending on the model considered, as shown in Figure 2.28.

As discussed previously, the top quark will be dynamically favored due to its high mass and therefore high Yukawa coupling, but this has another consequence as well, since the lifetime of this quark is extremely low, of the order of  $10^{-15}$  s [85]. This means that this particle usually decays before being able to form hadrons, so we can only detect the products of its decay, not the top

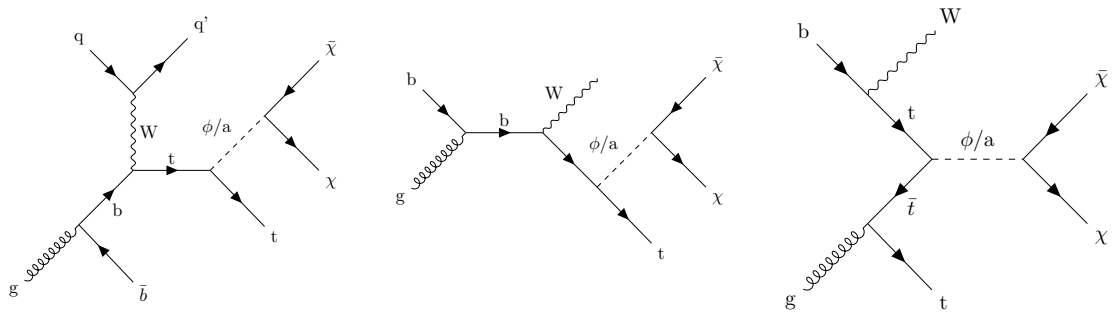


Figure 2.28: Feynman diagrams involving the production of DM with a single top quark with its associated t-channel W boson (on the left), or tW (on the center and on the right) production.

quark itself. In almost 100% of the cases, the top actually decays into a bottom quark and a W boson, which decays itself before being detected into quarks and/or leptons. Even though this will be detailed in Chapter 3, we can already conclude that the typical final state of such signature is therefore made out of MET coming from the DM, one b-tagged jet along with one or two W bosons, seen as a combination of jets and leptons, depending on the channel considered.

### 2.6.2 The $t\bar{t}$ production channel

The  $t\bar{t}$ +DM analysis is really similar, except that in this case, we have two top quarks in the final state, as represented in Figure 2.29.

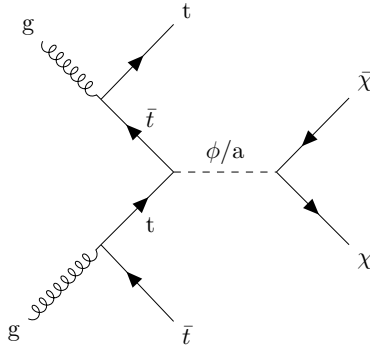


Figure 2.29: Schematic representation of a typical  $t\bar{t}$ +DM event.

The final state expected by such an event is therefore made of two b-tagged jets, along with two W bosons and some MET coming from the pair of DM particles. In this case as well, both scalar  $\phi$  and pseudoscalar  $a$  mediators will be considered, with a mass range from 10 to 500 GeV.

### 2.6.3 The dilepton final state

As previously explained, most of the models considered will produce exactly two W bosons, which are not stable long enough and therefore decay before reaching the detector, meaning that we cannot directly detect such bosons. However, we can detect the results of the decays of these W, since they can decay either to hadrons ( $67.6 \pm 0.27\%$  branching ratio) or to a lepton and a neutrino, giving us an additional contribution of MET ( $10.8 \pm 0.09\%$  for each lepton) [85].

This means that this kind of analyses featuring two W bosons in the final state can focus on different channels: either completely hadronic (if both the W decay into quarks), semileptonic or dileptonic (when both W bosons decay into two neutrinos and two leptons of opposite charge).

Given the Branching Ratio (BR) of the W decay, it is easy to see that the dileptonic channel, which will be the focus of this work, is not favored statistically. However, this channel features less backgrounds than other channels, resulting in a better signal isolation, and because leptons can usually be reconstructed in a better way than jets (cf. Chapter ??), resulting in lower uncertainties and in improved limits.

## 2.7 Previous relevant results

This analysis being performed at a center of mass energy  $\sqrt{s} = 13$  TeV, only the most relevant results to this energy obtained by both the CMS and ATLAS collaborations will be quoted.

First of all, the **ATLAS collaboration** published interesting results at this center of mass energy, considering an integrated luminosity of  $13.3 \text{ fb}^{-1}$ , and obtained the corresponding exclusion limits at the 95% CL, considering the  $t\bar{t}+\text{DM}$  model and both scalar and pseudoscalar spin-0 mediators for the interaction, as shown in Figure 2.30. In this case, and for the couplings considered, an exclusion up to  $\sim 375$  GeV has been achieved [17].

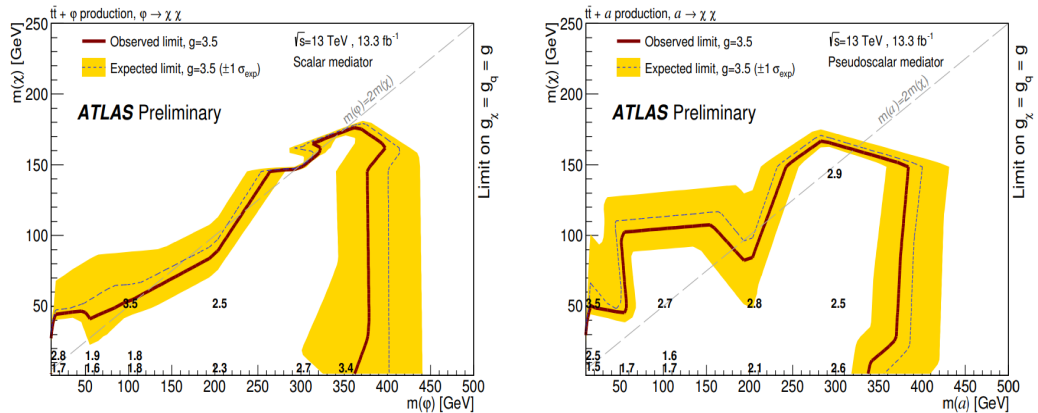


Figure 2.30: Limits on the DM and mediator masses obtained by ATLAS using  $13.3 \text{ fb}^{-1}$  of 13 TeV data, considering scalar (on the left) and pseudoscalar (on the right) mediators [17].

Considering the full 2016 dataset of  $36.1 \text{ fb}^{-1}$ , similar results have been obtained, as shown in Figure 2.31. In this case, and for lower coupling values, an exclusion up to around 100 GeV has been obtained considering scalar and pseudoscalar mediators [20].

The **CMS collaboration** published in 2018 a similar analysis, using the  $35.9 \text{ fb}^{-1}$  of data collected during the year 2016. This analysis combined the three different final states possible (hadronic, semileptonic and dileptonic) and computed the limits on the signal strength for different mediator and dark matter masses, considering both scalar and pseudoscalar mediators [22]. The results obtained can be found in Figure 2.32.

Last year, a CMS combination of the  $t/\bar{t}+\text{DM}$  and  $t\bar{t}+\text{DM}$  analyses has also been published [23], combining this time only the hadronic and semileptonic channels of both analyses. The limits obtained in this case are represented in Figure 2.33, where the limits obtained by each analysis

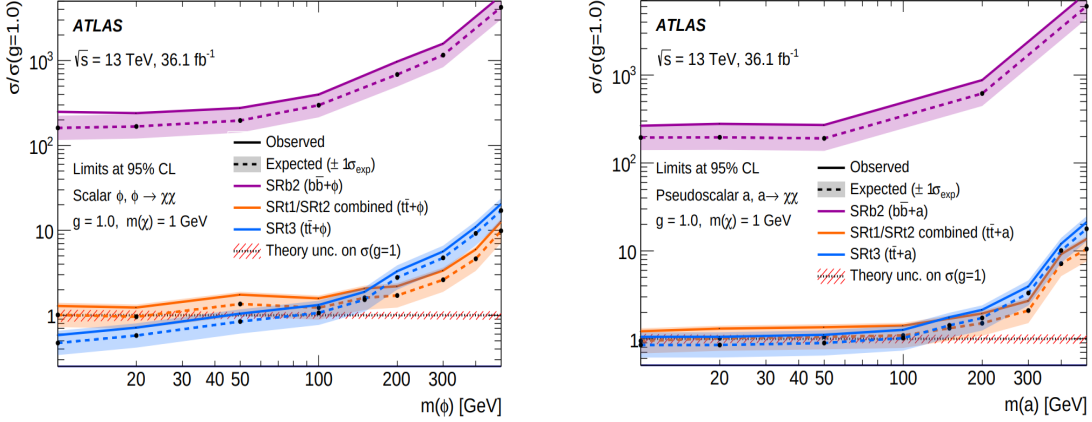


Figure 2.31: Exclusion limits at the 95% CL obtained by ATLAS considering scalar (on the left) and pseudoscalar (on the right) mediators, for a DM mass of 1 GeV [20].

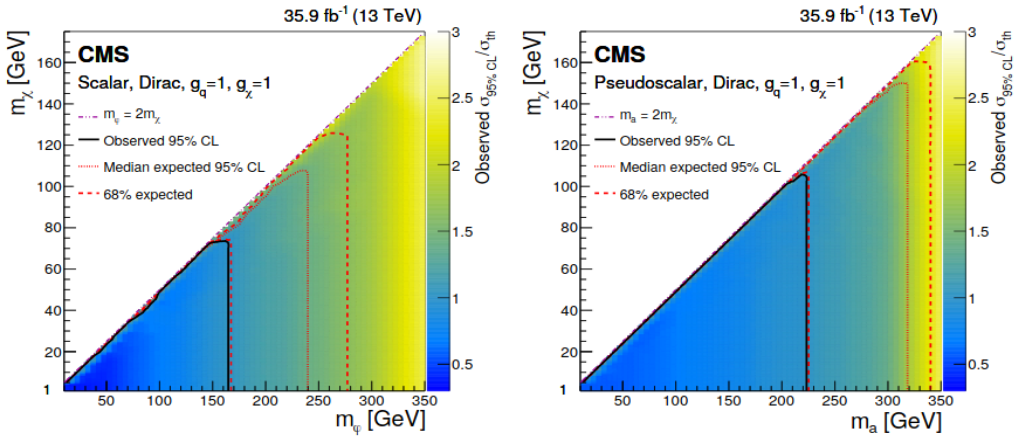


Figure 2.32: 95% CL exclusion plots on the signal strength computed as a function of the mediator and DM masses obtained by CMS considering a scalar (on the left) and a pseudoscalar (on the right) mediator for the interaction [22].

on their own along with the results of the combination, leading to a factor 2 improvement of the limits obtained, have been represented.

This combination managed to exclude the production of scalar mediators up to 290 GeV and pseudoscalar mediators up to 300 GeV, at the 95% CL for the couplings considered. This combined analysis actually leads to the most stringent exclusion limits of the LHC on the production of DM through these categories of spin-0 mediators.

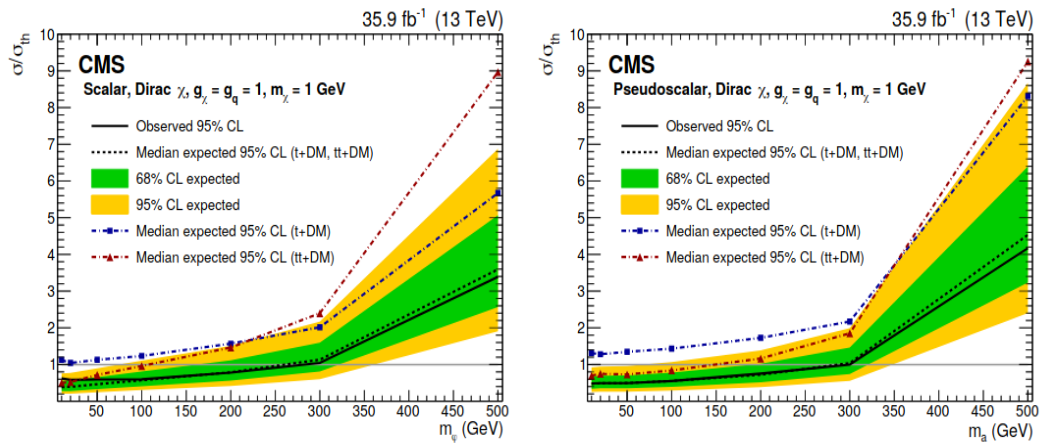


Figure 2.33: Expected and observed 95% CL limits on the DM production cross sections shown considering scalar (on the left) and pseudoscalar (on the right) mediators for the interaction [23].



# Chapter 3

## Event selection

This Chapter will be dedicated to the analysis itself, by defining first of all the different objects actually used in this case, along with the actual selection that has been applied to enhance the quality of such objects in this particular search in Section 3.1. Then, the different Signal Regions (SRs) defined in which a high purity of signal is expected are defined in Section 3.2 while all the different Control Regions (CRs) defined in order to check the behavior of the Monte Carlo (MC) simulation performed for the major backgrounds on this analysis, such as the single top or SM  $t\bar{t}$  production, will be introduced in Section 3.3.

Finally will come a description about the different variables expected to naturally introduce some discrimination of the  $t/\bar{t}$  and  $t\bar{t}+\text{DM}$  signals with respect to the different backgrounds in Section 3.4, along with a global description of the Machine Learning (ML) techniques employed in order to optimize the discriminating power of these variables in the best way possible.

### 3.1 Objects selection

We already described what to expect from a typical  $t/\bar{t}$  or  $t\bar{t}+\text{DM}$  signal: the typical signature of such signals is made out of a certain number of b tagged jets along with two leptons (electrons and/or muons) and some Missing Transverse Energy (MET) coming from the two DM particles created along the way. It is therefore extremely important to describe the Working Point (WP) chosen and the selection applied in order to select the objects of the analysis, such as the leptons and the jets used, in such a way to optimize the lepton reconstruction efficiency while reducing as much as possible the possible misidentification rates of such objects.

First of all, the different triggers used to collect the data will be detailed in Section 3.1.1. Then, the leptons used in this analysis will be introduced in Sections 3.1.2 (for electrons) and 3.1.3 (for muons). Finally, given the nature of the DM signal searched for, a complete description of the jets selected in the analysis will be necessary and performed in Section 3.1.4.

#### 3.1.1 Triggers selection

The triggers, described in Section ??, and particularly the trigger paths chosen are an important part of each analysis since they will describe the kind of data that can be collected and therefore analyzed. The triggers used in this analysis for the years 2016, 2017 and 2018 can be found in Tables 3.1, 3.2 and 3.1 respectively.

Dataset	Run range	<b>High-Level Trigger (HLT) trigger path</b>
SingleMu	[273158,284044]	HLT_IsoMu24_v* HLT_IsoTkMu24_v*
SingleEle	[273158,284044]	HLT_Ele27_WPTight_Gsf_v* HLT_Ele25_eta2p1_WPTight_Gsf_v*
DoubleEG	[273158,284044]	HLT_Ele23_Ele12_CaloIdL_TrackIdL_IsoVL_DZ_v*
DoubleMu	[273158,281612] [281613,284044]	HLT_Mu17_TrkIsoVVL_Mu8_TrkIsoVVL_v* HLT_Mu17_TrkIsoVVL_TkMu8_TrkIsoVVL_v* HLT_Mu17_TrkIsoVVL_Mu8_TrkIsoVVL_DZ_v* HLT_Mu17_TrkIsoVVL_TkMu8_TrkIsoVVL_DZ_v*
MuonEG	[273158,278272] [278273,284044]	HLT_Mu8_TrkIsoVVL_Ele23_CaloIdL_TrackIdL_IsoVL HLT_Mu23_TrkIsoVVL_Ele12_CaloIdL_TrackIdL_IsoVL HLT_Mu8_TrkIsoVVL_Ele23_CaloIdL_TrackIdL_IsoVL_DZ_v* HLT_Mu23_TrkIsoVVL_Ele12_CaloIdL_TrackIdL_IsoVL_DZ_v*

Table 3.1: 2016 trigger paths considered for this analysis.

Our analysis relying on the dilepton final state, the single lepton trigger are only considered in order to recover some of the efficiency lost in some cases when one lepton passes the tight identification criteria while the second one does not, and does therefore not trigger the event. The logical *or* of all the trigger paths are usually considered. Eventual events passing several triggers is taken into account as well to make sure to avoid any double counting due to this effect.

These triggers have been studied in order to make sure that they are efficient enough in the  $p_T$  region of the leptons of the analysis to avoid any undesired effect due to the turn-on of any trigger. These trigger efficiencies, calculated using a general tag and probe method and found for example for different runs of the 2017 data taking period in Figure 3.1 for a DoubleEG trigger, are then used to reweight the simulated samples.

Dataset	Run range	<b>HLT trigger path</b>
SingleMu	[297046,306462]	HLT_IsoMu27_v*
EGamma	[297046,306462]	HLT_Ele35_WPTight_Gsf_v* HLT_Ele23_Ele12_CaloIdL_TrackIdL_IsoVL_v*
DoubleMu	[297046,299329] [299368,306462]	HLT_Mu17_TrkIsoVVL_Mu8_TrkIsoVVL_DZ_v* HLT_Mu17_TrkIsoVVL_Mu8_TrkIsoVVL_DZ_Mass8_v*
MuonEG	[297046,306462] [297046,299329] [299368,306462]	HLT_Mu12_TrkIsoVVL_Ele23_CaloIdL_TrackIdL_IsoVL_DZ_v* HLT_Mu23_TrkIsoVVL_Ele12_CaloIdL_TrackIdL_IsoVL_DZ_v* HLT_Mu23_TrkIsoVVL_Ele12_CaloIdL_TrackIdL_IsoVL_DZ_v*

Table 3.2: 2017 trigger paths considered for this analysis.

Dataset	Run range	HLT trigger path
SingleMu	[315252,325172]	HLT_IsoMu24_v*
		HLT_Mu5_v*
	[314859,325175]	HLT_IsoMu27_v*
EGamma	[315252,325172]	HLT_Ele32_WPTight_Gsf_v*
		HLT_Ele35_WPTight_Gsf_v*
		HLT_Ele23_Ele12_CaloIdL_TrackIdL_IsoVL_v*
DoubleMu	[315252,325172]	HLT_Mu17_TrkIsoVVL_Mu8_TrkIsoVVL_DZ_Mass3p8_v*
		HLT_Mu17_TrkIsoVVL_Mu8_TrkIsoVVL_DZ_Mass8_v*
MuonEG	[315252,325172]	HLT_Mu23_TrkIsoVVL_Ele12_CaloIdL_TrackIdL_IsoVL_v*
		HLT_Mu12_TrkIsoVVL_Ele23_CaloIdL_TrackIdL_IsoVL_DZ_v*

Table 3.3: 2018 trigger paths considered for this analysis.

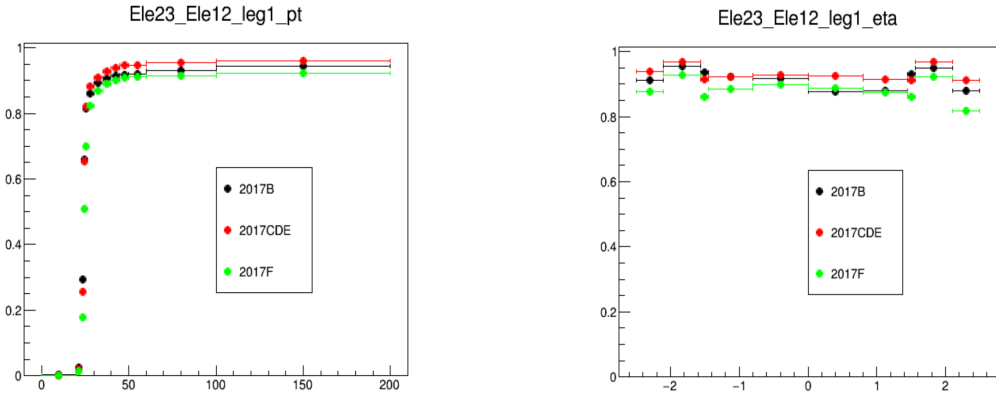


Figure 3.1: DoubleEG trigger efficiencies with respect to the  $p_T$  (on the left) and  $\eta$  (on the right), computed using a tag and probe method, for the 2017 data taking period.

### 3.1.2 Electrons selection

Several strategies are used in CMS in order to be able to identify prompt electrons and isolate this signal over background sources coming mainly from photon conversions, misidentification of jets or electrons coming from the semileptonic decay of the bottom and charm quarks. Several variables, which can be divided in the several following categories, allow to introduce some discrimination between these prompt and fake electrons:

- The **calorimetric observables** use the transverse shape of electromagnetic showers in the Electromagnetic Calorimeter (ECAL), the fact that these electromagnetic showers should be narrower than hadronic showers and the fraction of energy deposited in the Hadronic Calorimeter (HCAL) and in the preshower/endcaps of the ECAL itself for the discrimination. Many different variables belong to this category, such as:

- **hOverE** ( $\frac{H}{E}$ ), where  $H$  corresponds to the energy deposited in the HCAL and  $E$  the total energy deposited in the ECAL.

- **ooEmooP** ( $\frac{1}{E_{SC}} - \frac{1}{p}$ ), where  $E_{SC}$  is the Super Cluster (SC) energy and  $p$  the momentum of the track at the point of closest approach to the Primary Vertex (PV).

- **dEtaInSee**  $\Delta\eta$  (**dPhiInSee**  $\Delta\phi$ ), the  $\eta$  ( $\phi$ ) difference between the SC and the inner track extrapolated from the interaction vertex.
- **sigmaIetaIeta** ( $\sigma_{\eta\eta}$ ), the weighted cluster Root Mean Square (RMS) inside 5x5 regions of SCs along  $\eta$ .
- The **isolation variables**, requiring the electron candidates to be quite isolated with respect to nearby energetic activity since most of the non-prompt electrons, such as electrons within a jet, are emitted with a large amount of surrounding energy.
  - The **relIsoWithEA** is the main variable that belongs to this category, corresponding to the PF isolation defined in a cone of size  $\Delta R = 0.3$  around the electron direction and relative to the electron  $p_T$ , and taking into account the Pile Up (PU) contamination in this cone.
- The **tracking quality variables**, such as:
  - The **expected inner hits**, the number of pixels without corresponding hits in the trajectory of a reconstructed gsfTrack.
  - The **matched gsfTracks hits**, the  $\chi^2$  value calculated from the reconstructed gskTrack and its corresponding hits.
- The **conversion rejection variables**, mostly used to reject most of the photon conversion contamination when defining electrons, using variable such as:
  - The **transverse  $d_0$**  (or  $d_{xy}$ ) and **longitudinal  $d_z$  impact parameters**.
  - The **conversion veto**, checking if an electron candidate also matches at least one conversion candidate which also passes the selection cuts.

In this analysis, instead of relying on the four basic Physics Object Group (POG) official Working Points (WPs) (veto, loose, medium and tight) that can be defined with some quality cuts, we rely on the Multi-Variate Analysis (MVA) approach that consists in using a single discriminator variable to perform the discrimination between genuine and misidentified electrons, combining the information coming from more than 20 variables at once using Boosted Decision Trees (BDT).

Two WPs are then given directly by the CMS EGamma POG [128], corresponding to an electron selection efficiency of 80 and 90% respectively. For this analysis, the tight POG *mva\_90p\_Iso2016* (for 2016) and *mvaFall17V1Iso\_WP90* (for 2017 and 2018) WPs have been chosen for the electron definition, along with additional quality cuts defined in Tables 3.4 and 3.5 (as previously mentioned, these cuts sometimes differ quite a bit depending on whether the electron interacts with the ECAL barrel ( $|\eta| < 1.479$ ) or one of the endcaps ( $|\eta| \geq 1.479$ )).

The electron efficiencies computed for this particular selection can be seen in Figure 3.2.

### 3.1.3 Muons selection

The selection applied to muons is mostly based on the Muon POG, providing references efficiencies for standard selection, recommendations for the tight selection [129], with a few additional cuts on both the impact parameters.

At the end of the day, a muon can be labeled as **Tight POG** if:

- The PF muon reconstructed is a global muon.

Variable		Barrel cut ( $ \eta  \leq 1.479$ )	Endcap cut ( $ \eta  > 1.479$ )
<b>Basic selection</b>			
$ \eta $	<	-	2.5
<b>HLT safe selection</b>			
hOverE	<	0.060	0.065
ooEmooP	<	0.013	0.013
$ \text{dEtaInSee}(\Delta\eta) $	<	0.004	-
$ \text{dPhiInSee}(\Delta\phi) $	<	0.020	-
$\sigma_{\eta\eta}$	<	0.011	0.031
ecalPFClusterIso	<	0.160	0.120
hcalPFClusterISO	<	0.120	0.120
trackIso	<	0.08	0.08
GsfTrack $\chi^2/\text{NDOF}$	<	-	3.0
<b>Additional selection</b>			
lostHits	<	1	1
$d_{xy}$	<	0.05	0.1
$d_z$	<	0.1	0.2
pfRelIso03	<	0.0588	0.0571

Table 3.4: Quality cuts applied to define a 2016 tight electron in this analysis.

- The  $\chi^2/\text{NDOF}$  of the global muon track fit is less than 10 and at least one muon chamber hit is included in the global muon track fit
- Muon segments in at least two muon stations have been observed.
- Its tracker track has a transverse impact parameter  $d_{xy} < 0.2$  cm and a longitudinal impact parameter  $d_z < 0.5$  cm with respect to the PV .
- The number of pixel hits is larger than 0.
- At least 5 tracker layers with hits have been observed.

The selection applied to muons of this particular analysis is a bit tighter though, since the following cuts are applied on top of this selection:

- $p_T > 10$  GeV,  $|\eta| < 2.4$  and  $|d_z| < 0.1$  cm
- $|d_{xy}| < 0.01$  cm (if  $p_T < 20$  GeV) or  $|d_{xy}| < 0.02$  cm (if  $p_T \geq 20$  GeV)
- Tight muon isolation requirement ( $< 0.15$ ) with  $\Delta\beta$  correction and in a cone size  $\Delta R < 0.4$ , as defined in Equation 3.1, in order to reduce the number of muons coming from the hadronization process of bottom and charm quarks.

$$\text{ISO} = \frac{\sum p_T^{\text{ch. had. (PV)}} + \max(0, \sum E_T^{\text{neut. had.}} + \sum E_T^\gamma - 0.5 \times \sum p_T^{\text{ch. had. (PU)}})}{p_T(\mu)} \quad (3.1)$$

Variable		Barrel cut ( $ \eta  \leq 1.479$ )	Endcap cut ( $ \eta  > 1.479$ )
<b>Basic selection</b>			
$ \eta $	<	-	2.5
convVeto	=	1	1
$d_{xy}$	<	0.05	0.1
$d_z$	<	0.1	0.2
pfRelIso03	<	0.06	0.06

Table 3.5: Quality cuts applied to define a 2017/2018 tight electron in this analysis.

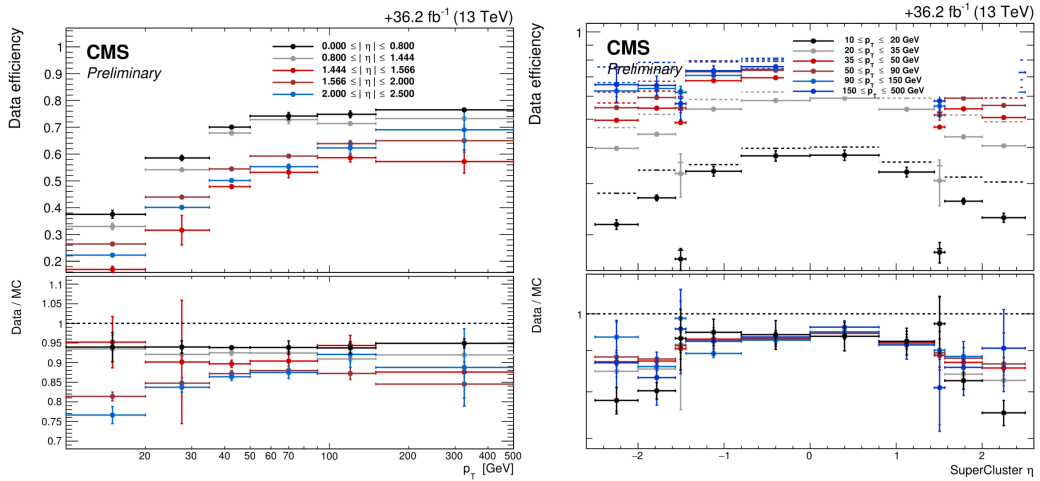


Figure 3.2: Tight electron efficiencies for this analysis, based on the Egamma POG `mva_90p_Iso2016` WP, for the data taking period of 2016.

This selection leads to efficiencies higher than 80% for all the muon momenta and pseudorapidities range, as shown in Figure 3.3.

### 3.1.4 Jet selection

Jets are an important part of this analysis as well given the final state searched for in this case. As explained in Section ??, the jets are clustered from the PF candidates using the anti-kT algorithm (with a typical distance parameter  $R = 0.4$ ).

A selection is then applied on these jets in order to separate noise from real jets. In this analysis, this selection follows the tight WP definition given by the CMS JET/MET POG [130], whose selection depends on the pseudorapidity of the jet and on the year of data taking, as shown in Tables 3.6 and 3.7. The tight WP has been chosen since it offers an efficiency higher than 98-99% for all the jets and a background rejection higher than 98% for jets having  $|\eta| < 3.0$ .

A slightly different selection (loose PU jet ID) is applied to jets having a  $p_T > 50$  GeV in order to reject jets coming from PU interactions in 2017 and 2018, as shown in Table 3.8.

The b-jets are then also select using the recommendations given by the B-Tagging and Vertexing POG [131]. The loose deepCSV b-tagging WP is used in this case, as explained in Section ??, for which the rate for misidentifying a light jet as a b-jet is around 10%. A jet is considered a b-jet in

$p_T/\eta$	-2.4:-2.1	-2.1:-1.6	-1.6:-1.2	-1.2:-0.8	-0.8:-0.3	-0.3:-0.2	-0.2:0.0	0.0:0.2	0.2:0.3	0.3:0.8	0.8:1.2	1.2:1.6	1.6:2.1	2.1:2.4
10:15	0.9995	1.0016	0.9985	0.9907	0.9844	1.0183	1.0089	1.0089	1.0265	0.9862	0.9808	0.9882	0.9927	0.9972
15:20	0.9805	0.9870	0.9950	0.9867	0.9935	0.9686	0.9927	0.9927	0.9771	0.9924	0.9826	0.9986	0.9912	0.9797
20:25	0.9756	0.9829	0.9949	0.9823	0.9914	0.9712	0.9906	0.9910	0.9590	0.9917	0.9776	0.9927	0.9873	0.9822
25:30	0.9793	0.9850	0.9942	0.9794	0.9912	0.9659	0.9899	0.9886	0.9610	0.9899	0.9784	0.9932	0.9874	0.9805
30:40	0.9773	0.9828	0.9947	0.9782	0.9891	0.9685	0.9903	0.9883	0.9614	0.9887	0.9770	0.9940	0.9876	0.9828
40:60	0.9766	0.9851	0.9957	0.9796	0.9908	0.9713	0.9911	0.9894	0.9638	0.9898	0.9786	0.9945	0.9871	0.9774
60:100	0.9618	0.9794	0.9963	0.9773	0.9917	0.9597	0.9914	0.9886	0.9655	0.9883	0.9764	0.9948	0.9858	0.9796
100:200	0.9803	0.9743	0.9831	0.9740	0.9949	0.9634	0.9954	0.9814	0.9482	0.9870	0.9732	0.9962	0.9782	0.9895

Color Definition

Scale Factors	0.99-1.01	0.98-0.99,1.01-1.02	0.97-0.98,1.02-1.03	0.96-0.97	0.95-0.96	< 0.95
---------------	-----------	---------------------	---------------------	-----------	-----------	--------

(a) 2016 muon efficiencies

$p_T/\eta$	-2.4:-2.1	-2.1:-1.6	-1.6:-1.2	-1.2:-0.8	-0.8:-0.3	-0.3:-0.2	-0.2:0.0	0.0:0.2	0.2:0.3	0.3:0.8	0.8:1.2	1.2:1.6	1.6:2.1	2.1:2.4
10:15	0.9880	0.9827	0.9981	0.9961	1.0018	1.0099	1.0129	1.0129	1.0193	0.9893	0.9767	0.9978	0.9901	0.9852
15:20	0.9735	0.9831	0.9955	0.9849	0.9995	0.9582	0.9932	0.9932	0.9400	0.9891	0.9813	0.9970	0.9899	0.9807
20:25	0.9737	0.9839	0.9976	0.9863	0.9940	0.9561	0.9936	0.9963	0.9757	0.9915	0.9800	0.9975	0.9892	0.9771
25:30	0.9741	0.9819	0.9975	0.9852	0.9931	0.9580	0.9936	0.9952	0.9619	0.9914	0.9790	0.9979	0.9905	0.9826
30:40	0.9719	0.9794	0.9973	0.9842	0.9935	0.9570	0.9932	0.9942	0.9635	0.9921	0.9781	0.9972	0.9900	0.9815
40:60	0.9709	0.9815	0.9979	0.9849	0.9941	0.9556	0.9945	0.9953	0.9636	0.9924	0.9790	0.9966	0.9896	0.9800
60:100	0.9622	0.9779	0.9959	0.9842	0.9935	0.9525	0.9938	0.9944	0.9563	0.9918	0.9747	0.9967	0.9868	0.9887
100:200	0.9649	0.9732	0.9899	0.9851	0.9884	0.9645	1.0060	0.9953	0.9831	0.9872	0.9738	0.9981	0.9868	0.9635

Color Definition

Scale Factors	0.99-1.01	0.98-0.99	0.97-0.98	0.96-0.97	0.95-0.96	< 0.95
---------------	-----------	-----------	-----------	-----------	-----------	--------

(b) 2017 muon efficiencies

$p_T/\eta$	-2.4:-2.1	-2.1:-1.6	-1.6:-1.2	-1.2:-0.8	-0.8:-0.3	-0.3:-0.2	-0.2:0.0	0.0:0.2	0.2:0.3	0.3:0.8	0.8:1.2	1.2:1.6	1.6:2.1	2.1:2.4
10:15	0.9686	0.9806	0.9996	0.9801	0.9975	0.9895	1.0053	1.0053	0.9446	0.9908	0.9763	0.9984	0.9967	0.9726
15:20	0.9683	0.9817	0.9974	0.9836	0.9951	0.9513	0.9925	0.9925	0.9678	0.9901	0.9849	0.9945	0.9888	0.9810
20:25	0.9681	0.9826	0.9979	0.9874	0.9963	0.9670	0.9936	0.9986	0.9725	0.9921	0.9835	0.9967	0.9899	0.9786
25:30	0.9679	0.9821	0.9977	0.9858	0.9960	0.9779	0.9943	0.9918	0.9795	0.9941	0.9804	0.9964	0.9890	0.9742
30:40	0.9688	0.9789	0.9970	0.9848	0.9956	0.9778	0.9933	0.9946	0.9740	0.9930	0.9814	0.9957	0.9885	0.9749
40:60	0.9672	0.9802	0.9967	0.9856	0.9964	0.9752	0.9950	0.9952	0.9743	0.9943	0.9821	0.9958	0.9875	0.9761
60:100	0.9652	0.9756	0.9959	0.9835	0.9957	0.9725	0.9919	0.9946	0.9760	0.9931	0.9803	0.9945	0.9853	0.9702
100:200	0.9500	0.9750	0.9944	0.9839	0.9976	0.9688	0.9984	0.9890	0.9460	0.9925	0.9778	0.9954	0.9780	0.9881

Color Definition

Scale Factors	0.99-1.01	0.98-0.99	0.97-0.98	0.96-0.97	0.95-0.96	< 0.95
---------------	-----------	-----------	-----------	-----------	-----------	--------

(c) 2018 muon efficiencies

Figure 3.3: Tight muon efficiencies for this analysis, based on the Muon POG tight WP with additional cuts for 2016, 2017 and 2018.

this analysis if it passes the following cuts:

- $p_T > 20 \text{ GeV}$
- $|\eta| < 2.4$
- $\text{deepCSV} > 0.1241$

## 3.2 Signals regions

It is important to note that a strict **blinding policy** has been followed for this search, in order to avoid optimizing the analysis based on what has already seen. The data available to be plotted in the following signal regions has therefore been limited to  $1 \text{ fb}^{-1}$  for each year.

Two signal regions have been defined in order to isolate on one hand the  $t/\bar{t}+\text{DM}$  process and on the other hand the  $t\bar{t}+\text{DM}$  signal.

Variable	$ \eta  \leq 2.4$	$ \eta  \leq 2.7$	$2.7 <  \eta  \leq 3.0$	$ \eta  > 3.0$
Neutral Hadron Fraction	< 0.90	< 0.90	< 0.98	-
Neutral EM Fraction	< 0.99	< 0.99	> 0.01	< 0.90
Number of Constituents	> 1	> 1	-	-
Charged Hadron Fraction	> 0	-	-	-
Charged Multiplicity	> 0	-	-	-
Charged EM Fraction	< 0.99	-	-	-
Number of Neutral Particles	-	-	> 2	> 10

Table 3.6: JET/MET POG tight WP for 2016.

Variable	$ \eta  \leq 2.4$	$ \eta  \leq 2.7$	$2.7 <  \eta  \leq 3.0$	$ \eta  > 3.0$
Neutral Hadron Fraction	< 0.90	< 0.90	-	> 0.02
Neutral EM Fraction	< 0.90	< 0.90	> 0.02 and < 0.99	< 0.90
Number of Constituents	> 1	> 1	-	-
Charged Hadron Fraction	> 0	-	-	-
Charged Multiplicity	> 0	> 0	-	-
Number of Neutral Particles	-	-	> 2	> 10

Table 3.7: JET/MET POG tight WP for 2017 and 2018.

### 3.2.1 $t/\bar{t}$ +DM region

As shown in Figure 3.4

To be added once defined

### 3.2.2 $t\bar{t}$ +DM region

As shown in Figure 3.5

Variable	$ \eta  \leq 2.4$	$ \eta  \leq 2.7$	$2.7 <  \eta  \leq 3.0$	$ \eta  > 3.0$
Neutral Hadron Fraction	< 0.90	< 0.90	< 0.99	> 0.02
Neutral EM Fraction	< 0.90	< 0.90	-	< 0.90
Number of Constituents	> 1	> 1	-	-
Charged Hadron Fraction	> 0	-	-	-
Charged Multiplicity	> 0	-	-	-
Number of Neutral Particles	-	-	-	> 2 and < 15

Table 3.8: JET/MET POG tight WP for 2017 and 2018, for jets having a  $p_T > 50$  GeV.

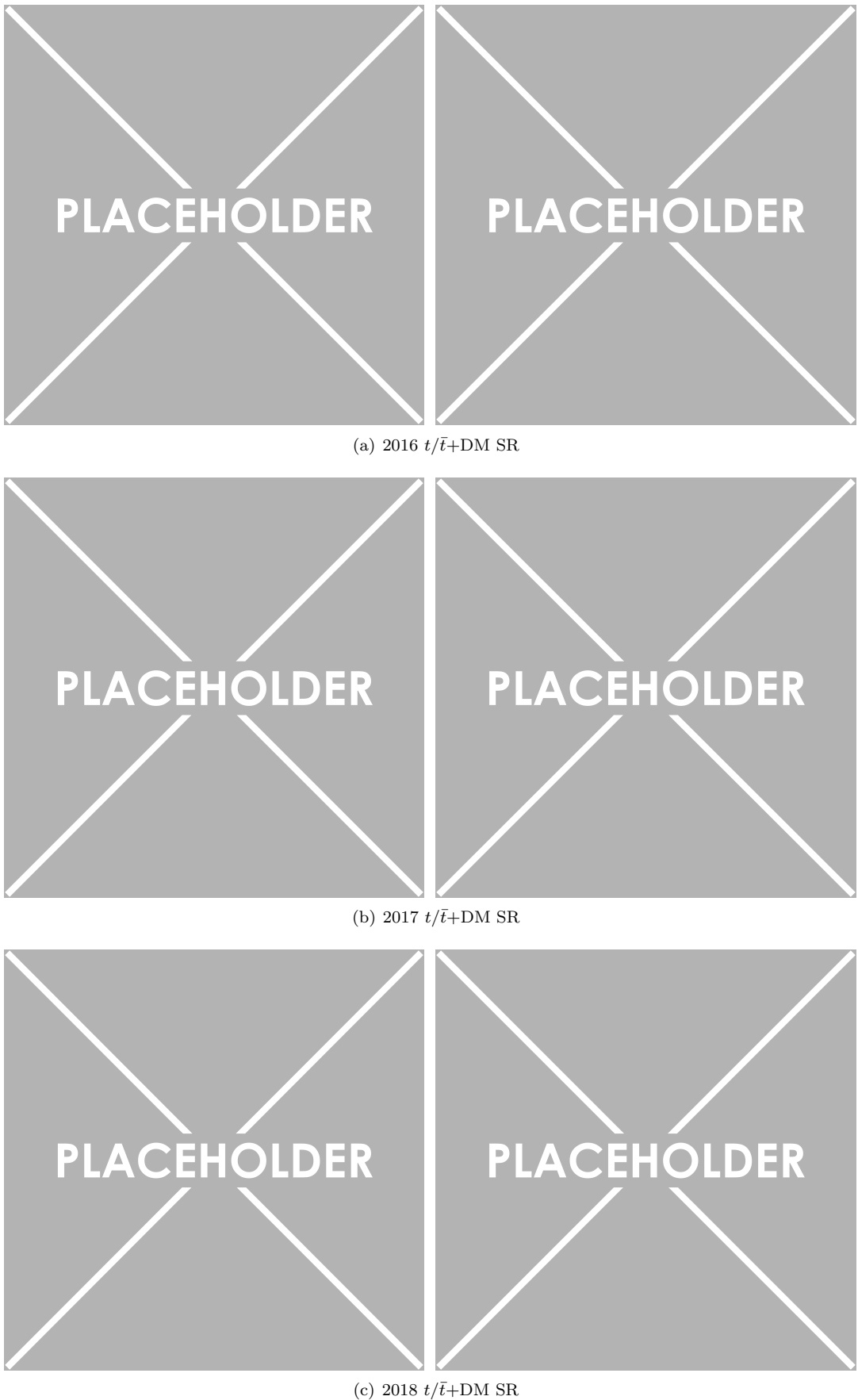


Figure 3.4: Two different variables ( $m_{ll}$ , on the left, and Pileup Per Particle Identification (PUPPI) MET, on the right) represented in the signal region defined to study the  $t/\bar{t}$ +DM process.

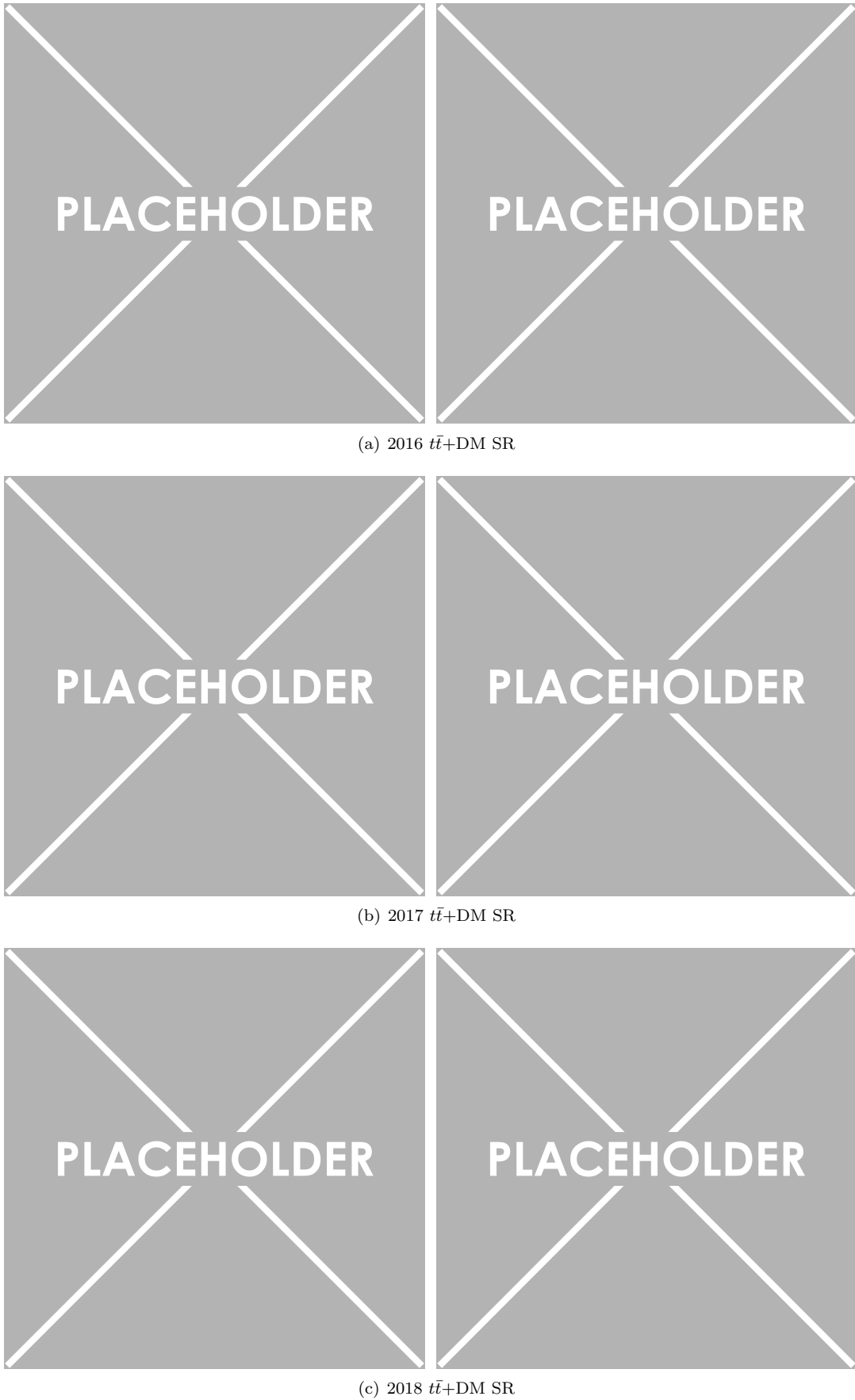


Figure 3.5: Two different variables ( $m_{ll}$ , on the left, and PUPPI MET, on the right) represented in the signal region defined to study the  $t\bar{t}$ +DM process.

To be added once defined

### 3.3 Control regions

Different control regions where the data/MC agreement can be checked have been defined in order to check the validity of the MC simulations performed for the SM processes corresponding to the main backgrounds of this analysis.

In this context, the DY control region will be defined in Section 3.3.1 while the SM  $t\bar{t}$ , WW and ttV processes will be checked in the Sections 3.3.2, ?? and 3.3.3 respectively.

#### 3.3.1 DY control region

As shown in Figure 3.6

To be added once defined

#### 3.3.2 Top control region

As shown in Figure 3.7

To be added once defined

#### 3.3.3 ttV control region

As shown in Figure 3.8

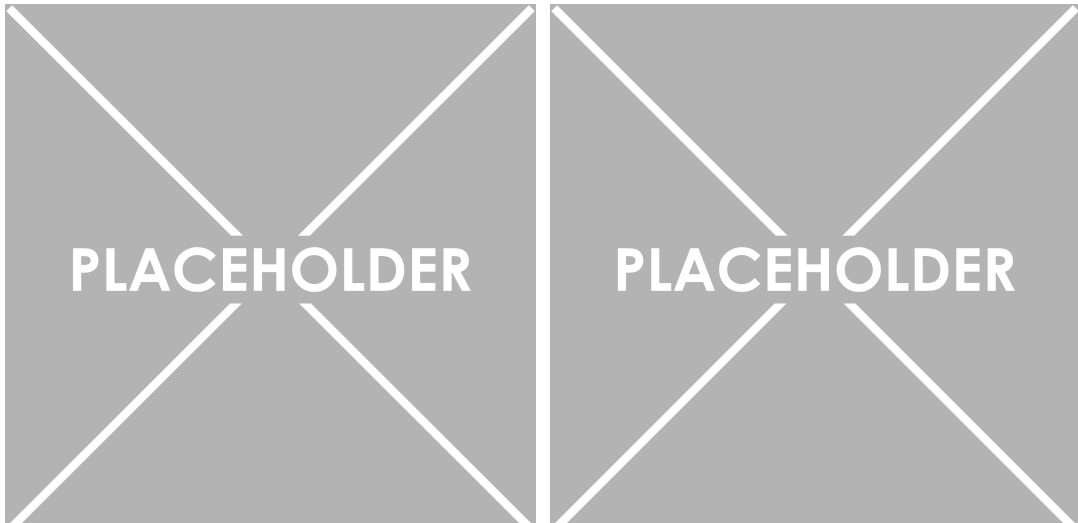
To be added once defined

#### 3.3.4 Same sign control region

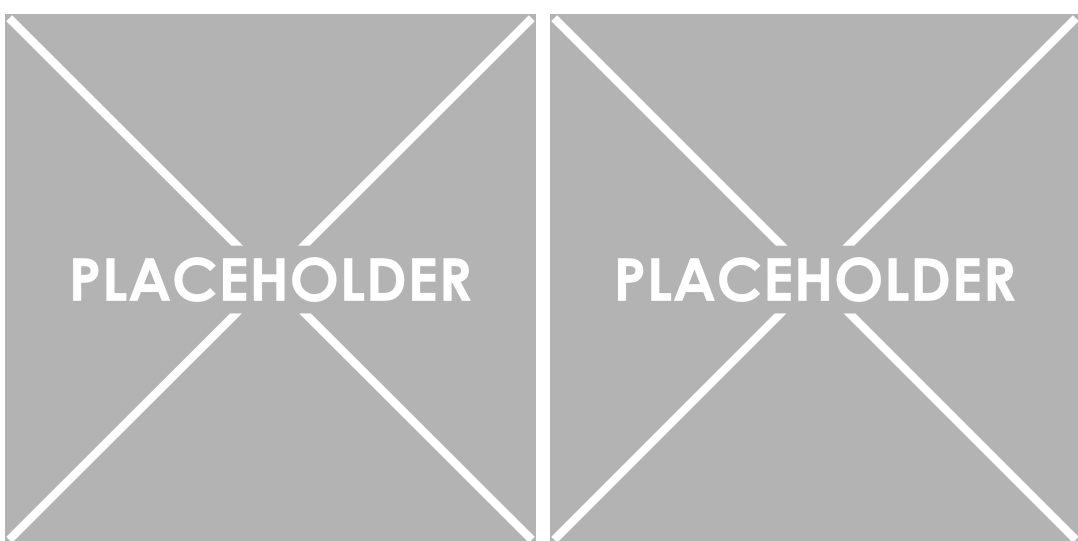
A same sign control region has also been defined in order to check the non-prompt background, calculated using a data-driven tight-to-loose method described in Section ???. This CR is defined with the following cuts:

- Exactly 2 same sign leptons
- $p_{T,1} > 20$  (25) GeV for  $e$  ( $\mu$ )
- $p_{T,2} > 13$  GeV
- $|\eta| < 2.5$  for both leptons
- $m_{ll} > 12$  GeV
- PuppiMET  $> 20$  GeV
- $p_T^{ll} > 30$  GeV
- $m_{th} > 60$  GeV

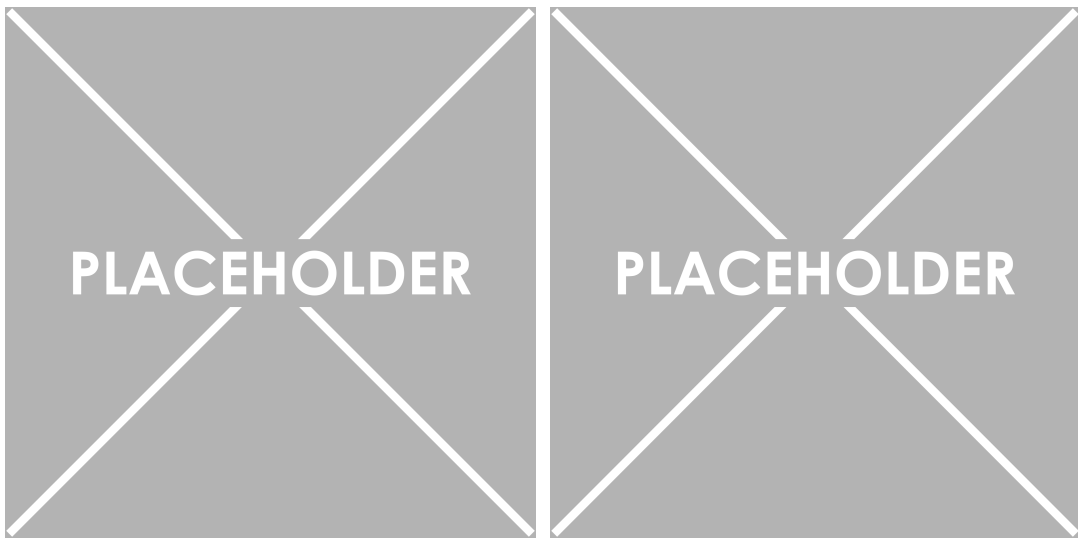
Several regions are then defined according to this cut, depending on the data taking period, on the channel, on the number of jets observed and on the  $p_T$  of the second lepton. Some plots can be found in Figure 3.9.



(a) 2016 DY CR

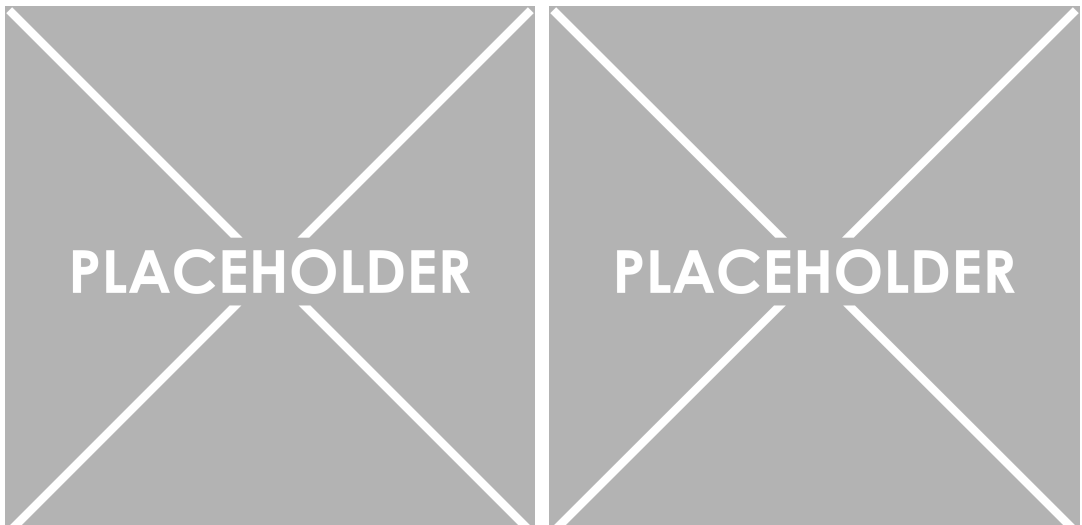


(b) 2017 DY CR

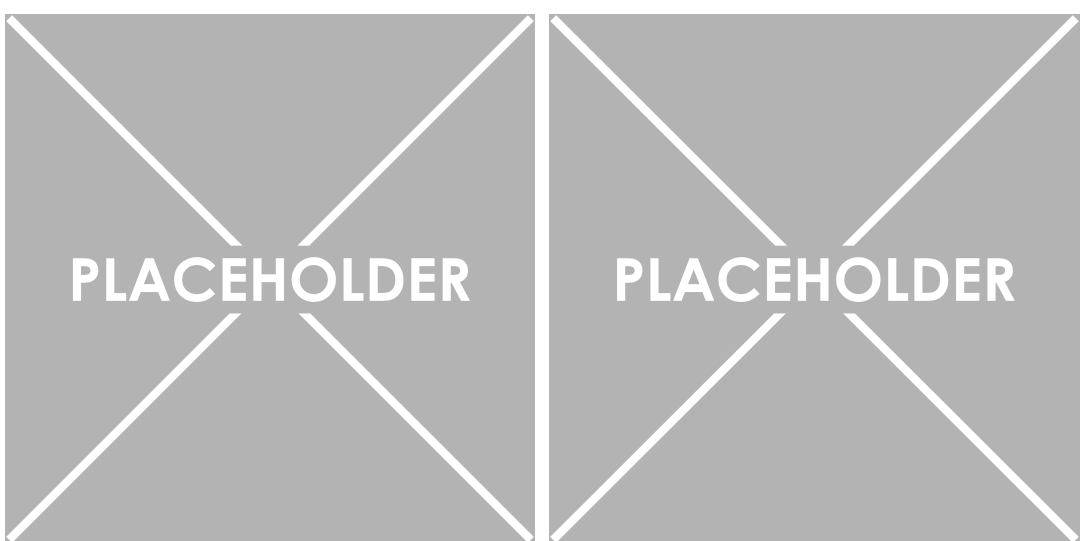


(c) 2018 DY CR

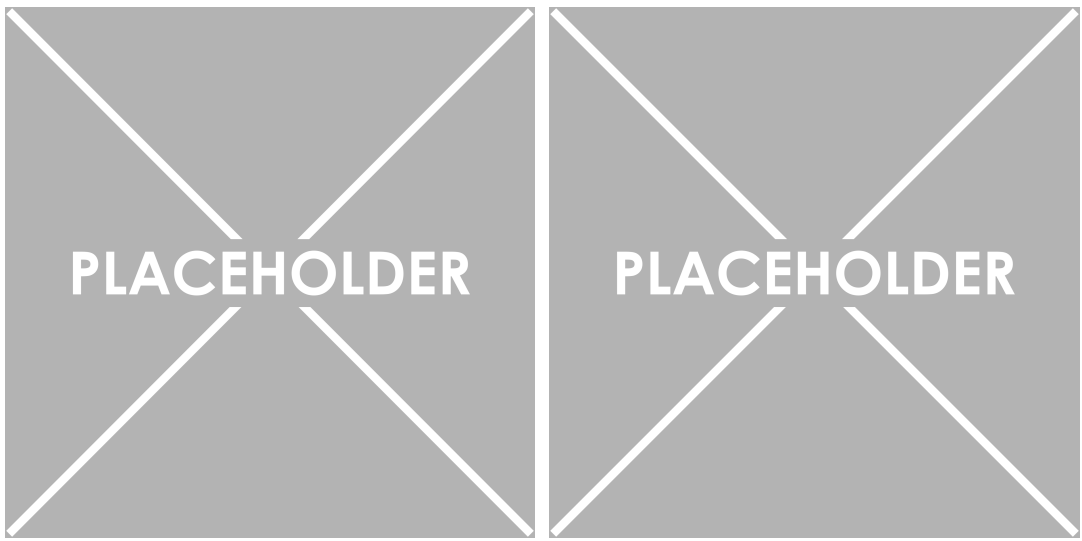
Figure 3.6: Two different variables ( $m_{ll}$ , on the left, and PUPPI MET, on the right) represented in the DY control region defined.



(a) 2016 top CR

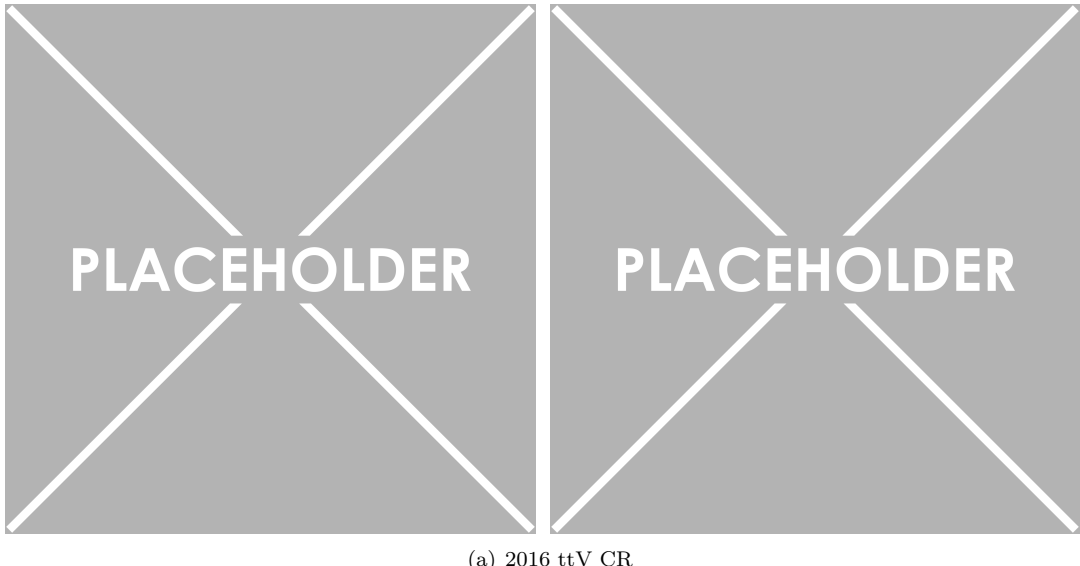


(b) 2017 top CR

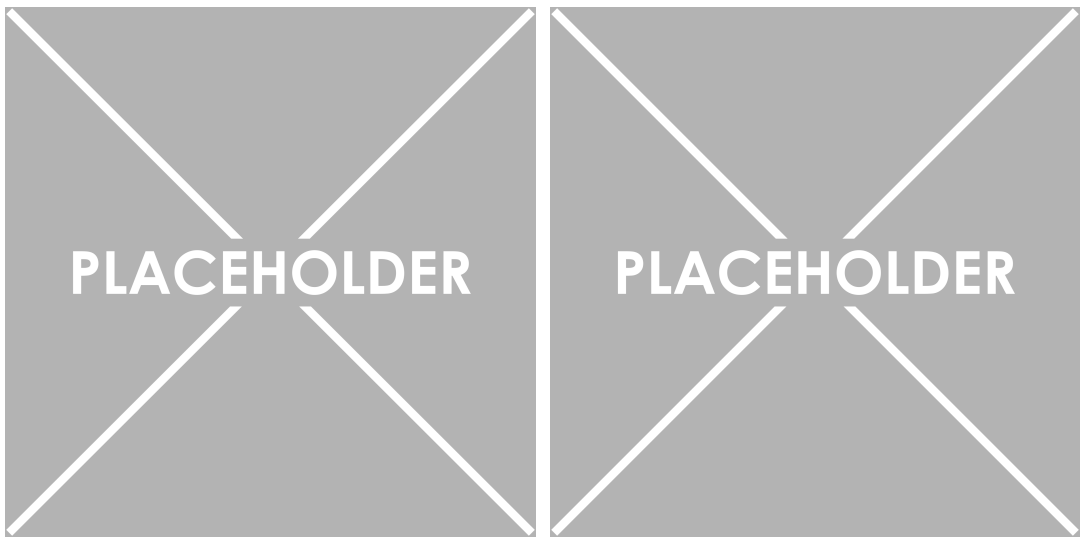


(c) 2018 top CR

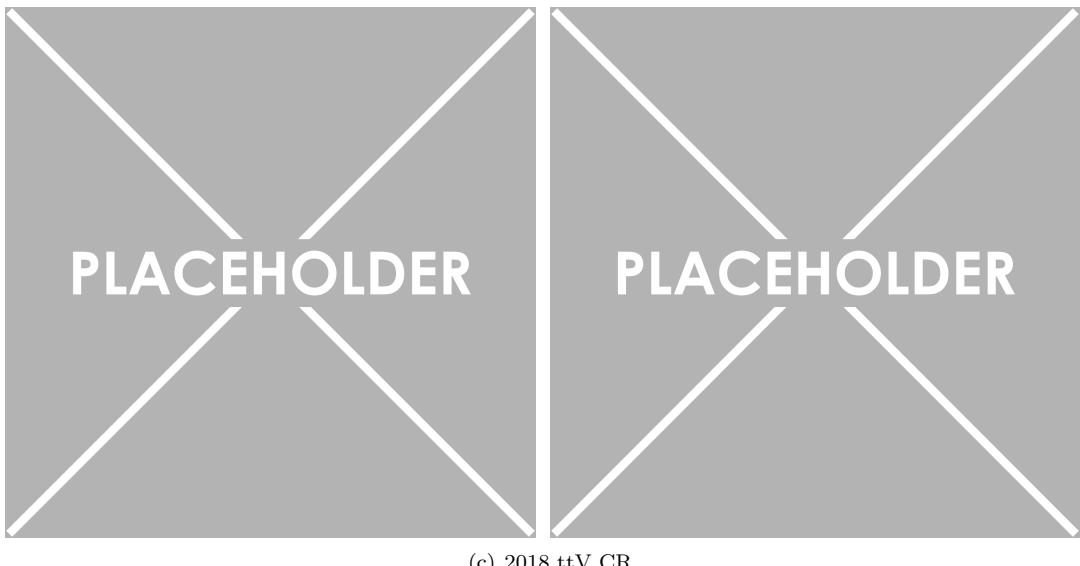
Figure 3.7: Two different variables ( $m_{ll}$ , on the left, and PUPPI MET, on the right) represented in the top control region defined.



(a) 2016  $ttV$  CR

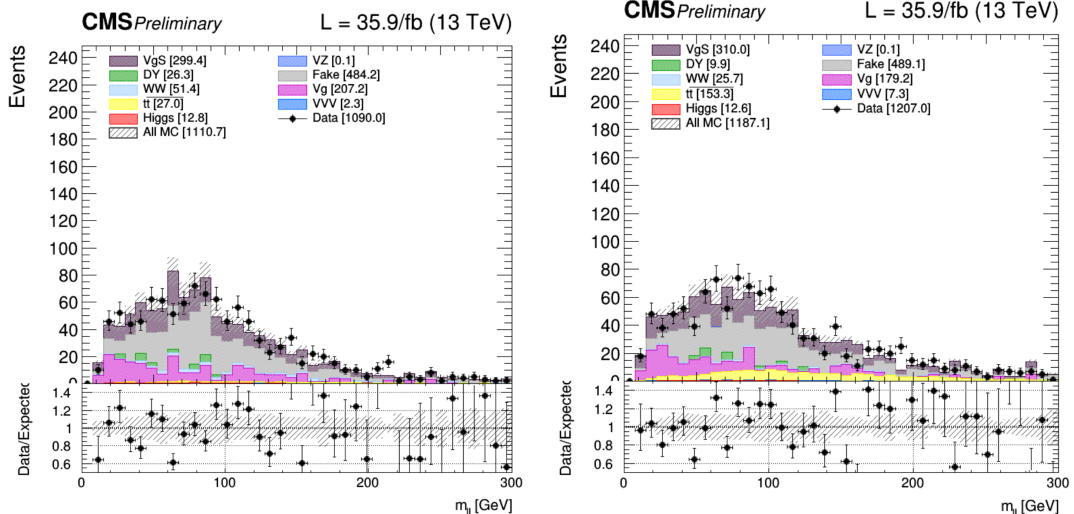


(b) 2017  $ttV$  CR

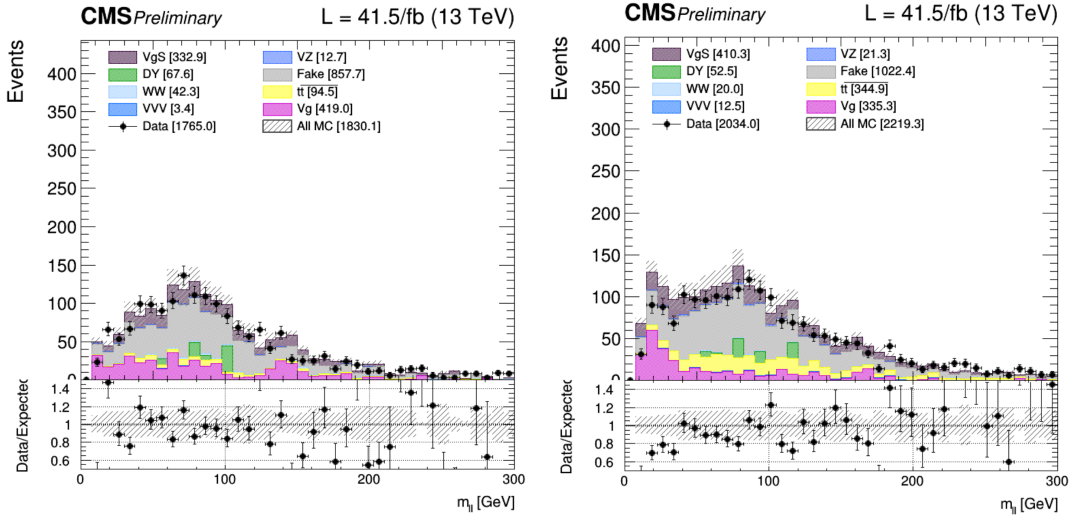


(c) 2018  $ttV$  CR

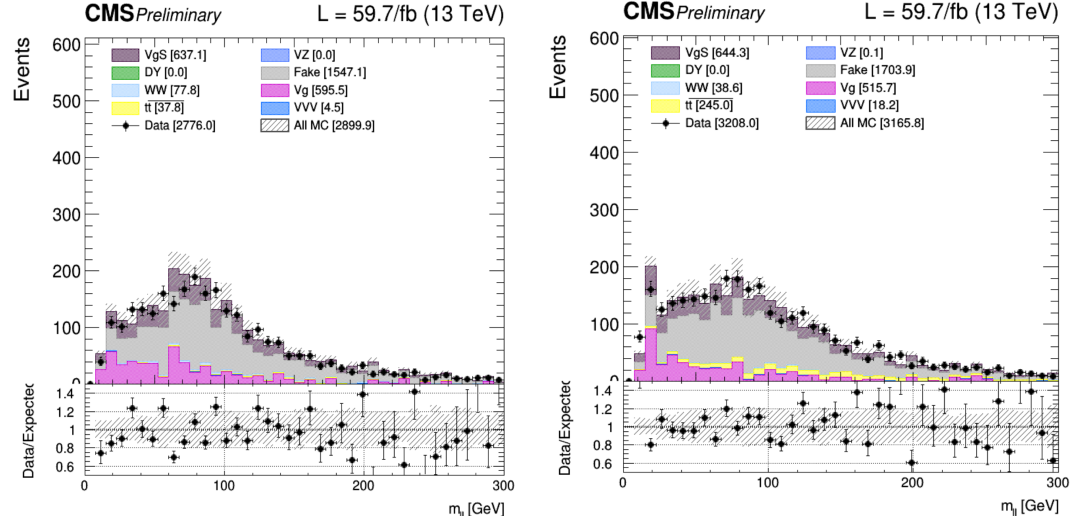
Figure 3.8: Two different variables ( $m_{ll}$ , on the left, and PUPPI MET, on the right) represented in the  $ttV$  control region defined.



(a) 2016 same sign control plots



(b) 2017 same sign control plots



(c) 2018 same sign control plots

Figure 3.9: Same sign control region  $m_{ll}$  distributions for the years 2016, 2017 and 2018 and for the  $e\mu$  channel and for the 0-jet (on the left) and 1j (on the right) categories.

In order to cover for most of the discrepancies between the data and the simulation observed in the distributions of this control region, a flat 30% systematic uncertainty is typically associated to this background, as will be discussed in more details in Section 4.1.

## 3.4 Background-signal discrimination

### 3.4.1 Discriminating variables

#### Missing Transverse Energy (MET)

This variable has already been defined in Section ??, and corresponds to the imbalance in transverse momentum which can be left by different phenomena, such as the apparition of a SM neutrino or the existence of DM particles, able to escape the detector without being detected.

This variable is expected to induce some discrimination between the signal and the backgrounds because, even tough the  $t\bar{t}$  in the dilepton final state is expected to produce two neutrinos and therefore some MET, the  $t\bar{t}$ +DM signal model is expected to have mostly the same contribution to the MET from its own two neutrinos, and an additional contributions from the pair  $\chi\bar{\chi}$  produced. The MET spectrum is therefore expected to reach higher values for the signal than the backgrounds.

TALK ABOUT SINGLE TOP?

#### Stransverse mass

The  $m_{T2}$  variable, also called **stransverse mass**, is an extension of the definition of the transverse mass  $m_T$  to cases when pairs of particles with the same flavor decay into one visible and one invisible particle, such as what happens in the  $W \rightarrow l\nu$  decay, for example.

In this particular case, two particles contribute to the presence of Missing Transverse Energy (MET) and the individual contribution of each particle ( $\not{p}_{T_1}$  and  $\not{p}_{T_2}$ ) to this missing energy cannot be inferred. The stransverse mass is then defined according to Equation 3.2, where  $\not{p}_{T_i} = \overrightarrow{p_{T_i}}$  is the (visible) transverse momentum of the particle  $i$  and  $\alpha$  is the angle between the visible and invisible  $p_T$  of the decay considered [120].

$$\begin{cases} M_{T2}^2 = \min_{\not{p}_{T_1} + \not{p}_{T_2} = \not{p}_{T_{\text{tot}}}} \left( \max \left( m_T^2(\not{p}_{T_1}, \not{p}_{T_1}), m_T^2(\not{p}_{T_2}, \not{p}_{T_2}) \right) \right) \\ m_T^2(\not{p}_T, \not{p}'_T) = 4 |\not{p}_T| |\not{p}'_T| \sin^2 \left( \frac{\alpha}{2} \right) \end{cases} \quad (3.2)$$

This equation can be understood in the following way: to compute the  $m_{T2}$  variable, different combinations  $(\not{p}_{T_1}, \not{p}_{T_2})$  satisfying the condition  $\not{p}_{T_1} + \not{p}_{T_2} = \not{p}_{T_{\text{tot}}}$  need to be probed, keeping only the combination which results in the lowest value.

In this particular analysis,  $M_{T2}(ll)$  is calculated, since the role of the visible particles is played by the two final state leptons. This variable is expected to introduce some discrimination because, according to the definition just given, the  $M_{T2}(ll)$  variable for a SM  $t\bar{t}$  process is expected to have an endpoint exactly at the mass of the W boson, while an eventual  $t\bar{t}$ +DM signal does not have

this limitation in the  $M_{T2}(ll)$  spectrum because of the pair of DM particles produced, which also contributes to the total MET of the event.

However, in practice, we do observe a tail in this spectrum even for SM  $t\bar{t}$  without DM, because of the instrumental MET sometimes observed or the fact that some selected leptons are not actually prompt leptons but can be jets misidentified as leptons by the detector.

TALK ABOUT SINGLE TOP?

### 3.4.2 Neural network



# Chapter 4

## Results and interpretations

### 4.1 Systematics and uncertainties

### 4.2 Results



## Chapter 5

# Conclusions

### 5.1 Future prospects



# **Appendices**



# Appendix A

## Samples used

### A.1 Data samples

All the data samples considered for this analysis are listed in Tables A.1, A.2 and A.3. The luminosity of each dataset has been computed using the Brilcalc tool provided by CMS [132], while the number of generated events has been obtained using the CERN official Data Aggregation System (DAS).

### A.2 Signal samples

To be completed once the files are actually available

### A.3 Backgrounds samples

All the background MC samples considered for this analysis are listed in Tables A.4, A.5 and A.6 for 2016, 2017 and 2018 respectively.

Dataset	Events (size)	$\mathcal{L}$ [fb $^{-1}$ ]
<b>Run 2016B</b>		
/DoubleEG/Run2016B_ver2-Nano1June2019_ver2-v1/NANOAOD	143073268 (99.4Gb)	
/DoubleMuon/Run2016B_ver2-Nano1June2019_ver2-v1/NANOAOD	82535526 (53.2Gb)	
/MuonEG/Run2016B_ver2-Nano1June2019_ver2-v1/NANOAOD	32727796 (26.8Gb)	5.8
/SingleElectron/Run2016B_ver2-Nano1June2019_ver2-v1/NANOAOD	246440440 (167.8Gb)	
/SingleMuon/Run2016B_ver2-Nano1June2019_ver2-v1/NANOAOD	158145722 (96.4Gb)	
<b>Run 2016C</b>		
/DoubleEG/Run2016C-Nano1June2019-v1/NANOAOD	47677856 (35.3Gb)	
/DoubleMuon/Run2016C-Nano1June2019-v1/NANOAOD	27934629 (19.7Gb)	
/MuonEG/Run2016C-Nano1June2019-v1/NANOAOD	15405678 (12.8Gb)	2.6
/SingleElectron/Run2016C-Nano1June2019-v1/NANOAOD	97259854 (69.3Gb)	
/SingleMuon/Run2016C-Nano1June2019-v1/NANOAOD	67441308 (42.4Gb)	
<b>Run 2016D</b>		
/DoubleEG/Run2016D-Nano1June2019-v1/NANOAOD	53324960 (39.6Gb)	
/DoubleMuon/Run2016D-Nano1June2019-v1/NANOAOD	33861745 (24.1Gb)	
/MuonEG/Run2016D-Nano1June2019-v1/NANOAOD	23482352 (19.4Gb)	4.2
/SingleElectron/Run2016D-Nano1June2019-v1/NANOAOD	148167727 (104.4Gb)	
/SingleMuon/Run2016D-Nano1June2019-v1/NANOAOD	98017996 (61.3Gb)	
<b>Run 2016E</b>		
/DoubleEG/Run2016E-Nano1June2019-v1/NANOAOD	49877710 (37.9Gb)	
/DoubleMuon/Run2016E-Nano1June2019-v1/NANOAOD	28246946 (20.8Gb)	
/MuonEG/Run2016E-Nano1June2019-v2/NANOAOD	22519303 (19.0Gb)	4.0
/SingleElectron/Run2016E-Nano1June2019-v1/NANOAOD	117321545 (86.5Gb)	
/SingleMuon/Run2016E-Nano1June2019-v1/NANOAOD	90984718 (58.7Gb)	
<b>Run 2016F</b>		
/DoubleEG/Run2016F-Nano1June2019-v1/NANOAOD	34577629 (26.9Gb)	
/DoubleMuon/Run2016F-Nano1June2019-v1/NANOAOD	20329921 (15.3Gb)	
/MuonEG/Run2016F-Nano1June2019-v1/NANOAOD	16002165 (13.6Gb)	3.1
/SingleElectron/Run2016F-Nano1June2019-v1/NANOAOD	70593532 (51.4Gb)	
/SingleMuon/Run2016F-Nano1June2019-v1/NANOAOD	65489554 (42.4Gb)	
<b>Run 2016G</b>		
/DoubleEG/Run2016G-Nano1June2019-v1/NANOAOD	78797031 (61.6Gb)	
/DoubleMuon/Run2016G-Nano1June2019-v1/NANOAOD	45235604 (34.2Gb)	
/MuonEG/Run2016G-Nano1June2019-v1/NANOAOD	33854612 (29.0Gb)	7.6
/SingleElectron/Run2016G-Nano1June2019-v1/NANOAOD	153363109 (109.2Gb)	
/SingleMuon/Run2016G-Nano1June2019-v1/NANOAOD	149912248 (94.6Gb)	
<b>Run 2016H</b>		
/DoubleEG/Run2016H-Nano1June2019-v1/NANOAOD	85388734 (67.7Gb)	
/DoubleMuon/Run2016H-Nano1June2019-v1/NANOAOD	48912812 (37.3Gb)	
/MuonEG/Run2016H-Nano1June2019-v1/NANOAOD	29236516 (26.0Gb)	8.6
/SingleElectron/Run2016H-Nano1June2019-v1/NANOAOD	128854598 (93.8Gb)	
/SingleMuon/Run2016H-Nano1June2019-v1/NANOAOD	174035164 (110.2Gb)	

Table A.1: Datasets collected in 2016 and considered for this analysis.

Dataset	Events (size)	$\mathcal{L}$ [fb $^{-1}$ ]
<b>Run 2017B</b>		
/DoubleEG/Run2017B-Nano1June2019-v1/NANOAOD	58088760 (46.6Gb)	4.8
/DoubleMuon/Run2017B-Nano1June2019-v1/NANOAOD	14501767 (10.8Gb)	
/SingleElectron/Run2017B-Nano1June2019-v1/NANOAOD	60537490 (42.2Gb)	
/SingleMuon/Run2017B-Nano1June2019-v1/NANOAOD	136300266 (86.2Gb)	
/MuonEG/Run2017B-Nano1June2019-v1/NANOAOD	4453465 (4.1Gb)	
<b>Run 2017C</b>		
/DoubleEG/Run2017C-Nano1June2019-v1/NANOAOD	65181125 (53.8Gb)	9.7
/DoubleMuon/Run2017C-Nano1June2019-v1/NANOAOD	49636525 (39.5Gb)	
/SingleElectron/Run2017C-Nano1June2019-v1/NANOAOD	136637888 (102.5Gb)	
/SingleMuon/Run2017C-Nano1June2019-v1/NANOAOD	165652756 (109.5Gb)	
/MuonEG/Run2017C-Nano1June2019-v1/NANOAOD	15595214 (15.0Gb)	
<b>Run 2017D</b>		
/DoubleEG/Run2017D-Nano1June2019-v1/NANOAOD	25911432 (21.6Gb)	4.2
/DoubleMuon/Run2017D-Nano1June2019-v1/NANOAOD	23075733 (18.6Gb)	
/SingleElectron/Run2017D-Nano1June2019-v1/NANOAOD	51526710 (38.5Gb)	
/SingleMuon/Run2017D-Nano1June2019-v1/NANOAOD	70361660 (47.2Gb)	
/MuonEG/Run2017D-Nano1June2019-v1/NANOAOD	9164365 (8.9Gb)	
<b>Run 2017E</b>		
/DoubleEG/Run2017E-Nano1June2019-v1/NANOAOD	56233597 (49.8Gb)	9.3
/DoubleMuon/Run2017E-Nano1June2019-v1/NANOAOD	51589091 (44.4Gb)	
/SingleElectron/Run2017E-Nano1June2019-v1/NANOAOD	102121689 (81.3Gb)	
/SingleMuon/Run2017E-Nano1June2019-v1/NANOAOD	154630534 (111.0Gb)	
/MuonEG/Run2017E-Nano1June2019-v1/NANOAOD	19043421 (19.2Gb)	
<b>Run 2017F</b>		
/DoubleEG/Run2017F-Nano1June2019-v1/NANOAOD	74307066 (67.1Gb)	13.5
/DoubleMuon/Run2017F-Nano1June2019-v1/NANOAOD	79756560 (68.0Gb)	
/SingleElectron/Run2017F-Nano1June2019-v1/NANOAOD	128467223 (105.2Gb)	
/SingleMuon/Run2017F-Nano1June2019-v1/NANOAOD	242135500 (178.3Gb)	
/MuonEG/Run2017F-Nano1June2019-v1/NANOAOD	25776363 (26.3Gb)	

Table A.2: Datasets collected in 2017 and considered for this analysis.

Dataset	Events (size)	$\mathcal{L} [\text{fb}^{-1}]$
<b>Run 2018A</b>		
/DoubleMuon/Run2018A-Nano25Oct2019-v1/NANO AOD	75499908 (62.6Gb)	
/EGamma/Run2018A-Nano25Oct2019-v1/NANO AOD	327843843 (261.8Gb)	13.5
/SingleMuon/Run2018A-Nano25Oct2019-v1/NANO AOD	241608232 (167.7Gb)	
/MuonEG/Run2018A-Nano25Oct2019-v1/NANO AOD	32958503 (32.3Gb)	
<b>Run 2018B</b>		
/DoubleMuon/Run2018B-Nano25Oct2019-v1/NANO AOD	35057758 (28.3Gb)	
/EGamma/Run2018B-Nano25Oct2019-v1/NANO AOD	153822427 (123.1Gb)	6.8
/SingleMuon/Run2018B-Nano25Oct2019-v1/NANO AOD	119918017 (82.3Gb)	
/MuonEG/Run2018B-Nano25Oct2019-v1/NANO AOD	16211567 (15.8Gb)	
<b>Run 2018C</b>		
/DoubleMuon/Run2018C-Nano25Oct2019-v1/NANO AOD	34565869 (27.6Gb)	
/EGamma/Run2018C-Nano25Oct2019-v1/NANO AOD	147827904 (119.2Gb)	6.6
/SingleMuon/Run2018C-Nano25Oct2019-v1/NANO AOD	110032072 (75.7Gb)	
/MuonEG/Run2018C-Nano25Oct2019-v1/NANO AOD	15652198 (15.3Gb)	
<b>Run 2018D</b>		
/DoubleMuon/Run2018D-Nano25Oct2019_ver2-v1/NANO AOD	168605834 (128.6Gb)	
/EGamma/Run2018D-Nano25Oct2019-v1/NANO AOD	751348648 (583.6Gb)	32.0
/SingleMuon/Run2018D-Nano25Oct2019-v1/NANO AOD	513867253 (344.5Gb)	
/MuonEG/Run2018D-Nano25Oct2019_ver2-v1/NANO AOD	71961587 (68.6Gb)	

Table A.3: Datasets collected in 2018 and considered for this analysis.

Process	Sample	Cross section [pb]
DY	DYJetsToLL_M-10to50_TuneCUETP8M1_13TeV-madgraphMLM-pythia8	18610.0
	DYJetsToLL_M-50_TuneCUETP8M1_13TeV-madgraphMLM-pythia8	6025.20
TTTo2L2Nu	TTTo2L2Nu_TuneCUETP8M2_ttHtranche3_13TeV-powheg-pythia8	87.310
Single top	ST_s-channel_4f_leptonDecays_13TeV-amcatnlo-pythia8_TuneCUETP8M1	3.360
	ST_t-channel_antitop_4f_inclusiveDecays_13TeV-powhegV2-madspin-pythia8_TuneCUETP8M1	26.38
	ST_t-channel_top_4f_inclusiveDecays_13TeV-powhegV2-madspin-pythia8_TuneCUETP8M1	44.33
	ST_tW_antitop_5f_inclusiveDecays_13TeV-powheg-pythia8_TuneCUETP8M1	35.60
	ST_tW_top_5f_inclusiveDecays_13TeV-powheg-pythia8_TuneCUETP8M1	35.60
WW	WWTo2L2Nu_13TeV-powheg	12.178
	WWJJToLNuLNu_EWK_noTop_13TeV-madgraph-pythia8	0.34520
	GluGluWWTo2L2Nu_MCFM_13TeV	0.5905
V $\gamma$ /V $\gamma^*$	WGToLNuG_TuneCUETP8M1_13TeV-madgraphMLM-pythia8	405.271
	ZGTo2LG_TuneCUETP8M1_13TeV-amcatnloFXFX-pythia8	131.300
	WZTo3LNu_mllmin01_13TeV-powheg-pythia8	58.59
VZ	ZZTo2L2Nu_13TeV_powheg_pythia8	0.5640
	ZZTo2L2Q_13TeV_powheg_pythia8	3.22
	ZZTo4L_TuneCP5_13TeV_powheg_pythia8	1.212
	WZTo2L2Q_13TeV_amcatnloFXFX_madspin_pythia8	5.595
VVV	ZZZ_TuneCUETP8M1_13TeV-amcatnlo-pythia8	0.01398
	WZZ_TuneCUETP8M1_13TeV-amcatnlo-pythia8	0.05565
	WWZ_TuneCUETP8M1_13TeV-amcatnlo-pythia8	0.16510
	WWW_4F_TuneCUETP8M1_13TeV-amcatnlo-pythia8	0.18331
Non-Prompt	Data-driven (tight-to-loose method)	

Table A.4: Main 2016 MC simulations for the different background processes considered for this analysis and their respective cross sections.

Process	Sample	Cross section [pb]
DY	DYJetsToLL_M-10to50_TuneCP5_13TeV-madgraphMLM-pythia8	18610
	DYJetsToLL_M-50_TuneCP5_13TeV-madgraphMLM-pythia8	6189.39
TTTo2L2Nu	TTTo2L2Nu_TuneCP5_13TeV-powheg-pythia8	87.310
Single top	ST_s-channel_4f_leptonDecays_mtop1715_TuneCP5_PSweights_13TeV-amcatnlo-pythia8	3.360
	ST_t-channel_antitop_4f_inclusiveDecays_TuneCP5_13TeV-powhegV2-madspin-pythia8	26.38
	ST_t-channel_top_4f_inclusiveDecays_TuneCP5_13TeV-powhegV2-madspin-pythia8	44.33
	ST_tW_antitop_5f_inclusiveDecays_TuneCP5_13TeV-powheg-pythia8	35.60
	ST_tW_top_5f_inclusiveDecays_TuneCP5_13TeV-powheg-pythia8	35.60
WW	WWTo2L2Nu_NNPDF31_TuneCP5_PSweights_13TeV-powheg-pythia8	12.178
	WWJJToLNuLNu_EWK_noTop_TuneCP5_13TeV-madgraph-pythia8	0.34520
	GluGluToWWTo*_13TeV_MCFM701_pythia8	0.06387
V $\gamma$ /V $\gamma^*$	WGToLNuG_TuneCP5_13TeV-madgraphMLM-pythia8	405.271
	ZGToLLG_01J_5f_TuneCP5_13TeV-amcatnloFXFX-pythia8	58.83
	WZTo3LNu_mllmin01_NNPDF31_TuneCP5_13TeV_powheg_pythia8	58.59
VZ	ZZTo2L2Nu_13TeV_powheg_pythia8	0.5640
	ZZTo2L2Q_13TeV_amcatnloFXFX_madspin_pythia8	3.22
	ZZTo4L_TuneCP5_13TeV_powheg_pythia8	1.212
	WZTo2L2Q_13TeV_amcatnloFXFX_madspin_pythia8	5.595
VVV	ZZZ_TuneCP5_13TeV-amcatnlo-pythia8	0.01398
	WZZ_TuneCP5_13TeV-amcatnlo-pythia8	0.05565
	WWZ_4F_TuneCP5_13TeV-amcatnlo-pythia8	0.16510
	WWW_4F_TuneCP5_13TeV-amcatnlo-pythia8	0.18331
Non-Prompt	Data-driven (tight-to-loose method)	

Table A.5: Main 2017 MC simulations for the different background processes considered for this analysis and their respective cross sections.

Process	Sample	Cross section [pb]
DY	DYJetsToLL_M-10to50_TuneCP5_13TeV-madgraphMLM-pythia8	18610.0
	DYJetsToLL_M-50_TuneCP5_13TeV-amcatnloFXFX-pythia8	6189.39
TTTo2L2Nu	TTTo2L2Nu_TuneCP5_13TeV-powheg-pythia8	87.310
Single top	ST_s-channel_4f_leptonDecays_TuneCP5_13TeV-madgraph-pythia8	3.360
	ST_t-channel_antitop_4f_InclusiveDecays_TuneCP5_13TeV-powheg-madspin-pythia8	26.38
	ST_t-channel_top_4f_InclusiveDecays_TuneCP5_13TeV-powheg-madspin-pythia8	44.33
	ST_tW_antitop_5f_inclusiveDecays_TuneCP5_13TeV-powheg-pythia8	35.60
	ST_tW_top_5f_inclusiveDecays_TuneCP5_13TeV-powheg-pythia8	35.60
WW	WWTo2L2Nu_NNPDF31_TuneCP5_13TeV-powheg-pythia8	12.178
	WWJJToLNuLNu_EWK_TuneCP5_13TeV-madgraph-pythia8	0.4286
	GluGluToWWTo*_TuneCP5_13TeV_MCFM701_pythia8	0.06387
V $\gamma$ /V $\gamma^*$	WGToLNuG_TuneCP5_13TeV-madgraphMLM-pythia8	405.271
	ZGToLLG_01J_5f_TuneCP5_13TeV-amcatnloFXFX-pythia8	131.300
	WZTo3LNu_mllmin01_NNPDF31_TuneCP5_13TeV_powheg_pythia8	58.59
VZ	ZZTo2L2Nu_TuneCP5_13TeV_powheg_pythia8	0.5640
	ZZTo2L2Q_13TeV_amcatnloFXFX_madspin_pythia8	3.22
	ZZTo4L_TuneCP5_13TeV_powheg_pythia8	1.212
	WZTo2L2Q_13TeV_amcatnloFXFX_madspin_pythia8	5.595
VVV	ZZZ_TuneCP5_13TeV-amcatnlo_pythia8	0.01398
	WZZ_TuneCP5_13TeV-amcatnlo_pythia8	0.05565
	WWZ_TuneCP5_13TeV-amcatnlo_pythia8	0.16510
	WWW_4F_TuneCP5_13TeV-amcatnlo_pythia8	0.18331
Non-Prompt	Data-driven (tight-to-loose method)	

Table A.6: Main 2018 MC simulations for the different background processes considered for this analysis and their respective cross sections.



## Appendix B

### **Neural network optimization**



# List of figures

2.1	Representation of the 12 fermions of the SM [24] along with the main force carriers and the Higgs boson, discovered in 2012 and completing the SM. . . . .	6
2.2	Expected and observed rotation curves of the galaxy NGC 6503 [9]. The black dots correspond to the data and the <i>luminous</i> line corresponds to the rotation curve decreasing as $r^{-1/2}$ expected from Newtonian dynamics. . . . .	8
2.3	Anisotropies at the $10^{-5}$ level in the temperature of the CMB, as observed by the Planck satellite in 2018 [33]. . . . .	9
2.4	Power spectrum of the CMB obtained by Planck, representing the fluctuations of the temperature of the radiation with respect to the angular angle of observation [35].	10
2.5	Mass distributions obtained by the Magellan telescope in the visible (on the left) and the Chandra telescope on the X-rays spectrum (on the right) telescopes of the Bullet Cluser. Being shifted compared to each other, this is yet another clear evidence for the existence of DM [37]. . . . .	11
2.6	Computer simulations for cold (on the left) and warm (on the right) DM scenarios and their impact on a galactic halo at 0 redshift [40]. . . . .	12
2.7	Schematic representation of the freeze-out process, representing the abundance of a 500 GeV DM as $Y_\chi$ with respect to the time and the impact of increasing cross-section annihilation values on this freeze-out abundance [41]. . . . .	13
2.8	Halo fraction upper limits at the 95% CL compared to the mass of the lensing object for different MACHO models considered by the EROS (on the top) and the MACHO (on the bottom) collaborations [45]. . . . .	14
2.9	Neutrino cross section of interaction from the charged current as measured by different experiments over a large range of energies, for both neutrinos $\nu$ and antineutrinos $\bar{\nu}$ [46]. . . . .	15
2.10	3.57 keV emission line detected with a $4.5\sigma$ CL by the XMM-Newton telescope in 2014, which could be a hint of the presence of DM [50]. . . . .	16
2.11	Axions exclusion summary plot and projected coverage of axion searches experiments, such as ADMX, CAST and IAXO [56]. . . . .	17
2.12	Schematic view of the three main DM detection strategies: direct, indirect and collider production searches [59]. . . . .	19
2.13	Nuclear recoil spectra induced in different materials for a given DM WIMP of 100 GeV, assuming a WIMP-nucleon SI cross section [60]. . . . .	20

2.14 Schematic representation of the annual modulation of the WIMP wind introduced by the motion of rotation of the Earth around the Sun [62]. . . . .	20
2.15 Impact of different experimental parameters on the final limits depending on the cross section and WIMP mass (on the left) or sensitivity and exposure (on the right), with respect to the expected limits (black curve) [63]. . . . .	21
2.16 Schematic representation of the three main strategies to detect directly the interaction between DM particles and an ordinary nucleus [63]. . . . .	22
2.17 Exclusion limits obtained by various direct detection experiments considering a SI interaction cross section for low WIMP (on the left) or high WIMP masses (on the right) [63]. . . . .	23
2.18 Observed and expected annual modulation in single hits events in the 2-6 keV energy range by the DAMA experiment [64]. . . . .	23
2.19 Upper limits on the DM annihilation cross section considering $b\bar{b}$ (on the left) and $\mu^+\mu^-$ (on the right) final states as a function of the WIMP mass, for different clusters studied [67]. . . . .	24
2.20 Neutrino spectra for a scalar DM candidate of 1 TeV for different indirect detection experiments and the corresponding background level expected [69]. . . . .	25
2.21 Limits of the decay width of the interaction with respect to the DM mass obtained by both IceCube and AMS [70]. . . . .	26
2.22 Schematic representation of a typical EFT modelization of an LHC event with an ISR object used to trigger the event [59]. . . . .	28
2.23 Schematic representation of a typical collider DM production through s-channel and t-channel processes [72]. . . . .	28
2.24 Schematic representation of a typical mono-X event, with an ISR jet in this case going back-to-back with some MET [59]. . . . .	29
2.25 Observed and expected 95% exclusion limits obtained by different searches of the CMS collaboration as a function the spin-0 scalar (on the left) or pseudoscalar (on the right) mediator. . . . .	30
2.26 Observed and expected 95% exclusion limits obtained by different searches of the CMS collaboration as a function of the spin-1 mediator, considering axial-vector (on the left) and axial (on the right) interactions. . . . .	31
2.27 CMS 90% exclusion limits compared to the most famous direct detection experiments for the SD (on the left) and SI (on the right) scenarios, obtained using similar couplings. . . . .	31
2.28 Feynman diagrams involving the production of DM with a single top quark with its associated t-channel W boson (on the left), or tW (on the center and on the right) production. . . . .	32
2.29 Schematic representation of a typical $t\bar{t}$ +DM event. . . . .	32
2.30 Limits on the DM and mediator masses obtained by ATLAS using $13.3 \text{ fb}^{-1}$ of 13 TeV data, considering scalar (on the left) and pseudoscalar (on the right) mediators [17]. . . . .	33

2.31	Exclusion limits at the 95% CL obtained by ATLAS considering scalar (on the left) and pseudoscalar (on the right) mediators, for a DM mass of 1 GeV [20]. . . . .	34
2.32	95% CL exclusion plots on the signal strength computed as a function of the mediator and DM masses obtained by CMS considering a scalar (on the left) and a pseudoscalar (on the right) mediator for the interaction [22]. . . . .	34
2.33	Expected and observed 95% CL limits on the DM production cross sections shown considering scalar (on the left) and pseudoscalar (on the right) mediators for the interaction [23]. . . . .	35
3.1	DougleEG trigger efficiencies with respect to the $p_T$ (on the left) and $\eta$ (on the right), computed using a tag and probe method, for the 2017 data taking period. . . . .	39
3.2	Tight electron efficiencies for this analysis, based on the Egamma POG <i>mva_90p_Iso2016</i> WP, for the data taking period of 2016. . . . .	42
3.3	Tight muon efficiencies for this analysis, based on the Muon POG tight WP with additional cuts for 2016, 2017 and 2018. . . . .	43
3.4	Two different variables ( $m_{ll}$ , on the left, and PUPPI MET, on the right) represented in the signal region defined to study the $t/\bar{t}$ +DM process. . . . .	45
3.5	Two different variables ( $m_{ll}$ , on the left, and PUPPI MET, on the right) represented in the signal region defined to study the $t\bar{t}$ +DM process. . . . .	46
3.6	Two different variables ( $m_{ll}$ , on the left, and PUPPI MET, on the right) represented in the DY control region defined. . . . .	48
3.7	Two different variables ( $m_{ll}$ , on the left, and PUPPI MET, on the right) represented in the top control region defined. . . . .	49
3.8	Two different variables ( $m_{ll}$ , on the left, and PUPPI MET, on the right) represented in the ttV control region defined. . . . .	50
3.9	Same sign control region $m_{ll}$ distributions for the years 2016, 2017 and 2018 and for the $e\mu$ channel and for the 0-jet (on the left) and 1j (on the right) categories. . . . .	51



# List of tables

3.1	2016 trigger paths considered for this analysis. . . . .	38
3.2	2017 trigger paths considered for this analysis. . . . .	38
3.3	2018 trigger paths considered for this analysis. . . . .	39
3.4	Quality cuts applied to define a 2016 tight electron in this analysis. . . . .	41
3.5	Quality cuts applied to define a 2017/2018 tight electron in this analysis. . . . .	42
3.6	JET/MET POG tight WP for 2016. . . . .	44
3.7	JET/MET POG tight WP for 2017 and 2018. . . . .	44
3.8	JET/MET POG tight WP for 2017 and 2018, for jets having a $p_T > 50$ GeV. . . . .	44
A.1	Datasets collected in 2016 and considered for this analysis. . . . .	62
A.2	Datasets collected in 2017 and considered for this analysis. . . . .	63
A.3	Datasets collected in 2018 and considered for this analysis. . . . .	64
A.4	Main 2016 MC simulations for the different background processes considered for this analysis and their respective cross sections. . . . .	65
A.5	Main 2017 MC simulations for the different background processes considered for this analysis and their respective cross sections. . . . .	66
A.6	Main 2018 MC simulations for the different background processes considered for this analysis and their respective cross sections. . . . .	67



# Bibliography

- [1] G. Altarelli, "The Standard Model of Particle Physics", CERN-PH-TH/2005-206, 2005
- [2] CMS Collaboration, "The CMS Experiment at the CERN LHC", JINST 3 S08004, 2008
- [3] ATLAS Collaboration, "The ATLAS Experiment at the CERN Large Hadron Collider", JINST 3 S08003, 2008
- [4] F. Englert and R. Brout, "Broken symmetry and the mass of gauge vector mesons", Phys. Rev. Lett. 13, pp. 321-323, 1964
- [5] P. W. Higgs, "Broken symmetries and the masses of gauge bosons", Phys. Rev. Lett. 13, pp. 508-509, 1964
- [6] S. Chatrchyan et al., "Observation of a new boson at a mass of 125 GeV with the CMS experiment at the LHC", Phys. Lett. B716, pp. 30-61, 2012 [arXiv: 1207.7235]
- [7] G. Aad et al., "Observation of a new particle in the search for the Standard Model Higgs boson with the ATLAS detector at the LHC", Phys. Lett. B716, pp. 1-29, 2012 [arXiv: 1207.7214]
- [8] V.C. Rubin, W.K. Ford and N. Thonnard, "Rotational properties of 21 SC galaxies with a large range of luminosities and radii, from NGC 4605 (R=4kpc) to UGC 2885 (R=122kpc)", Astrophysical Journal 238, pp. 471-487, 1980
- [9] K.G. Begeman, A.H. Broeils and R.H. Sanders, "Extended rotation curves of spiral galaxies - Dark haloes and modified dynamics", Monthly Notices of the Royal Astronomical Society, vol. 249, issue 3, ISSN 0035-8711, 1991
- [10] A. Robertson, R. Massey and V. Eke, "What does the Bullet Cluster tell us about self-interacting dark matter?", Monthly Notices of the Royal Astronomical Society, vol. 465, issue 1, 2017 [arXiv: 1605.04307]
- [11] J.B. Mu?oz, C. Dvorkin and A. Loeb, "21-cm Fluctuations from Charged Dark Matter", Phys. Rev. Lett. 121, 121301 (2018) [arXiv: 1804.01092]
- [12] A. Natarajan, "A closer look at CMB constraints on WIMP dark matter", Phys. Rev. D85, 2012 [arXiv:1201.3939 ]
- [13] G. D'Ambrosio G.F. Giudice, G. Isidori and A. Strumia, "Minimal Flavour Violation: an effective field theory approach", Nucl.Phys. 645, pp 155-187, 2002 [arXiv:0207.036 ]
- [14] CMS Collaboration, "Search for the production of dark matter in association with top-quark pairs in the single-lepton final state in proton-proton collisions at  $\sqrt{s} = 8$  TeV", JHEP, vol. 6 121, 2015
- [15] CMS Collaboration, "Search for the Production of Dark Matter in Association with Top Quark Pairs in the Di-lepton Final State in pp collisions at  $\sqrt{s} = 8$  TeV", CMS-PAS-B2G-13-004, 2014

- [16] "Search for dark matter in events with heavy quarks and missing transverse momentum in pp collisions with the ATLAS detector", Eur. Phys. J. C (2015) 75:92
- [17] ATLAS Collaboration, Search for the Supersymmetric Partner of the Top Quark in the Jets+Emiss Final State at  $\sqrt{s} = 13$  TeV", ATLAS-CONF-2016-077
- [18] ATLAS Collaboration, "Search for top squarks in final states with one isolated lepton, jets, and missing transverse momentum in  $\sqrt{s} = 13$  TeV pp collisions with the ATLAS detector", ATLAS-CONF-2016-050, 2016
- [19] ATLAS Collaboration, "Search for direct top squark pair production and dark matter production in final states with two leptons in  $\sqrt{s} = 13$  TeV pp collisions using  $13.3 \text{ fb}^{-1}$  of ATLAS data", ATLAS-CONF-2016-076, 2016
- [20] ATLAS Collaboration, "Search for dark matter produced in association with bottom or top quarks in  $\sqrt{s} = 13$  TeV pp collisions with the ATLAS detector", Eur. Phys. J. C 78 (2018) 18 [arXiv: 1710.11412]
- [21] CMS Collaboration, Search for dark matter produced in association with heavy-flavor quark pairs in proton-proton collisions at  $\sqrt{s} = 13$  TeV", Eur. Phys. J. C (2017) 77: 845
- [22] CMS Collaboration, "Search for dark matter particles produced in association with a top quark pair at  $\sqrt{s} = 13$  TeV", Phys. Rev. Lett. 122, 011803 (2019) [arXiv: 1807.06522]
- [23] CMS Collaboration, "Search for dark matter produced in association with a single top quark or a top quark pair in proton-proton collisions at  $\sqrt{s} = 13$  TeV", JHEP, vol. 03 141, 2019 [arXiv: 1901.01553]
- [24] S. Manzoni, "The Standard Model and the Higgs Boson", Physics with Photons Using the ATLAS Run 2 Data, Springer Theses, 2019
- [25] A.B. Balantekin, A. Gouvea and B.Kayser, "Addressing the Majorana vs. Dirac Question with Neutrino Decays", FERMILAB-PUB-18-418-T, NUHEP-TH/18-09 [arXiv: 1808.10518]
- [26] J. Woithe, G.J. Wiener and F. Van der Vecken, "Let's have a coffee with the Standard Model of particle physics!", Physics education 52, number 3, 2017
- [27] H. Poincare, "The Milky Way and the Theory of Gases", Popular Astronomy, vol. 14, pp.475-488, 1906
- [28] F. Zwicky, "Die Rotverschiebung von extragalaktischen Nebeln", Helvetica Physica Acta , vol. 6, pp. 110-127, 1933
- [29] S. Van den Bergh, Phys Rev D "The early history of dark matter", Dominion Astrophysical Observatory, 1999
- [30] V.C. Rubin, W.K. Ford, "Rotation of the Andromeda Nebula from a Spectroscopic Survey of Emission Regions", Astrophysical Journal 159, p. 379, 1970
- [31] A. A. Penzias, R.W. Wilson, "A Measurement of Excess Antenna Temperature at 4080 Mc/s", Astrophysical Journal 142, pp. 419-421
- [32] D.J. Fixsen, "The temperature of the cosmic microwave background", Astrophysical Journal, 2009
- [33] Planck Collaboration, "Planck 2018 results. I. Overview and the cosmological legacy of Planck", 2018 [arXiv: 1807.06205]

- [34] R. Tojeiro, "Understanding the Cosmic Microwave Background Temperature Power Spectrum", 2006
- [35] Planck Collaboration, "Planck 2018 results. VI. Cosmological parameters", 2018 [arXiv: 1807.06209]
- [36] "Astrophysical Constants and Parameters", 2019
- [37] D. Clowe et all., "A Direct Empirical Proof of the Existence of Dark Matter", *Astrophysical Journal Letters* 648, 2006
- [38] L. Heurtier, H. Partouche, "Spontaneous Freeze Out of Dark Matter From an Early Thermal Phase Transition", CPHT-RR065.112019 [arXiv: 1912.02828]
- [39] K.R. Dienes, J. Fennick, J. Kumar, B. Thomas "Dynamical Dark Matter from Thermal Freeze-Out", *Phys. Rev. D* 97, 063522 (2018) [arXiv: 1712.09919]
- [40] C.S. Frenk, S.D.M. White, "Dark matter and cosmic structure", *Annalen der Physik*, p. 22 , 2012 [arXiv: 1210.0544]
- [41] R. Kirk, "Dark matter genesis"
- [42] M. Drewes et all., "A White Paper on keV Sterile Neutrino Dark Matter", 2016 [arXiv: 1602.04816]
- [43] C. Alcock et all., "The MACHO Project: Microlensing Results from 5.7 Years of LMC Observations", *Astrophys.J.* 542 (2000) 281-307
- [44] P. Tisserand et all., "Limits on the Macho content of the Galactic Halo from the EROS-2 Survey of the Magellanic Clouds", *A & A* 469, pp. 387-404 (2007)
- [45] EROS and MACHO collaborations, "EROS and MACHO Combined Limits on Planetary Mass Dark Matter in the Galactic Halo", 1998
- [46] Particle Data Group, "Neutrino Cross Section Measurements", PDG 2019
- [47] K. McFarland, "Neutrino Interactions", 2008 [arXiv: 0804.3899]
- [48] E. Morgan, "Aspects of WIMP Dark Matter Searches at Colliders and Other Probes", Springer theses, 2016
- [49] F. Couchot et all., "Cosmological constraints on the neutrino mass including systematic uncertainties", *A & A* 606, A104 (2017)
- [50] E. Bulbul et all., "Detection of An Unidentified Emission Line in the Stacked X-ray spectrum of Galaxy Clusters", 2014 [arXiv: 1402.2301]
- [51] A. Boyarsky et all., "An unidentified line in X-ray spectra of the Andromeda galaxy and Perseus galaxy cluster", *Phys. Rev. Lett.* 113, 251301 (2014) [arXiv: 1402.4119]
- [52] A. Boyarsky et all., "Checking the dark matter origin of 3.53 keV line with the Milky Way center", *Phys. Rev. Lett.* 115, 161301 (2015) [arXiv: 1408.2503]
- [53] T. Jeltema1 and S.Profumo, "Deep XMM Observations of Draco rule out at the 99% Confidence Level a Dark Matter Decay Origin for the 3.5 keV Line", 2015 [arXiv: 1512.01239]
- [54] D. Wu, "A Brief Introduction to the Strong CP Problem", Superconducting Super Collider Laboratory, 1991

- [55] R.D. Peccei, H.R. Quinn, "CP Conservation in the Presence of Pseudoparticles", Phys. Rev. Lett. 38, 1440, 1977
- [56] P.W. Graham et all., "Experimental Searches for the Axion and Axion-like Particles", Annual Review of Nuclear and Particle Science 65, 2015 [arXiv: 1602.00039]
- [57] CAST collaboration, "New CAST limit on the axion-photon interaction", Nature Physics 13, pp. 584-590 (2017)
- [58] S.K. Vempati, "Introduction to MSSM", 2012 [arXiv: 1201.0334]
- [59] B. Penning, "The Pursuit of Dark Matter at Colliders - An Overview", 2017 [arXiv: 1712.01391]
- [60] M. Schumann, "Direct Detection of WIMP Dark Matter: Concepts and Status", J. Phys. G46 (2019) no.10, 103003 [arXiv: 1903.03026]
- [61] S.C. Martin et all., "The RAVE survey: constraining the local Galactic escape speed", Mon.Not.Roy.Astron.Soc.379:755-772, 2007
- [62] K. Freese, M. Lisanti, C. Savage, "Annual Modulation of Dark Matter: A Review", [arXiv: 1209.3339v3]
- [63] T.M. Undagoitia and L. Rauch, "Dark matter direct-detection experiments", J. Phys. G43 (2016) no.1, 013001 [arXiv: 1509.08767]
- [64] R. Bernabei et all., "First results from DAMA/LIBRA and the combined results with DAMA/NaI", Eur.Phys.J.C56:333-355, 2008 [arXiv: 0804.2741]
- [65] J.M. Gaskins, "A review of indirect searches for particle dark matter", Contemporary Physics, 2016 [arXiv: 1604.00014]
- [66] F.S. Queiroz, "Dark Matter Overview: Collider, Direct and Indirect Detection Searches", Max-Planck Institute of Physics
- [67] LAT collaboration, "Constraints on Dark Matter Annihilation in Clusters of Galaxies with the Fermi Large Area Telescope", JCAP 05(2010)025 [arXiv: 1002.2239]
- [68] A.A. Moiseev et all., "Dark Matter Search Perspectives with GAMMA-400", 2013 [arXiv: 1307.2345]
- [69] L. Covi et all., "Neutrino Signals from Dark Matter Decay", JCAP 1004:017, 2010 [arXiv: 0912.3521]
- [70] B. Lu and H. Zong, "Limits on the Dark Matter from AMS-02 antiproton and positron fraction data", Phys. Rev. D 93, 103517 (2016) [arXiv: 1510.04032]
- [71] J. Abdallah et all., "Simplified Models for Dark Matter Searches at the LHC", Phys. Dark Univ. 9-10 (2015) 8-23 [arXiv: 1506.03116]
- [72] H. An, L. Wang, H. Zhang, "Dark matter with t-channel mediator: a simple step beyond contact interaction", Phys. Rev. D 89, 115014 (2014) [arXiv: 1308.0592]
- [73] ATLAS Collaboration, "Search for dark matter and other new phenomena in events with an energetic jet and large missing transverse momentum using the ATLAS detector", JHEP 01 (2018) 126 [arXiv: 1711.03301]
- [74] CMS Collaboration, "Search for new physics in the monophoton final state in proton-proton collisions at  $\sqrt{s} = 13$  TeV", J. High Energy Phys. 10 (2017) 073 [arXiv: 1706.03794]

- [75] CMS Collaboration, "Search for dark matter produced with an energetic jet or a hadronically decaying W or Z boson at  $\sqrt{s} = 13$  TeV", JHEP 07 (2017) 014 [arXiv: 1703.01651]
- [76] CMS Collaboration, "Search for new physics in final states with an energetic jet or a hadronically decaying W or Z boson and transverse momentum imbalance at  $\sqrt{s} = 13$  TeV", Phys. Rev. D 97, 092005 (2018) [arXiv: 1712.02345]
- [77] ATLAS Collaboration, "Search for dark matter in association with a Higgs boson decaying to two photons at  $\sqrt{s} = 13$  TeV with the ATLAS detector", Phys. Rev. D 96 (2017) 112004 [arXiv: 1706.03948]
- [78] CMS Collaboration, "Search for associated production of dark matter with a Higgs boson decaying to  $b\bar{b}$  or  $\gamma\gamma$  at  $\sqrt{s} = 13$  TeV", JHEP 10 (2017) 180 [arXiv: 1703.05236]
- [79] Atlas Collaboration, "Search for new phenomena in dijet events using 37 fb<sup>-1</sup> of pp collision data collected at  $\sqrt{s} = 13$  TeV with the ATLAS detector", Phys. Rev. D 96, 052004 (2017) [arXiv: 1703.09127]
- [80] CMS Collaboration, "Search for narrow and broad dijet resonances in proton-proton collisions at  $\sqrt{s} = 13$  TeV and constraints on dark matter mediators and other new particles", JHEP 08 (2018) 130 [arXiv: 1806.00843]
- [81] C. Munoz, "Models of Supersymmetry for Dark Matter", FTUAM 17/2, IFT-UAM/CSIC-17-005, 2017 [arXiv: 1701.05259]
- [82] CMS Collaboration, "Searches for invisible decays of the Higgs boson in pp collisions at  $s_{\text{sqrt}s} = 7, 8,$  and  $13$  TeV", JHEP 02 (2017) 135 [arXiv: 1610.09218]
- [83] J. Alimena et all., "Searching for long-lived particles beyond the Standard Model at the Large Hadron Collider", 2019 [arXiv: 1903.04497]
- [84] A. Albert et all., "Recommendations of the LHC Dark Matter Working Group: Comparing LHC searches for heavy mediators of dark matter production in visible and invisible decay channels", 2017 [arXiv: 1703.05703]
- [85] M. Tanabashi et al., Particle Data Group, Phys. Rev. D98, 030001 (2018)
- [86] R. Schicker, "The ALICE detector at LHC", 2005
- [87] LHCb Collaboration, "LHCb Detector Performance", Int. J. Mod. Phys. A 30, 1530022 (2015) [arXiv: 1412.6352]
- [88] J.T. Boyd, "LHC Run-2 and Future Prospects", 2020
- [89] E. Gschwendtner, "AWAKE, A Particle-driven Plasma Wakefield Acceleration Experiment", CERN Yellow Report CERN 2016-001, pp.271-288 [arXiv: 1705.10573]
- [90] M. Thomson, "Modern Particle Physics", Cambridge University Press, 2013
- [91] G. Apollinari et all., "High Luminosity Large Hadron Collider HL-LHC", CERN Yellow Report CERN-2015-005, pp.1-19 [arXiv: 1705.08830]
- [92] CMS Collaboration, "The CMS experiment at the CERN LHC", JINST 3 (2008) S08004
- [93] CMS Collaboration, "Precision measurement of the structure of the CMS inner tracking system using nuclear interactions", JINST 13 (2018) P10034 [arXiv: 1807.03289]
- [94] M.S. Kim, "CMS reconstruction improvement for the muon tracking by the RPC chambers", 2013 JINST 8 T03001 [arXiv: 1209.2646]

- [95] CMS Collaboration, "Performance of the CMS muon detector and muon reconstruction with proton-proton collisions at  $\sqrt{s} = 13$  TeV", JINST 13 (2018) P06015 [arXiv: 1804.04528]
- [96] CMS Collaboration, "Particle-Flow Event Reconstruction in CMS and Performance for Jets, Taus, and MET", CMS-PAS-PFT-09-001, 2009
- [97] CMS Collaboration, "Description and performance of track and primary-vertex reconstruction with the CMS tracker", JINST 9 (2014) P10009 [arXiv: 1405.6569]
- [98] V. Knunz, "Measurement of Quarkonium Polarization to Probe QCD at the LHC", Springer theses, 2015
- [99] CMS Collaboration, "Performance of electron reconstruction and selection with the CMS detector in proton-proton collisions at  $\sqrt{s} = 8$  TeV", JINST 10 (2015) P06005 [arXiv: 1502.02701]
- [100] J. Rembser, "CMS Electron and Photon Performance at 13 TeV", J. Phys. Conf. Ser. 1162 012008, 2019
- [101] P.L.S. Connor, "Review of jet reconstruction algorithms", Ryan Atkin J. Phys. Conf. Ser. 645 012008, 2015
- [102] CMS Collaboration, "Jet energy scale and resolution in the CMS experiment in pp collisions at 8 TeV", JINST 12 (2017) P02014 [arXiv: 1607.03663]
- [103] F. Beaudette, "The CMS Particle Flow Algorithm", 2014 [arXiv: 1401.8155]
- [104] CMS Collaboration, "Identification of heavy-flavour jets with the CMS detector in pp collisions at 13 TeV", JINST 13 (2018) P05011 [arXiv: 1712.07158]
- [105] CMS Collaboration, "Performance of missing transverse momentum reconstruction in proton-proton collisions at  $\sqrt{s} = 13$  TeV using the CMS detector", JINST 14 (2019) P07004 [arXiv: 1903.06078]
- [106] L. Sonnenschein, "Analytical solution of ttbar dilepton equations", Phys.Rev.D73:054015, 2016
- [107] M.H. Seymour and M. Marx, "Monte Carlo Event Generators", MCnet-13-05, 2013 [arXiv:1304.6677]
- [108] B. Cabouat, J.R. Gaunt and K. Ostrolenk, "A Monte-Carlo Simulation of Double Parton Scattering", JHEP11(2019)061 [arXiv: 1906.04669]
- [109] R. Placakyte, "Parton Distribution Functions", 2011 [arXiv:1111.5452]
- [110] J. Alwall et all., "MadGraph 5 : Going Beyond", 2011 [arXiv:1106.0522]
- [111] C. Oleari, "The POWHEG-BOX", Nucl.Phys.Proc.Suppl.205-206:36-41 [arXiv:1007.3893]
- [112] S. Frixione et all., "The MC@NLO 4.0 Event Generator", CERN-TH/2010-216 [arXiv: 1010.0819]
- [113] B. Webber, "Parton shower Monte Carlo event generators", Scholarpedia
- [114] M. Bahr et all., "Herwig++ Physics and Manual", Eur.Phys.J.C58:639-707, 2008 [arXiv: 0803.0883]
- [115] T. Sjostrand, "A Brief Introduction to PYTHIA 8.1" Comput.Phys.Commun.178:852-867, 2008 [arXiv: 0710.3820]

- [116] A. Karneyeu et all., "MCPLLOTS: a particle physics resource based on volunteer computing", European Physical Journal C 74 (2014) [arXiv: 1306.3436]
- [117] V. Lefebure and S. Banerjee, "CMS Simulation Software Using Geant4", CMS-NOTE-1999-072, 1999
- [118] S. Banerjee, "Validation of Geant4 Physics Models Using Collision Data from the LHC", J. Phys.: Conf. Ser. 898 042005
- [119] A. Rizzi, G. Petrucciani and M. Peruzzi, "A further reduction in CMS event data for analysis: the NANO AOD format", J. Phys.: Conf. Ser. 214 06021
- [120] C.G. Lester and D.J. Summers, "Measuring masses of semi-invisibly decaying particles pair produced at hadron colliders", Phys.Lett.B463:99-103, 1999
- [121] K. Bloom, "CMS software and computing for LHC Run 2", ICHEP 2016 [arXiv: 1611.03215]
- [122] W. Tanenbaum, "A ROOT/IO Based Software Framework for CMS", ECONF C0303241:TUKT010, 2003
- [123] CMS Collaboration, "CMS Luminosity Measurements for the 2016 Data Taking Period", CMS-PAS-LUM-17-001, 2017
- [124] CMS Collaboration, "CMS Luminosity Measurements for the 2017 Data Taking Period", CMS-PAS-LUM-17-001, 2018
- [125] CMS Collaboration, "CMS Luminosity Measurements for the 2018 Data Taking Period", CMS-PAS-LUM-17-001, 2019
- [126] CMS Twiki, "Reweighting recipe to emulate Level 1 ECAL prefiring"
- [127] CMS Collaboration, "Measurement of the differential cross sections for top quark pair production as a function of kinematic event variables in pp collisions at  $\sqrt{s} = 7$  and 8 TeV", Phys. Rev. D 94 (2016) 052006 [arXiv: 1607.00837]
- [128] CMS Twiki, "Electron and Photon Physics Object Offline Guide"
- [129] CMS Twiki, "Baseline muon selections for Run-II", 2019
- [130] CMS Twiki, "Jet Identification"
- [131] CMS Twiki, "Heavy flavor identification at CMS with deep neural networks"
- [132] CMS Collaboration, "BRIL Work Suite"